
UNIVERSITY *of the*
WESTERN CAPE

# Targeted delivery of GFP loaded polymeric nanoparticles to CD4 expressing cells using a CD4 specific aptamer

**Tayla Michele Mirfin**

A thesis submitted in partial fulfilment of the requirements for the degree Magister Scientiae in the Department of Biotechnology, University of the Western Cape.

**Supervisor:** Professor Mervin Meyer

**Co-supervisor:** Professor Admire Dube

December 2020

# Table of Contents

## Keywords

Aptamers

Alginate

Chitosan

CD4

Electrostatic complexation

HIV

Ionotropic gelation

Polymeric nanoparticles

Nanomedicine

# Abstract

Human Immunodeficiency Virus (HIV), which is the cause of Acquired Immunodefiency Syndrome (AIDS) is a major global public health issue affecting over 37 million people worldwide and is responsible for claiming over 32 million lives since the discovery of the disease in 1981. Through effective diagnosis, treatment and prevention HIV is a manageable disease. Today, advanced antiretrovirals, known as HAART, serve as effective, first-line drug regimens, consisting of a variety of viral inhibitors, and have successfully helped viral suppression. However, issues arise with antiretrovirals due to patient non-adherence and the development of drug resistant mutations. Coupled with dormant HIV reservoirs, viral extinction is attenuated. It is therefore essential that effective alternative treatments are investigated. The exploration of nanomedicine for targeted drug delivery has shown an ability to prolong the drug circulation time, target drugs to specific sites in the body, and enhance drug effectiveness. A previous study demonstrated a novel therapeutic strategy that was based on a mutant version of the caspase-3 enzyme that can induce apoptosis in HIV infected cells. This therapeutic strategy has the potential to wipe out reservoirs of HIV infection. However, the therapeutic strategy lacked selectivity because the delivery mechanism was based on protein transduction technology which will result in the non-selective delivery of the drug. In this study, preliminary work towards the development of a targeted nanoparticle delivery system for this mutant caspase-3 enzyme is described. The study describes the synthesis of green fluorescent protein loaded alginate/chitosan nanoparticles that were functionalized with a DNA aptamer intended to target the nanoparticles to CD4 expressing cells, that are also targeted by HIV. The THP-1 cell line was used due to the ability of the cells to express CD4 receptors on the cell surface. The nanoparticles were synthesized through ionotropic gelation. The size, polydispersity, zeta potential and morphology were investigated by Dynamic Light Scattering and Scanning Electron Microscopy, respectively. The strongly negative zeta potential studies revealed stability of the nanoparticles in suspension and Scanning Electron Microscopy results showed an indicative collapse of the polymer network for the empty nanoparticles (i.e. nanoparticles not loaded with GFP), whereas solid, cuboid nanoparticles were shown for the GFP-loaded nanoparticles. Image-based fluorescence cytometry demonstrated

that the GFP-loaded nanoparticles bind to the THP-1 cells that express the CD4 receptor. The results obtained are indicative of a potential drug delivery system for HIV treatment however, adjustments would need to be made to the current study to further develop this nanocarrier.

# Declaration

I declare that *'Targeted delivery of GFP loaded Alginate/Chitosan nanoparticles to CD4 expressing cells using a CD4 specific aptamer'* is my own work that has not been submitted for any degree or examination in any other university and that all the sources I have used or quoted have been acknowledged in the references.



Signed: 

Date: December 2020

# Dedication

To my Pa, you were my hero.

# Acknowledgements

Firstly, my sincerest gratitude goes to my supervisors Professor Mervin Meyer and Professor Admire Dube for giving me the opportunity to work in the overly exciting and ever-evolving field of nanomedicine. Also, special thanks to the MSc Nanoscience Programme for the financial support and for offering me this life-changing experience. My special appreciation goes towards Dr Sarah D'Souza for always being a brain to pick, a willing lunch partner and an incredibly special friend. Your on-going support has meant the absolute world to me and without it I would have been so lost! My appreciation also extends to Darius Riziki Martin, who was always willing to offer a helping hand, and friendly encouragement. Special thanks to everyone in the School of Pharmacy for being so warm and welcoming, and to Professor Admire Dube for making the team feel like family. My thanks also extend to the Biotechnology department. Additional thanks go to Dr Lauren Swartz and Dr Nicole Sibuyi for your help whenever I needed it. And finally, a very heartfelt thanks to Ms Toni Olivier and Ms Noluthando Tshuma for a friendship filled with giggles, support, and many deep meaningful chats.

# Abbreviations

AIDS – Acquired Immunodeficiency Syndrome

Alg – Sodium alginate

Apt – Amine modified CD4 aptamer

ARVs – Antiretrovirals

BSA - Bovine serum albumin

Ca – Calcium

CD4 - Cluster of differentiation 4

COOH – Carboxylic acid

$COO^-$ - Carboxyl end groups

CS – Chitosan

DNA – Deoxynucleic acid

dsDNA – Double stranded DNA

*E. coli* – Escherichia coli

EDC – 1-Ethyl-3-(3-dimethylaminopropyl)-carbodiimide

FDA - Food and Drug Administration

HAART – Highly Active Antiretroviral Therapy

HCl – Hydrochloric acid

HIV – Human Immunodeficiency Virus

IFN γ – Interferon gamma

IL – Interleukin

IPTG - Isopropyl β-D-1-thiogalactopyranoside

kDa – Kilodaltons

LA – Lysogeny agar

LB - Lysogeny broth

NaOH – Sodium hydroxide

NHS - N-hydroxysuccinimide

NK - Natural killer

PDI – Polydispersity index

RMPI – Roswell Park Memorial Institute medium

RNA – Ribonucleic acid

SELEX - System Enrichment of Ligands by Exponential enrichment

SDS – Sodium Dodecyl Sulfate

SDS-PAGE - Sodium dodecyl sulphate polyacrylamide gel



TEMED - N,N,N',N'-tetramethylethane-1,2-diamine

RPMI – Roswell Park Memorial Institute

NP/s – Nanoparticle/s

NDDS - Nanoparticle drug delivery systems

UNAIDS – Joint United Nations Programme of HIV/AIDS

WHO – World Health Organization

ZP – Zeta potential

# Chapter 1 INTRODUCTION

Human Immunodeficiency Virus (HIV), which causes of Acquired Immunodeficiency Syndrome (AIDS), is a major global public health issue affecting over 37 million people worldwide and is responsible for claiming over 32 million lives since the discovery of the disease in 1981 (UNAIDS, 2019; WHO, 2019a). HIV is a uniquely challenging pathogen that can lead to destruction of host immunity through its high replicative capacity and ability to evade host immunity. In addition, the virus has the ability to cease replication and contribute to latent infection within cells thus creating viral reservoirs, and can continue to silently replicate (Siliciano and Greene, 2011; Ananworanich *et al.*, 2016; Couturier and Lewis, 2018; Wang *et al.*, 2018). Therefore, complete eradication of the virus is never absolute.

Through effective diagnosis, treatment and prevention HIV/AIDS is a manageable disease. Before 1996, few treatment options existed for HIV infection. The clinical management of HIV largely consisted of prophylaxis against common opportunistic pathogens and the introduction of HIV-1 specific antiviral drugs that were given as monotherapy (Young, 1988; Arts and Hazuda, 2012). Today, advanced antiretroviral treatments, known as HAART, serve as effective, first-line drug regimens, consisting of a variety of viral inhibitors, and have successfully helped about 54% of people globally in suppressing the virus (UNAIDS, 2019; Avert, 2020). However, issues arise with antiretrovirals due to patient non-adherence and drug resistant mutations. Coupled with dormant HIV reservoirs, viral extinction is attenuated. Therefore, the development of a steadfast and effective alternative treatment is essential to explore other avenues of viral obliteration (Brady *et al.*, 2010; Couturier and Lewis, 2018; Bandera *et al.*, 2019; Mbunkah *et al.*, 2019).

Advancements in disease diagnostics, management and treatment are ever-evolving, particularly through nanotechnology applications. Nanotechnology has had a tremendous impact on medical sciences, specifically in terms of nanoparticle drug delivery systems (NDDS) (Doshi and Mitragotri, 2009; D'Mello *et al.*, 2017; Patra *et al.*, 2018). In comparison to conventional medicines, NDDS have shown an ability to prolong the drug circulation time, target drugs to specific sites in the body, and enhance drug effectiveness (Onoue, Yamada and Chan, 2014; Bobo *et al.*, 2016; Choi

and Han, 2017; Ventola, 2017; Flühmann *et al.*, 2018). Additionally NDDS can improve drug absorption across biological tissues and into cells, improving bioavailability, and extending the duration of action (Onoue, Yamada and Chan, 2014). Therefore, through the utilization of NDDS, HIV treatment regimens can be enhanced, with the aim of complete viral eradication.

In this study, polymeric nanoparticles (NPs) are explored as a targeted delivery a system for a protein drug that has previously been shown to be a possible treatment for HIV/AIDS. The aim of the current study is to evaluate the targeted delivery of proteins to CD4+ cells, which are the cells that are primarily infected by HIV. In order to track the delivery of the NPs to the cells, the NPs were loaded with a fluorescent protein, green fluorescent protein (GFP). To achieve targeted delivery the surface of the NPs were functionalized with a CD4-specific DNA aptamer. Implications of this study would denote the exploration of an alternative HIV treatment, wherein cells infected with the virus would be rendered apoptotic, and possible virus destruction would ensue.

# Chapter 2 LITERATURE REVIEW

## 2.1 Human Immunodeficiency Virus (HIV)

There are two main types of HIV, namely HIV-1 and HIV-2. Although HIV-2 holds significance in West African AIDS-related deaths, HIV-1 accounts for 95% of the infections globally and is the more infectious of the two (Avert, 2019). Therefore, more focus is placed on HIV-1 research globally.

### 2.1.1 Epidemiology of HIV

At the end of 2018 there were over 37 million people living with HIV globally including approximately 1.7 million people newly infected by the HIV-1 virus. On average, a staggering 32 million people have died from AIDS-related illnesses since the start of the epidemic in 1981. Reports indicate that by June 2019 24.5 million people had access to antiretrovirals (ARVs) worldwide, thus leaving 13.4 million people untreated or unaccounted for (UNAIDS, 2019).

South Africa has the largest and most high-profile HIV epidemic globally, with 7.7 million people living with HIV (about 20.4% of the general population). Although South Africa has the largest antiretroviral therapy (ART) program internationally, 10% of the infected population is still unaware of their status, with only 62% of those who are aware, taking medication (Avert, 2020). While great strides have been made to improve access to and availability of ARTs, there is still an alarming gap worldwide that warrants improvement and understanding to truly control this epidemic.

### 2.1.2 Pathogenesis of HIV

#### 2.1.2.1 Normal host immunity

The first line of defense against viral pathogens can be attributed to cells of the innate immune system, such as myeloid cells (e.g. monocytes, neutrophils, macrophages (MΦ) and dendritic cells (DCs)) (Swanstrom and Coffin, 2012; Legrice and Gotte, 2013; Glowicz, 2015; Doitsh and Greene, 2016; Wacleche *et al.*, 2018). When homeostasis is perturbed, these cells engage in non-specific phagocytosis with a subsequent pro-inflammatory response. This pro-inflammatory response

aids in immune response by increasing signaling (via chemokines) to more myeloid cells, encouraging increased phagocytosis with resultant pathogenic neutralization and destruction (Lambotin *et al.*, 2010; Pennock *et al.*, 2013; Sattentau and Stevenson, 2016; Wacleche *et al.*, 2018).

DCs then produce cytokines such as interleukin-12 (IL-12) and interleukin-15 (IL-15), which stimulate natural killer cells (NK) to further degrade pathogenic invaders through cytotoxic actions (Lambotin *et al.*, 2010). DCs also process the pathogenic antigen and present it, on its cellular surface (via the major histocompatibility complex (MHC) class I or class II antigenic peptide) to the effector T lymphocytes of the adaptive immune system, namely the T helper (CD4+) and cytotoxic T (CD8+) lymphocytes (Lambotin *et al.*, 2010; Pennock *et al.*, 2013; Sattentau and Stevenson, 2016; Wacleche *et al.*, 2018). The presentation by DCs allows for the early response against a particular pathogen to be translated into a memory response as a result of the activation of the adaptive immune system (i.e. the production antibodies) (Lambotin *et al.*, 2010; Wacleche *et al.*, 2018). T lymphocytes are responsible for the cell-mediated immune response of the adaptive immune system (Doitsh and Greene, 2016).

Critical to almost all functions of the adaptive immune response is the activation of T lymphocytes from their naïve state (Pennock *et al.*, 2013; Chavez, Calvanese and Verdin, 2015). Upon emerging from the thymus, these naïve T lymphocytes migrate through secondary lymphoid tissues (spleen and lymph nodes) and the peripheral circulation until they recognize the specific pathogenic antigen they have been programmed to identify on the antigen-presenting cells (APCs). Succeeding a coordinated interaction between receptors on the T lymphocyte and an APC, these T lymphocytes become activated (Lambotin *et al.*, 2010; Pennock *et al.*, 2013).

Following activation, T lymphocytes co-ordinate the proliferation of more immune cells (cytotoxic T lymphocytes, helper T lymphocytes, B cells and MΦ) essential for further pathogenic degradation, via chemical signaling of cytokines and chemokines, **Fig. 2.1** (Andersen *et al.*, 2005; Pennock *et al.*, 2013; Wacleche *et al.*, 2018). The cytotoxic T lymphocytes co-ordinate cellular apoptosis of these APCs via enzymatic activation of the caspase cascade or by release of cytotoxic

enzymes, perforin and granzyme, into the intercellular space, subsequently killing neighboring cells (Andersen *et al.*, 2005; Lambotin *et al.*, 2010; Pennock *et al.*, 2013).

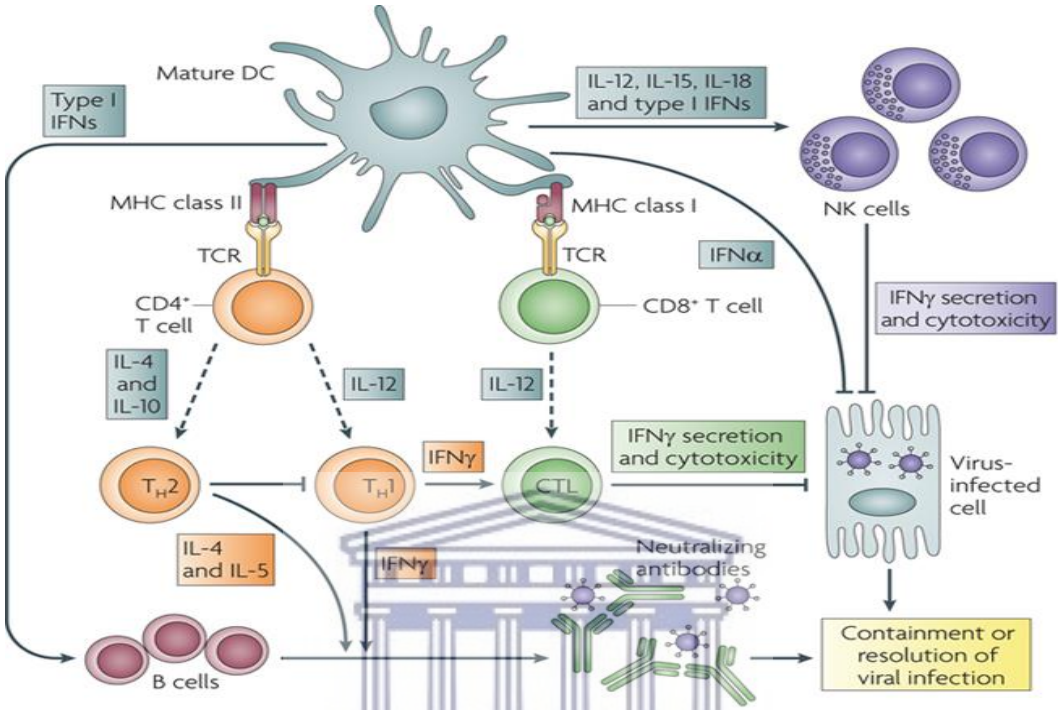


**Fig. 2.1 Function of dendritic cells in normal host immune response.** Following the uptake of a viral antigen, DCs produce various cytokines important for pathogen destruction and antibody production. DCs migrate to lymphoid tissue to prime naïve CD4+ and CD8+ T lymphocytes (via MHC I/II) as well as activate NK cells through the production of inflammatory cytokines. Following the activation and maturation of the naïve T-lymphocytes, more immune cells (cytotoxic T lymphocytes, helper T lymphocytes and B cells) are proliferated, essential for further pathogenic destruction (Lambotin, *et al*., 2010).

One of the earliest insults to the immune system after HIV infection is the direct infection and depletion of the CD4+ T lymphocytes (Brenchley and Douek, 2008; Klatt, Funderburg and Brenchley, 2013). CD4+ cell depletion rapidly occurs within the mucosal tissues where high numbers of activated memory CD4+ T lymphocytes reside whereas a slower, more progressive, depletion of CD4+ T lymphocytes in peripheral tissues and blood ensues (Klatt, Funderburg and Brenchley, 2013). This depletion impairs the normal cell mediated immunity and therefore allows infection of opportunistic pathogens to arise, resulting in acquired immunodeficiency syndrome (AIDS) (Andersen *et al*., 2005; Medzhitov, 2007).

### 2.1.2.2 Genomic structure of HIV-1

HIV-1 is a member of Lentivirinae, which belongs to the family Retroviridae. The genome of HIV encodes 16 viral proteins, each playing an essential role in the HIV replicative life cycle (**Table 2.1**) (Turner and Summers, 1999; Engelman and Cherepanov, 2013; Chen, Wang and Liu, 2016). The three major genes of the HIV genome are *Gag, Pol* and *Env.* These genes code for structural proteins, viral enzymes and envelope proteins. The remaining genes code for regulatory proteins and accessory proteins, all needed at various stages of the HIV life cycle to achieve efficient viral interaction, infection and replication within host cells (Engelman and Cherepanov, 2013; Chen, Wang and Liu, 2016; Freed, 2016).

**Table 2.1 Vital genes and their functions within HIV-1.** The three major genes are *Gag, Pol* and *Env*; encoding for the most essential proteins needed for successful function and replication of HIV-1 (Turner and Summers, 1999; Engelman and Cherepanov, 2013; Galvis, 2014; Chen, Wang and Liu, 2016; Luo *et al.*, 2019)**.**

| Gene | Components encoded |
|---|---|
| ***Gag*** | Proteins of the viral capsid that encapsulate viral genomic RNA (e.g. p24, p17, p9 and p7) |
| ***Pol*** | Viral enzymes such as reverse transcriptase, protease and integrase |
| ***Env*** | Viral envelope glycoproteins (i.e. gp120 and gp41) |
| ***Tat*** **(Transactivator of transcription)** | Regulatory proteins that control transcription of the provirus |
| ***Rev*** | Regulatory proteins that control patterns of viral RNA processing |
| ***Nef,Vif, Vpu/Vpx, Vpr*** | Proteins that contribute to effective viral replication and infectivity. E.g. *Vpr* gene products mediate the transport of the reverse transcribing viral complex across the nuclear membrane.<br>* Vpu is found exclusively in HIV-1, while Vpx in HIV-2 |
| **6 Accessory genes** | Controls patterns of viral and cellular gene expression |

#### 2.1.2.3 Host destruction from a single virion

Upon entering a host, a single virion replicates to generate viremia and persistent infection in all the lymphoid tissue in the body, with preference to CD4+ cells. These cells include T helper cells, monocytes, MΦ and DCs (Swanstrom and Coffin, 2012; Zeng, Haase and Schacker, 2012; Galvis, 2014; Chen, Wang and Liu, 2016; Sattentau and Stevenson, 2016). The viral load from time of initial infection to the time of overt immunodeficiency undergoes remarkable changes with RNA copies exceeding $10^5$; corresponding to depletion of host immunity (Swanstrom and Coffin, 2012; Galvis, 2014). Furthermore, seroconversion (antibody development) to positive HIV-1 serology occurs within 4 to 10 weeks post-exposure with the median time of 63 days (Galvis, 2014).

HIV-1 enters active CD4+ cells, with preference to T lymphocytes, by binding to specific surface receptors (Swanstrom and Coffin, 2012; Chen, Wang and Liu, 2016). The virus does this by means of its envelope proteins, gp120 and gp41, which successfully bind to the CD4 receptor of the immune cells, while using the cell's CCR5 or CXCR4 receptors as co-receptors (Arts and Hazuda, 2012; Shaw and Hunter, 2012; Engelman and Cherepanov, 2013; Galvis, 2014; Chen, Wang and Liu, 2016). The CCR5 co-receptor is expressed on macrophages and activated T helper lymphocytes, while CXCR4 is expressed on resting and memory T-helper lymphocytes (Galvis, 2014). This allows for membrane fusion and subsequent injection of the viral RNA into the cell via the viral capsid. Degradation of this capsid results in the release of viral enzymes and the single stranded viral RNA (Brenchley and Douek, 2008; Engelman and Cherepanov, 2013).

Viral reverse transcriptase (RT) is the most important enzyme, which allows for the synthesis of single stranded viral DNA using viral RNA as a template. RT is the viral version of DNA polymerase as it polymerizes DNA precursors. A complement strand of the viral DNA (cDNA) is then synthesized resulting in the final product which is a double stranded viral DNA (Engelman and Cherepanov, 2013; Jakobsen *et al.*, 2013; Galvis, 2014; Chavez, Calvanese and Verdin, 2015; Knyazhanskaya *et al.*, 2016). This DNA is then congruently introduced into the host DNA by viral integrase – an enzyme responsible for transporting the viral DNA into the host nucleus and cleaving the viral DNA at the 3' termini (known as 3' processing), as well as the host DNA at the 5' termini. The enzyme joins the 3' termini of the virus to cleaved 5' phosphates of the host DNA.

Host enzymes complete the integration process by repairing the un-joined strand gaps created by viral integrase, resulting in a stable provirus. HIV is known as a retrovirus as it subverts the central dogma (i.e. DNA to RNA to proteins) and generates viral DNA from viral RNA (Engelman and Cherepanov, 2013; Galvis, 2014; Knyazhanskaya *et al.*, 2016; Klatt, 2019). It should be noted that not all reverse transcription products in HIV infection result in positive proviral nuclear integration, because reverse transcription of HIV is a very error-prone process. Thus, cytosolic accumulation of viral DNA fragments can trigger an innate immune response (Jakobsen *et al.*, 2013).

The virus can then follow various paths resulting in latent infection or active infection with viral budding. Viral latency occurs when the integrated DNA does not actively transcribe into viral mRNA. A leading theory postulates that latency is established from infected activated CD4+ T lymphocytes that revert to a resting memory state. This results in the development of HIV reservoirs, supporting viral persistence and host immunity evasion (Swanstrom and Coffin, 2012; Stevenson, 2015; Ananworanich *et al.*, 2016; Doitsh and Greene, 2016; Henrich *et al.*, 2017; Bandera *et al.*, 2019).

Active infection involves the transcription of viral genome into enveloped glycoproteins (containing gp120 and gp41 surface receptors) which cluster on the host cell surface. Simultaneously, viral polyproteins are transcribed - a consequence of *GagPol* gene expression (Engelman and Cherepanov, 2013; Chen, Wang and Liu, 2016; Freed, 2016). HIV-1 protease is a crucial enzyme responsible for the cleavage of the viral *Gag* and *GagPol* polyproteins (p17, p24, p7 of the viral core) during virion maturation and together with viral RNA, are brought to the cell surface to complete virion maturation (Arts and Hazuda, 2012; Freed, 2016; Klatt, 2019). This enzyme is thus perceived as a key target for the development of anti-HIV treatment strategies. This site of virion maturation will then commemorate the development of a new, mature HIV particle equipped for further infection following budding from the cell (Engelman and Cherepanov, 2013; Chen, Wang and Liu, 2016; Doitsh and Greene, 2016; Freed, 2016). Usually, budding would be inhibited by a host cellular protein tetherin, however viral *Vpu* counteracts this function therefore allowing budding to commence (Galvis, 2014).

Unlike non-enveloped viruses that usually exit infected cells by inducing their lysis, enveloped viruses (HIV) leave their cellular hosts by budding, keeping the plasma membrane intact. Therefore, other features of HIV and its interaction with the host are responsible for the immense CD4+ T cell loss in AIDS (Zeng, Haase and Schacker, 2012; Engelman and Cherepanov, 2013; Doitsh and Greene, 2016).

### 2.1.3 Stages of HIV infection

HIV/AIDS is a chronic disease that typically begins as an acute, symptomatic illness, followed by a period of viral latency and ends with opportunistic infection resulting from the destruction of the host immunity (**Fig. 2.2**) (Shaw and Hunter, 2012; Galvis, 2014; Freed, 2016; Bandera et al., 2019).

#### 2.1.3.1 Transmission and disease development

Transmission of HIV-1 results in the establishment of a new infection, typically starting from a single virus particle via mucosal exposure or percutaneous inoculation (Shaw and Hunter, 2012; Swanstrom and Coffin, 2012). The infection begins with an acute, symptomatic, flu-like illness, lasting six to twelve weeks, which is associated with high viremia and a sharp drop in peripheral blood CD4+ T cell counts (Douek, Picker and Koup, 2003; Klatt, Funderburg and Brenchley, 2013; Ananworanich *et al.*, 2016; Couturier and Lewis, 2018; Bandera *et al.*, 2019). Following this, there is establishment of a considerable reservoir of latently infected cells (i.e. immune cells found in lymphoid and myeloid tissue), and development of an acquired HIV-1-specific immune response (Douek, Picker and Koup, 2003; Ananworanich *et al.*, 2016; Couturier and Lewis, 2018; Bandera *et al.*, 2019).

Sequentially, a 100- to 1000-fold fall in the viral load is observed with a partial rise in the CD4+ T lymphocyte count and a generally asymptomatic period of chronic infection, lasting on average 10 years. The asymptomatic period is marked by gradual depletion of peripheral CD4+ T lymphocytes counts with accompanying slow rise in viremia, with eventual onset of AIDS and evident immunodeficiency (Douek, Picker and Koup, 2003; Brenchley and Douek, 2008; Galvis, 2014; Lorenzo-Redondo *et al.*, 2016)

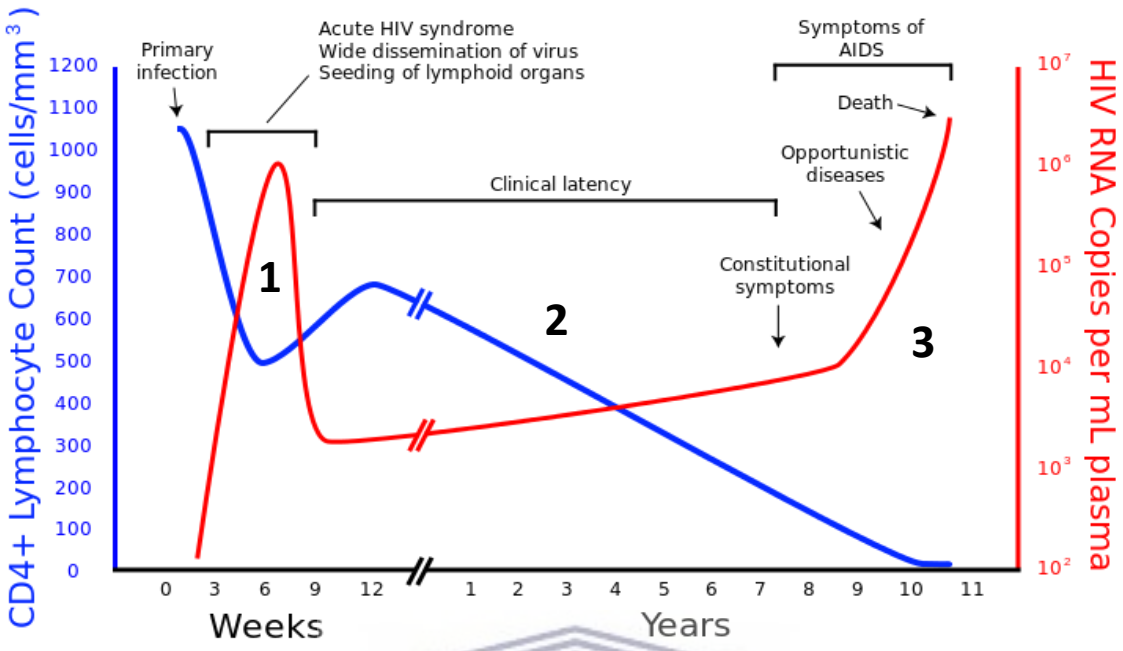


**Fig. 2.2 Changes in CD4+ cell count and HIV RNA copy numbers during HIV infection.** An HIV-1 individual that is left untreated will undergo three phases: (1) Acute phase lasting for 6–12 weeks with flu-like symptoms, peak virus load and drop in CD4+ T cells; (2) Chronic asymptomatic phase lasting on average 7–10 years, virus replication reaches a steady level; (3) AIDS onset is associated with increasing virus replication and declining CD4+ cell counts to <200cells/µl (time to AIDS onset varies between individuals from as little as 2 years to more than 15 years after seroconversion). Note that the patterns of CD4+ cell decline, virus load increase and actual values of viral RNA load vary greatly from one patient to another (Galvis, 2014).



### 2.1.3.2 Host immunodeficiency

Chronic HIV infection is marked by the substantial decline of more than half the total count CD4+ helper T lymphocytes within lymphoid tissue (<200 cells/µl), with resultant immunodeficiency (Sainski *et al.*, 2011; Zeng, Haase and Schacker, 2012; Doitsh and Greene, 2016; Di *et al.*, 2019). The ensuing infection with marked immunodeficiency results in the development of AIDS, augmenting the allowance of opportunistic tumors and infections to beset the individual, that would ordinarily be inconsequential in normal immunity (Zeng, Haase and Schacker, 2012; Klatt, Funderburg and Brenchley, 2013; Luo *et al.*, 2019).

Originally, cellular destruction was thought to be attributed to the virus lysing and thus, destroying the cell upon budding and aiding in the spreading of the virus. However, it was

consequently found that only 5-10% of the dying CD4+ T lymphocytes are infected with the virus, while the remaining 90-95% of cells are uninfected (Monroe *et al.*, 2014; Doitsh and Greene, 2016). This finding probed further understanding as to why and how the CD4+ T lymphocyte population is exponentially eradicated.

### 2.1.3.3 Intercellular programmed cell death

Cell death can occur via various intracellular pathways with apoptosis and pyroptosis holding great significance during HIV infection (see **Fig. 2.3**) (Monroe *et al.*, 2014; Doitsh and Greene, 2016; Knyazhanskaya *et al.*, 2016). Early innate sensing of HIV infection includes the activation of anti-viral responses, most notably cytokine production through pattern recognition receptors (PRRs). PRRs are sensors of the innate immune system recognizing evolutionary conserved structures on pathogens (Kawai and Akira, 2010; Nissen *et al.*, 2014). This may serve a protective role for the host by creating a pro-inflammatory environment, resulting in restricted viral replication (Kawai and Akira, 2010; Jakobsen *et al.*, 2013; Nissen *et al.*, 2014).

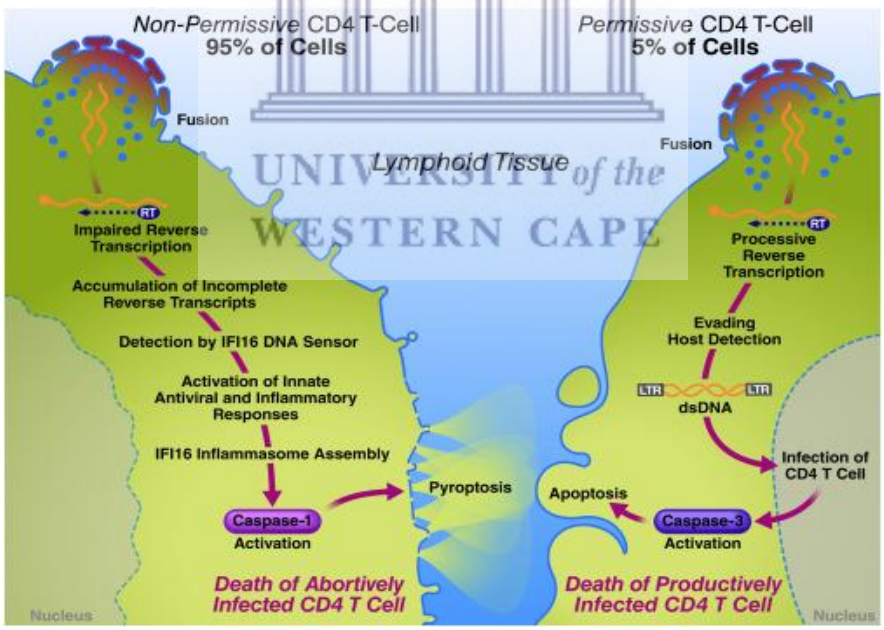


**Fig. 2.3 Role of caspase-3-mediated apoptosis and caspase-1-mediated pyroptosis in CD4+ T lymphocytes death during HIV infection.** If the virus infects an activated and, thus, permissive cell, productive infection ensues, with the activation of silent caspase-3-mediated apoptosis. Conversely, if the virus infects a resting, non-permissive cell, pyroptosis ensues; - a highly inflammatory form of programmed cell death (Doitsh and Greene, 2016).

Conversely, it is well established that innate immune responses, with secretion of cytokines, contribute to chronic immune activation, the development of immunodeficiency and progression to AIDS (Jakobsen *et al.*, 2013; Nissen *et al.*, 2014; Doitsh and Greene, 2016).

Upon successful integration of an HIV virion, the cellular sensor, DNA-dependent protein kinase (DNA PK), detects breaks in the cellular DNA – the consequence of viral integrase. This detection triggers the activation of the enzyme caspase-3, which initiates the events of apoptosis (a non-inflammatory programmed cell death) (Jakobsen *et al.*, 2013; Monroe *et al.*, 2014; Chavez, Calvanese and Verdin, 2015; Doitsh and Greene, 2016). An additional apoptotic trigger occurs when HIV protease (a viral cleaving enzyme) cleaves and therefore, activates cellular proteins called caspases, specifically caspase-8, which in turn activates caspase-3, resulting in apoptosis. The instant caspases are activated, programmed cell death initiates (Sainski *et al.*, 2011; Swanstrom and Coffin, 2012).

Additionally, a study done by Monroe *et al.*, 2014, demonstrates that cell death can occur following the detection of rogue, unintegrated viral transcripts by intracellular protein, interferon-gamma-inducible protein 16 (IFI16). Upon detection, IFI16 initiates an inflammatory cascade by means of inflammasome assembly, which in turn activates caspase-1. Caspase-1 stimulates the production of the cytokine, interleukin 1β (IL-1β), creating a highly inflammatory environment within the cell. This considerable spike in inflammation will lead to cellular self-destruction known as pyroptosis (Jakobsen *et al.*, 2013; Monroe *et al.*, 2014; Nissen *et al.*, 2014; Doitsh and Greene, 2016).



Once the cell erupts, the highly concentrated IL-1β is released into the extracellular space, with consequential pyroptosis of bystander CD4+ lymphocytes. This is the root rationale behind the exponential eradication of the (mostly uninfected) CD4+ lymphocytes in chronic immunodeficient HIV infection (Monroe *et al.*, 2014; Nissen *et al.*, 2014). The cycle of abortive infection, inflammatory death, and recruitment of new cells to these sites of inflammation explains how this innate host response is undermined and therefore, vastly contributes to HIV/AIDS pathogenesis. It is important to note that the elicitation of pyroptosis requires cell-to-

cell spread of the virus; free virions are unable to activate this response (Nissen *et al.*, 2014; Doitsh and Greene, 2016).

#### 2.1.3.4 Extracellular programmed cell death

Extracellular eradication of CD4+ lymphocyte occurs upon the recognition of the HIV surface proteins by cytotoxic T lymphocytes. Cytotoxic T lymphocytes elicit cellular apoptosis. Alternatively, HIV specific antibodies are produced following weeks to months of infection, allowing for further immune detection and destruction of infected cells. It should be noted, however, that antibodies are specific to certain strains of HIV. As HIV lacks proof-reading abilities and commonly synthesizes inconsistent complement strands, previously produced antibodies could be rendered obsolete (Engelman and Cherepanov, 2013; Jakobsen *et al.*, 2013; Mbunkah *et al.*, 2019).

### 2.1.4 Current treatments for HIV

Before 1996, few antiretroviral treatment options existed for HIV-1 infection. The clinical management of HIV-1 largely consisted of prophylaxis against common opportunistic pathogens and the introduction of HIV-1 specific antiviral drugs (known as NRTIs) that were given as monotherapy (Young, 1988; Arts and Hazuda, 2012). Shortfalls in HIV vaccination are also apparent. Amongst the array of attempted vaccines, the most promising appear to be passive immunization with monoclonal antibodies, and the Tat therapeutic vaccine, in which anti-Tat antibodies are produced – highly uncommon in a natural infection. Although these vaccines show promise, there is yet to be one that prevails (Gray *et al.*, 2016; Adamson *et al.*, 2017). Issues with vaccines arise due to differing individual genetics, a lack of acquired immunity, HIV host evasion, and the highly error-prone process of HIV replication, leading to inconsistencies in the virus (Gray *et al.*, 2016; Yaqub, 2018). Therefore, focus was placed on developing effective HIV drug regimens. The treatment of HIV-1 infection was revolutionized in the mid-to-late 1990s by the development of protease and RT inhibitors that saw the introduction of combined drug regimens, known today as highly active antiretroviral therapy (HAART), that constitute the first-line ART regimen (**Table 2.2**) (Collier *et al.*, 1996; D'Aquila *et al.*, 1996; Gulick *et al.*, 1997; Brady *et al.*, 2010; Arts and Hazuda, 2012).

HAART reduces viral load to almost undetectable levels, allowing a longer and healthier life for those infected (Cheng, Zhang and Zhao, 2019; van der Merwe, 2019). According to World Health Organization (WHO) guidelines, it was formerly recommended that HAART be initiated when the CD4 count is below 500 cells/µl however, the WHO and the US Department of Health and Human Services (HHS) later recommended that HAART treatment, in all HIV positive individuals, should be implemented immediately, regardless of the CD4 count. South Africa adopted the "Treat All" policy in 2017, which follows the above recommendations (HHS, 2014; Anthony *et al.*, 2019; WHO, 2019b).

Modern HAART regimens make use of drugs that target viral enzymes or act as receptor antagonists to the virus at different stages within the HIV life cycle. These include entry/fusion inhibitors (including coreceptor antagonists), nucleoside and non-nucleoside reverse transcriptase inhibitors (NRTIs and NNRTIs), protease inhibitors and integrase inhibitors (PIs and InSTIs). The first-line treatment regimen usually consists of two NRTIs in combination with a third drug from one of the other classes (Bandera *et al.*, 2019; NIH, 2020). As of 2019, there are at least 39 antiretrovirals that have been approved by the United States Food and Drug Administration (US FDA) and fall into the above classes (NIH, 2020).



**Table 2.2. Antiretroviral drug classes and their associated modes of action.** Adapted from (Quiñones-Mateu and Arts, 2001; Arts and Hazuda, 2012; Clutter *et al.*, 2017; Klatt, 2019; NIH, 2020)

| Drug class | Mode of action | Examples |
|---|---|---|
| **Entry/Fusion Inhibitor** | Fusion inhibitors are peptides that interfere with the receptor-mediated entry by mimicking the HR2 region found on gp41. During viral replication, the HR2 region binds to the HR1 region, facilitating the fusion of the viral envelope. Antagonistic binding of the inhibitor to the HR1 region inhibits the fusion process of the viral envelope.<br>Entry inhibitors are soluble preparations of CD4 that bind to viral gp120, preventing attachment to cellular CD4.<br>CCR5 antagonists are also included in this drug class. This drug binding induces and stabilizes a receptor conformation that is not recognized by either CCR5 | Enfuvirtide<br>Maraviroc<br>Vicriviroc<br>Cenicriviroc |

| | | |
|---|---|---|
| | agonists or HIV-1, inhibiting coreceptor binding in HIV-1 entry. | |
| **Nucleoside RT inhibitor (NRTI)** | NRTIs are nucleotide base analogues that inhibit reverse transcription by causing chain termination of viral DNA after nuclear incorporation. These drugs are activated upon becoming phosphorylated intracellularly by host kinases and cause chain termination due to a lack of 3’ hydroxyl group at the sugar moiety of the drug. This results in the inability to form the 5' to 3' phosphodiester linkage required for DNA elongation and formation of a provirus. | Abacavir<br>Emtricitabine<br>Lamivudine<br>Tenofovir disoproxil<br>Tenofovir alafenamide<br>Zidovudine (AZT) |
| **Non-nucleoside RT inhibitor (NNRTI)** | NNRTIs inhibit HIV-1 RT by binding directly and non-competitively to a hydrophobic pocket proximal to the active binding site. The binding of NNRTIs to RT changes the conformation of the substrate-binding site and reduces its catalytic, polymerase activity. | Delavirdine<br>Etravirine<br>Efavirenz<br>Nevirapine<br>Rilpivirine |
| **Protease inhibitor (PI)** | PIs are substrate analogues for the HIV protease enzyme, responsible for blocking the enzyme’s active binding site. This inhibits the viral maturation process resulting in a lack of fully functional virion formation. | Amprenavir<br>Atazanavir<br>Darunavir<br>Fosamprenavir<br>Indinavir<br>Lopinavir<br>Nelfinavir<br>Ritonavir<br>Saquinavir<br>Tipranavir |
| **Integrase strand transfer inhibitor (InSTIs)** | InSTIs target and block the enzyme integrase, inhibiting 3’ processing of the viral DNA, thereby interfering with the strand transfer of the viral DNA.<br>The selective effect on strand transfer is a result of the inhibitor (1) binding only to the specific complex between integrase and the viral DNA and (2) interacting with the two essential magnesium metal ion cofactors in the integrase active site and the DNA. InSTIs are therefore the only ARV class that interacts with two essential elements of the virus, the integrase enzyme as well as the viral DNA, which is the substrate for integration. | Bictegravir<br>Dolutegravir<br>Elvitegravir<br>Raltegravir |

### 2.1.5 Limitations of current HIV treatments

Since its introduction, ART has greatly reduced global morbidity and mortality rates and lengthened the lifespan of people living with HIV (Kiptoo *et al.*, 2013; Luo *et al.*, 2019). However, despite its potency, the efficacy of ART in halting viral replication can be jeopardized by development of drug resistance mutations, non-adherence and viral persistence in reservoirs (further discussed in section **2.1.5.3**) (Brady *et al.*, 2010; Couturier and Lewis, 2018; Bandera *et al.*, 2019; Mbunkah *et al.*, 2019). Notably, there is essentially no cross-resistance among antiretroviral drug classes, therefore multi-drug regimens work well. However, significant drug resistance within each class has been discovered (Arts and Hazuda, 2012; Clutter *et al.*, 2017; Klatt, 2019). Noteworthy side effects of ART are also experienced by up to 94% of patients and include gastrointestinal issues, such as nausea and diarrhea; headache, hypersensitivity, myopathy, Steven-Johnsons syndrome, skin rash and hepatotoxicity to name a few (Iacob, Iacob and Jugulete, 2017; Klatt, 2019).

#### 2.1.5.1 Drug resistant mutations

Drug resistance mutations are the leading cause of ART failure, becoming a challenge in achieving the long-term effectiveness of ART. Virologic failure (inability to successfully suppress HIV) due to drug resistant mutations is most likely a consequence of incomplete patient adherence to ART treatment (Kiptoo *et al.*, 2013; Clutter *et al.*, 2017; Klatt, 2019; Luo *et al.*, 2019). With the development of HIV-1 drug resistance mutations, the principal ART drugs are unable to inhibit the resistant virus and the viral load may be precipitously raised (Azam *et al.*, 2014; Anthony *et al.*, 2019). Subsequently, with depletion of the immune system through CD4 T lymphocyte exhaustion, patients are inevitably more prone to opportunistic infection, which is exhibited as a clinical therapy failure (Saini *et al.*, 2012; Bhargava *et al.*, 2014). Worse still, patients who failed in first-line antiretroviral drugs may also likely fail with the second-line drugs, creating severe public health issues (Anthony *et al.*, 2019; Luo *et al.*, 2019; WHO, 2019b).

Mutations within HIV-1 occur daily and spontaneously, with most being innocuous to the host, but detrimental to viral fitness, such as seen with PI and InSTI drug resistance (Arts and Hazuda, 2012; Clutter *et al.*, 2017; Bandera *et al.*, 2019). The high mutation rate of HIV-1 is due to the

absence of 3'→5' exonucleolytic proofreading activity of HIV-1 RT. Mutations introduce many "quasispecies" of HIV, particularly during the period following initial infection and habitually mutants least inhibited by antiretrovirals may become dominant subtypes. Additionally, in the absence of ART, selective evolutionary pressure to increase HIV variants with drug resistant mutations is low (Clutter *et al.*, 2017; Klatt, 2019). The high mutation rate of HIV during reverse transcription replication, or by transmission from an HIV-1-infected antiretroviral drug-treated person, enhances development of antiretroviral drug resistance (Lorenzo-Redondo *et al.*, 2016; Klatt, 2019; Mbunkah *et al.*, 2019) Resistance increases with the length of therapy, as multiple amino acid changes accumulate over time to yield virus variants (Clutter *et al.*, 2017; Klatt, 2019).

The drug resistance mutations to NRTIs and NNRTIs are one the leading causes of first-line ART failure (Luo *et al.*, 2019). For some drugs, such as the NRTI lamivudine and all NNRTIs, just a single mutation - notably the M184V or K103N mutations - can result in high-level drug resistance. This is clinically relevant, as NNRTIs including efavirenz and nevirapine have for many years made up the backbone of first-line treatment in low-resource settings (Anthony *et al.*, 2019; Avert, 2020). In a study by Luo*, et al*., where drug resistant mutations amongst 112 first-line ART users were investigated. The percentage of drug resistance was exceptionally high amongst patients taking the NNRTIs, efavirenz (71.84%) and nevirapine (74.76%), while resistance was also present for NRTIs such as lamivudine (66.02%) and tenofovir NRTI (21.36%) (Luo *et al.*, 2019). This proves the complexity and high prevalence of NRTI and NNRTI drug resistant mutations, signifying the leading cause of first-line ART failure.



#### 2.1.5.1.1 NRTI drug resistance

Resistance to NRTIs is mediated by two mechanisms: (1) ATP-dependent pyro-phosphorolysis, with chain termination reversal, and (2) the prevention of NRTI incorporation into the nascent chain (Arts and Hazuda, 2012; Clutter *et al.*, 2017). ATP-dependent pyro-phosphorolysis is the removal of NRTIs from the 3' end of the nascent chain by phosphorylytic excision (cleavage by inorganic phosphates), resulting in the reversal of the chain termination process. NRTI mutations occur in RT and are classified as nucleoside/nucleotide associated mutations (NAMs) or thymidine analog mutations (TAMs) - responsible for promoting pyro-phosphorolysis (Arts and

Hazuda, 2012; Clutter *et al.*, 2017; Klatt, 2019). A second mechanism of NRTI resistance is the prevention of NRTI incorporation into the growing chain, typically after discrimination by RT between the inhibitor and the native DNA substrate has been made. Mutations associated with this mechanism are commonly induced following treatment with lamivudine or emtricitabine (Arts and Hazuda, 2012; Clutter *et al.*, 2017; Klatt, 2019).

#### 2.1.5.1.2 NNRTI drug resistance

Whilst reductions in replicative fitness of HIV is observed amongst other drug classes; with NNRTIs, single nucleotide changes can result in high-level resistance with only a slight loss of replicative fitness (Arts and Hazuda, 2012; Anthony *et al.*, 2019). For example, NNRTI resistance mutations result in a slight decrease in RT polymerase activities due to their relatively low genetic barrier to resistance (i.e. allowance for mutations to happen relatively easily) (Quinones-Mateu and Arts, 2001; Arts and Hazuda, 2012; Clutter *et al.*, 2017; Klatt, 2019). This type of resistance also constitutes a slow reversion of these mutations, even in the absence of any drug, proving the stability of NNRTI resistant HIV and the contribution to transmitted drug resistance amongst a general population (Tebit *et al.*, 2010; Arts and Hazuda, 2012; Clutter *et al.*, 2017). There is a high level of cross-resistance within this drug class increasing the likelihood of transmission of drug resistant dominant strains. This is particularly apparent within low-to-middle income countries where routine drug resistance testing is not feasible (Clutter *et al.*, 2017; Klatt, 2019). In South Africa, in particular, the key drivers of NNRTI resistance transmission can be attributed to rapid ART scale-up, with inadequate resistance testing and switching to second-line treatment (Anthony *et al.*, 2019).

### 2.1.5.2 Non-adherence

In resource-limited settings, non-adherence is a major contributing factor to development of drug resistance and ultimately treatment failure (Kiptoo *et al.*, 2013; Clutter *et al.*, 2017; Luo *et al.*, 2019). The adherence to antiretroviral therapy remains unsatisfactory and varies between 27 and 80% across different populations in various studies, compared with the required level of 95% (Iacob, Iacob and Jugulete, 2017; Avert, 2020). The low adherence to ART is a multi-factorial process, raising considerable difficulties in long-term follow-up. Non-adherence can arise from

intentional or unintentional causes. Intentional non-adherence can be attributed to denial of diagnosis, lack of trust in the health-care providers/treatment, HIV associated stigmas and disappointment due to the inability to cure HIV infection. Unintentional reasons may be attributed to different personality types, forgetfulness, lack of knowledge or cognitive limitations such as depression (Iacob, Iacob and Jugulete, 2017; Laws *et al.*, 2019).

In sub-Saharan Africa the most reported reasons for non-adherence to ART are lack of knowledge, health concerns such as side effects, and socio-cultural prejudice towards HIV infected patients (Mongo-delis *et al.*, 2019). In a study in Kenya, the key factors affecting adherence were; being away from home, being busy/forgetting and stigma (Talam *et al.*, 2008). Another study based in Indonesia stated that minimizing the stigma associated with HIV could increase adherence to ART (Nurfalah, Yona and Waluyo, 2019). It appears that different regions have varying contributing factors to non-adherence, with focus on the negative stigma surrounding the disease and the associated shame of having the disease.

**2.1.5.3 HIV reservoirs**

HIV reservoirs are defined as a site entailing viral production, virion storage and viral persistence, with no active infection. They are predominantly established in lymphoid tissue, particularly resting memory cells, during acute infection, with myeloid tissue and adipose tissue constituting as major sites for viral latency too (Couturier and Lewis, 2018; Bandera *et al.*, 2019). Reservoirs are extremely stable with an estimated half-life of 44 months and virions in these resevoirs have the ability to proliferate without viral reactivation (Siliciano and Greene, 2011; Ananworanich *et al.*, 2016; Wang *et al.*, 2018).

One of the most active areas of research has focused on understanding the mechanisms involved in the establishment and maintenance of the HIV reservoir (Chavez, Calvanese and Verdin, 2015). A leading theory postulates that latency is established from infected, activated CD4+ T lymphocytes that revert to a resting memory state. According to this theory, the transition to a resting memory state is associated with a decrease in transcriptional protein complexes within the cell (e.g. NFκB - nuclear factor kappa-light-chain-enhancer of activated B cells), therefore silencing the HIV genome (Siliciano and Greene, 2011; Chavez, Calvanese and Verdin, 2015).

Whilst combinations of ART drugs usually suppress viral replication and reduce viral RNA to undetectable levels in blood, it is noteworthy that these treatments do not fully eradicate the virus due to the presence of these reservoirs (Ananworanich *et al.*, 2016; Lorenzo-Redondo *et al.*, 2016; Bandera *et al.*, 2019). This is because latently infected cells do not produce active viral transcripts, thereby escaping viral cytopathic effects and are ignored by the immune system. Furthermore, ARTs target active viral replication, therefore rendering them ineffective against these latent proviruses (Siliciano and Greene, 2011; Chavez, Calvanese and Verdin, 2015).

Significantly, early ART initiation does not prevent the establishment of these latently infected cells either, despite treatment starting within a few days of acute infection (Ananworanich *et al.*, 2016; Henrich *et al.*, 2017; Bandera *et al.*, 2019). This finding was corroborated in the study by Ananworanich, *et al.,* where it was shown that early ART commencement reduces, but does not obliterate, total HIV RNA concentrations by 20-fold after 2 weeks and 316-fold after 3 years. In another study by Henrich *et al*., two cases of extremely early initiations of ART demonstrated HIV reservoirs of reduced sizes, regardless of treatment having started a few days after infection. Therefore, despite efforts to prevent viral latency with confident virus destruction, the virus persists.



**2.2 Alternative therapeutic strategy for HIV treatment**

In a study by Vocero-Akbani, *et al.* (1999)*,* a new therapeutic strategy was described that induced cellular apoptosis of HIV-1 infected cells, through exploiting HIV protease. The study by Vocero-Akbani *et al*., aimed to develop a new treatment for HIV, due to increasing incidence of drug resistant HIV strains, without targeting the viral replicative machinery. It was described in **2.1.2.2** that HIV protease is an essential enzyme for HIV-1 maturation. Caspase-3 is another protease that plays a key role in apoptosis pathways described in section **2.1.3.3**. The cleavage and subsequent activation of this enzyme triggers downstream events that ultimately results in the induction of apoptosis. Under normal apoptotic conditions, caspase-3 is activated by other caspases, such as caspase-8 (Vocero-Akbani *et al.*, 1999; Sainski *et al.*, 2011). In their strategy Vocero-Akbani, *et al.,* developed a mutant form of caspase-3 that is only cleavable by HIV

protease (**Fig. 2.4**). The mutant form of caspase-3 (TAT-Casp3) is delivered to cells using TAT facilitated protein transduction technology. The study also demonstrates that the delivery of TAT-Casp3 to HIV infected Jurkat T cells can induce apoptosis in these cells.

The modified caspase-3 can be used as a with a 'Trojan horse' approach, in that can it enter cells disguised as a non-threatening protein however, result in apoptosis upon cleavage by HIV protease. This strategy is favorable as the protein remains inactive in uninfected cells, and therefore only eradicates infected cells. It could also be applied to other pathogens encoding specific proteases such as hepatitis C, cytomegalovirus and malaria (Vocero-Akbani *et al.*, 1999).

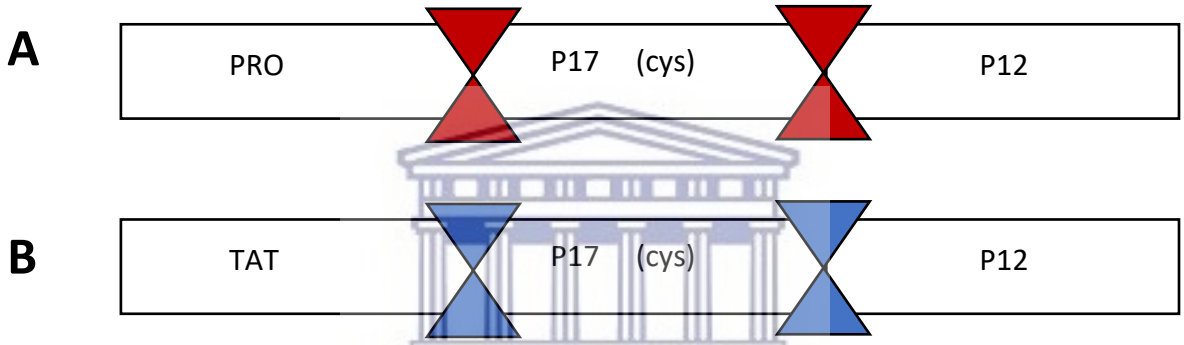


**Fig. 2.4 Modified TAT-Casp3 protein.** (A) Normal cellular caspase-3, (B) Modified caspase-3 protein with substituted HIV gag cleavage sites (blue). To introduce the modified protein into cells, the PRO domain was substituted with a transducing domain (TAT), resulting in a TAT-Casp3 fusion. Adapted from (Vocero-Akbani, *et al*., 1999).



### 2.2.1 Limitations of the modified TAT-Casp3 protein

Vocero-Akbani, *et al.* demonstrated an effective strategy to eradicate HIV-laden cells through exploitation of viral protease, however there are limitations. Untargeted delivery of the modified TAT-Casp3 protein would result in nonspecific accumulation of the therapeutic agent within uninfected cells and could reduce the overall therapeutic index (Zhou and Rossi, 2014; Maso *et al.*, 2019). Off-target concerns would also arise with unintended effects, such as possible carcinogenicity, immunogenicity and mutagenicity (Gauthier and Klok, 2010; Rudmann, 2013; Huang *et al.*, 2019).

In a study called the Human Protein Atlas (HPA) project, the functions of over 20,000 proteins were studied in tissues throughout the body, such as antibodies, enzymes and cancer-related proteins (Uhlen *et al.*, 2010). It was noted that not all those proteins were uniformly expressed in all the tissues of our body. This, therefore demonstrated that overlapping proteins within multiple human tissues exist. Because of this, after drug administration, one can expect to see administered drugs having an effect on proteins in multiple tissues (Uhlen *et al.*, 2010; Kim *et al.*, 2016). In relation to the TAT-Casp3 protein, a consequence of overlapping proteins could demonstrate the inability of the host to distinguish between host proteins and the modified TAT-Casp3 protein, warranting unpredictable adverse effects systemically, or possible drug interactions with conceivable immune activation and systemic inflammation (Rudmann, 2013; Kim *et al.*, 2016).

TAT-Casp3 is essentially a protein therapeutic agent and should this therapeutic be delivered intravenously, it may be neutralized by opsonization (a process that labels foreign particles in the body for ingestion and destruction by phagocytes). This can result in the removal and degradation of TAT-Casp3 via macrophages of the reticuloendothelial system (RES). Therefore opsonization would further contribute to a reduced therapeutic index (Onoue, Yamada and Chan, 2014). With the amalgamation of concerns listed, there could furthermore be unnecessary expenses endured that may affect the overall cost of treatment and warrant excessive cost to the patient. With relatively cheap treatment options already available for HIV/AIDS (i.e. ARVs), one would assume that this treatment option would be unsuccessful, despite its potential.



**2.3 Targeted therapeutics**

Targeted drug delivery systems represent a rapidly growing class of therapeutics, providing more efficient avenues to treat disease with higher specificity and efficacy (Maso *et al.*, 2019). The proposal of targeted drug delivery arose due to unwanted toxicities associated with nonspecific biodistribution of therapeutic agents, particularly in chemotherapeutics (Zhou and Rossi, 2014; Maso *et al.*, 2019; Palve *et al.*, 2020). In fact, the first targeted therapy was Tamoxifen (circa

1970s), an anti-cancer therapy, used to competitively bind to estrogen receptors associated with the progression of breast cancer (Allen, 2002; Yan, Rosen and Arteaga, 2011).

In recent years convenient, molecular platforms have been designed for drug delivery such as antibody-drug conjugates, polymer conjugates, dendrimers, lipid nanocarriers (liposomes and micelles), and polymeric nanoparticles (NPs) (Onoue, Yamada and Chan, 2014; Zhou and Rossi, 2014; Maso *et al.*, 2019). Nanodrug systems, in particular, are gaining popularity as they can offer several pharmacokinetic advantages, such as specific drug delivery, high metabolic stability, high membrane permeability, improved bioavailability, and longer duration of action (Onoue, Yamada and Chan, 2014).

Selective targeting can be achieved by taking advantage of the intrinsic features of these molecular platforms such as size, charge or the presence of a specific polymeric element recognized by cell receptors (Onoue, Yamada and Chan, 2014; Maso *et al.*, 2019). Targeting can also be achieved by direct functionalization of the molecular platform surface with a targeting moiety (e.g. antibody, peptide or aptamer) (Caballero-George, Marin and Briceño, 2013; Onoue, Yamada and Chan, 2014; Zhou and Rossi, 2017; Maso *et al.*, 2019). Each strategy must be developed for a defined disease with site-selective features to increase therapeutic outcome (Maso *et al.*, 2019).



**2.3.1 Aptamers**

Aptamers were first described in 1990 and are commonly referred to as 'chemical antibodies' (Ellington and Szostak, 1990; Tuerk and Gold, 1990; Shigdar *et al.*, 2013). The idea that nucleic acids could function as ligands and modulate the activity of target proteins originated from research on HIV and adenoviruses. It was demonstrated that these viruses encoded small, structured RNA molecules that bind to endogenous proteins and facilitated viral replication. These findings suggested to virologists that nucleic acid molecules, that bind proteins, have the potential to become therapeutic drug agents (Cullen and Greene, 1989; Song, Lee and Ban, 2012; Nimjee *et al.*, 2017). The term aptamer was first coined by Andy Ellington and stems from two words, "aptus" which is Latin for "to fit", and "meros" which is Greek for "part" or "region" (Ellington and Szostak, 1990; Nimjee *et al.*, 2017).

Aptamers are short, synthetic single chain DNA or RNA oligonucleotides (<100 nucleotides) that are generated by a random selection process. They react with high affinity, specificity and selectivity to various ligands, small molecules and proteins (Ellington and Szostak, 1990; Tuerk and Gold, 1990; Nezlin, 2016; Martin, 2018). Aptamers are used in various areas of biological research including immunological studies (Nezlin, 2016; Martin, 2018; Bauer *et al.*, 2019), cancer research (Medley *et al.*, 2011; Shigdar *et al.*, 2013; Ho *et al.*, 2015), targeted drug delivery (Shigdar *et al.*, 2011; Nimjee *et al.*, 2017), diagnostics (Chen and Yang, 2015; Martin, 2018; Bauer *et al.*, 2019), bio-imaging and analytics (Medley *et al.*, 2011; Song, Lee and Ban, 2012; Chen and Yang, 2015; Nezlin, 2016; Bauer *et al.*, 2019). Aptamers are also used as fluorescent, electrochemical, or colorimetric biosensors and in recent years they have received increased attention in the development of lateral flow assays where aptamers are used for antigen recognition (Chen and Yang, 2015; Martin, 2018).

### 2.3.2 Aptamers vs antibodies

Aptamers show several advantages over antibodies (**Table 2.3**), including their small size, low immunogenicity, easy chemical synthesis, adaptive modification, cell-free development and high stability, particularly in higher temperatures (Chen and Yang, 2015; Nezlin, 2016; Martin, 2018; Bauer *et al.*, 2019). Although antibodies are highly specific and bind with strong affinity to target ligands, their production is costly and time-consuming. Furthermore, antibodies are easily denatured under harsh conditions and since they are produced using a biological process, batch to batch variation is often a problem (Chen and Yang, 2015; Nezlin, 2016; Bauer *et al.*, 2019). For disease therapeutics and diagnostic applications, biological compartments are more accessible by aptamers and aptamers have a higher bioavailability than antibodies due to their 20- to 25-fold smaller sizes (Shigdar *et al.*, 2013; Chen and Yang, 2015). Hence, aptamers are fast becoming the desired substitute for all antibody-based applications (Bauer *et al.*, 2019).

**Table 2.3 Comparison of aptamers with antibodies** (Walter, Stahl and Scheper, 2012; Chen and Yang, 2015; Bauer et al., 2019).

| Characteristics | Aptamer | Antibody |
|---|---|---|
| **Applicable target** | Any targets from ions to whole cells, including non-immunogenic or toxic targets | Common proteins or haptens<br>Difficult for non-immunogenic or toxic targets |
| **Selection** | *In vitro* selection under a variety of conditions, with a variety of targets | Limited to physiologic conditions by animal immunization<br>Time-consuming and costly |
| **Production** | Efficient with chemical synthesis with a low cost | Time consuming and costly |
| **Batch Activity** | Uniform | Varied |
| **Stability** | Redox-insensitive. Difficult to aggregate due to lack of large hydrophobic cores. Tolerant of (or able to recover at) pH and temperature. | Redox-sensitive. Easy to aggregate. Sensitive to (or unable to recover at) pH and temperature. |
| **Shelf-life** | Long shelf life. Tolerant of transportation without any special cooling requirements | Short shelf life. Requiring a continuous cold chain |
| **Affinity** | In a low nanomolar to picomolar range | In a low nanomolar to picomolar range |
| **Detection range** | Better | Good |
| **Modification** | Easily modified with other active groups in scale with a low cost | Difficult and expensive to be modified |
| **Reusability** | Good reusability through a reversible conformation switch | Poor reusability due to irreversible conformation changes |
| **Oriented immobilization** | Easy, through various modifications | Difficult, through protein A/G (a recombinant fusion protein) |
| **Sensing design** | All molecular recognition element-based approaches<br>Nucleic acid amplification based ultrasensitive assays<br>Target-induced structural change based homogeneous assays | All molecular recognition element-based approaches |
| ***In vivo* application** | Low immunogenicity and high bioavailability due to a small size | High immunogenicity and low bioavailability due to a large size |

### 2.3.3 SELEX

SELEX (‘‘Systematic Evolution of Ligands by Exponential Enrichment’’) is a novel *in vitro* selection technique used for the generation of high affinity nucleic acid binders (aptamers) to almost any given target (Ellington and Szostak, 1990; Tuerk and Gold, 1990; Schütze *et al.*, 2011). SELEX is cyclic process which starts off with a large DNA library of possible aptamer sequences which is exposed to the target, followed by the separation of the bound and unbound sequences (**Fig. 2.5**). The bound sequences are eluted, amplified, and used as a DNA library in successive rounds (8-25 rounds) of SELEX to identify the sequences with the highest affinity to the target. These sequences are identified by cloning and DNA sequence analysis (Schütze *et al.*, 2011; Chen and Yang, 2015).

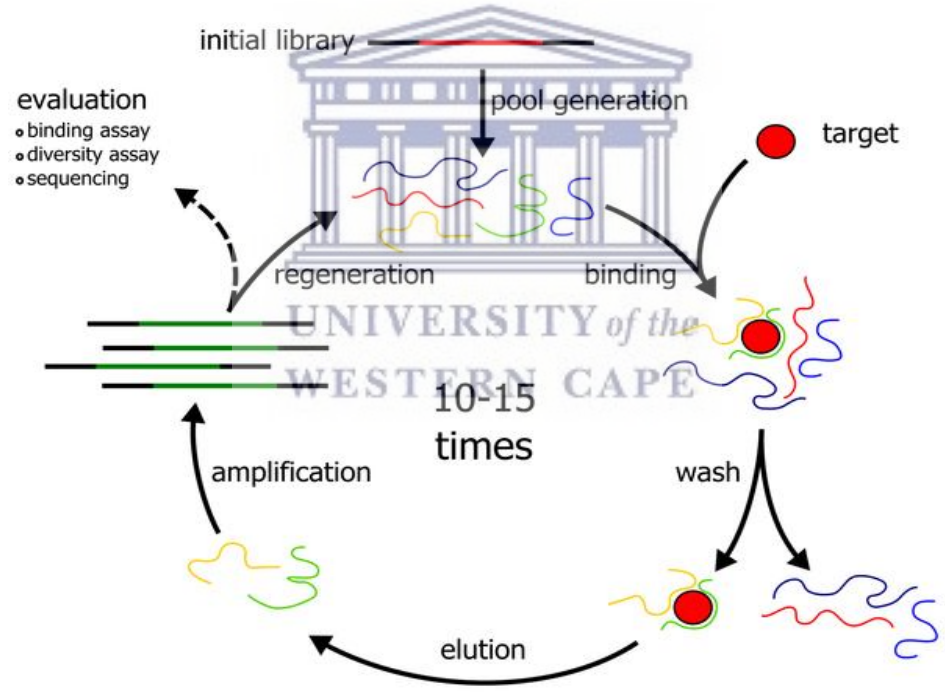


**Fig. 2.5 Aptamer selection process (SELEX)** The process involves (i) incubation of an initial random DNA library with the target of interest to allow target binding (ii) isolation of the DNA that binds to the target (iii) elution of desired DNA from target (iv) DNA amplification by PCR (v) preparation and regeneration of single-stranded DNA for the next-round library and (vi) eventual cloning and sequencing of the enriched library (Schutze, et *al.*, 2011).

There are several approaches available that can efficiently generate aptamers, including cell-based SELEX, purified protein-based SELEX, nitrocellulose (NC) membrane filtration- based SELEX, affinity-based chromatography, capillary electrophoresis-based SELEX, microfluidic-based SELEX, magnetic bead-based SELEX and tailored- SELEX (Martin, 2018).

### 2.4 Applications of nanotechnology in therapeutics

Nanomedicine is defined as the application of nanotechnology in view of making a medical diagnosis or treating or preventing diseases. See **Table 2.4** for some examples of approved nanodrugs. It exploits the improved and often novel physical, chemical and biological properties of materials at the nanometer scale, particularly 1-100 nm (EMEA, 2006; Flühmann *et al.*, 2018). The term nanomedicine encompasses nanopharmaceuticals (therapeutics), nanoimaging agents (diagnostics) and theranostics (a combination of diagnostics and therapeutics) (Ventola, 2017). In comparison to conventional medicines, nanomedicines have shown indispensable characteristics such as longer circulation time, higher binding capacity to target molecules, improved drug efficacy, reduced drug toxicity, increased solubility of drugs, higher accumulation in target tissues, ability to travel across biological barriers (e.g. blood-brain barrier), efficient lymphatic transport and reduced immunogenicity and oxidative stress in tissues (Onoue, Yamada and Chan, 2014; Bobo *et al.*, 2016; Choi and Han, 2017; Ventola, 2017; Flühmann *et al.*, 2018). Another favorable feature of nanomedicines, which has not been efficiently controlled using conventional medicines, is the ability to allow more specific drug targeting and delivery. This, in turn, would warrant greater drug safety, biocompatibility and improvement of *in vivo* pharmacokinetic properties due to a reduction of administration frequency, dose and overall toxicity (Onoue, Yamada and Chan, 2014; Bobo *et al.*, 2016; Choi and Han, 2017; Ventola, 2017).

**Table 2.4 Examples of FDA and EMA approved nanomedicines currently available for clinical application** (Hafner et al., 2014; Choi and Han, 2017; Ventola, 2017; Flühmann et al., 2018)

| Nanomedicine type | Brand (active drug) | Indication |
|---|---|---|
| **Liposomes** | DepoDur® (Morphine) | Pain relief |
| | Marqibo® (Vincristine) | Acute lymphoblastic leukemia |
| **Nanocrystals** | Zyphahera® (Olanzapine) | Schizophrenia |
| | Trevicta®(EU)/Trinza®(US) (Paliperidone palmitate) | Schizophrenia |
| **Polymeric drugs** | Copaxane® (Galtiramer acetate) | Multiple sclerosis |
| | Macugen® (Pegaptanib) | Wet macular degeneration |
| **Micelles** | Estrasorb® (Estradiol) | Menopausal hormone therapy |
| **Iron NPs** | Venofer® (iron sucrose) | Chronic renal failure and iron deficiency anemia |
| | Nanotherm® (iron oxide) | Photothermic cancer therapy |
| **Nanoemulsions** | Norvir® (Cyclosporine) | HIV infection, kidney transplant rejection |
| | Oncaspar® (Pegasparagase) | Acute lymphocytic leukemia |
| **Protein nanocarriers** | Abraxane® (Paclitaxel) | Chemotherapy |
| | Ontak ® (Diptheria toxin) | T-cell lymphoma |

### 2.4.1 Materials used in nanomedicine construction

Nanomaterials are classified as either organic or inorganic, according to their composition e.g. whether they are composed of inorganic metals, organic lipids, proteins or polymers (**Fig. 2.6**).

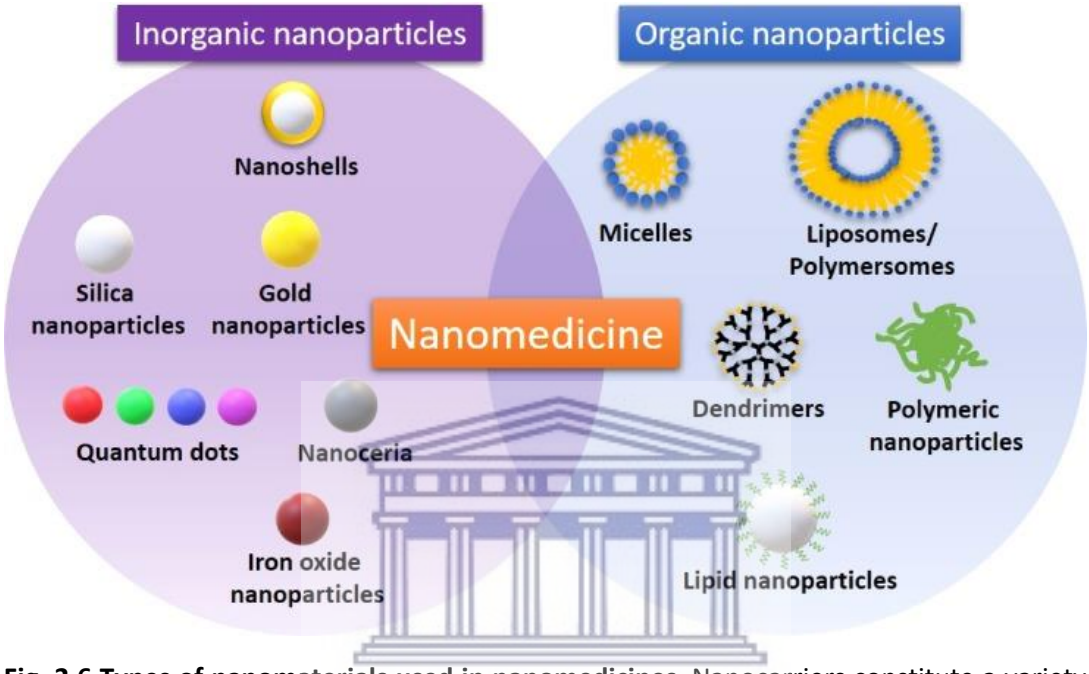


**Fig. 2.6 Types of nanomaterials used in nanomedicines**. Nanocarriers constitute a variety of shapes, distributions, and materials. Typically, they can be differentiated as either inorganic or organic. Inorganic NPs, comprising of metal oxides or pure metals, can be used for drug delivery, however due to their unique properties, they are often exploited for diagnostic imaging and photothermic therapies. Organic NPs are predominantly comprised of lipids or polymers. They are often used for drug delivery, as well as providing a means of creating 'stealth' particles that able to avoid degradation by biological processes (Martinelli, Pucci and Ciofani, 2019).



#### 2.4.1.1 Inorganic materials

Inorganic nanomaterials are composed of metal oxides or pure metals, such as gold, silver, iron and silica, with fullerenes included in this class too (**Table *2.5***) (Paliwal, Babu and Palakurthi, 2014; Lombardo, Kiselev and Caccamo, 2019; Martinelli, Pucci and Ciofani, 2019). Inorganic NPs are used as carriers of therapeutic agents, however they are often also exploited for diagnostic imaging of diseased tissue due to their unique magnetic, plasmonic, conducting, optical and

electrical properties (Giner-Casares *et al.*, 2016; Lombardo, Kiselev and Caccamo, 2019). Although inorganic NPs are usually well tolerated and mostly cleared from the body, their potential toxicities are not well studied thus far (Conde *et al.*, 2014; J. Li *et al.*, 2014; Lombardo, Kiselev and Caccamo, 2019).

Commonly, inorganic NPs have a core-shell structure, typically referred to as a nanoshell. Nanoshells usually consist of an inorganic core (such as gold, quantum dots (QDs), iron oxide and silica), surrounded by a shell area composed mainly of organic polymers or, occasionally, a metal. The shell is important in allowing possible further bioconjugation or simply to stabilize and protect the core from unwanted physiochemical interactions with the biological environment (Conde *et al.*, 2014; J. Li *et al.*, 2014; Lombardo, Kiselev and Caccamo, 2019).

#### 2.4.1.2 Organic materials

To date, a majority of the approved nanomedicines consist of organic materials (Bobo *et al.*, 2016; Choi and Han, 2017; Flühmann *et al.*, 2018). These nanocarriers can take the form of liposomes, polymeric NPs, micelles, dendrimers, solid lipid NPs (SLNs) and protein NP conjugates (**Table 2.6**) (Lombardo, Kiselev and Caccamo, 2019; Martinelli, Pucci and Ciofani, 2019). The types of materials used in organic nanoparticle construction include lipids (e.g. phospholipids, triglycerides, waxes, steroids, fatty acids); proteins (e.g. albumin, silk, collagen, elastin); synthetic polymers (e.g. poly(lactide-co-glycolide) (PLGA), polyethylene glycol (PEG)) and natural polymers, (e.g. chitosan and alginate) (Nasir, Kausar and Younus, 2015; Banik, Fattahi and Brown, 2016; Bobo *et al.*, 2016; Choi and Han, 2017; Jain *et al.*, 2018; Martinelli, Pucci and Ciofani, 2019).

Biodegradable, natural polymers have gained considerable attention in nanomedicine development, due to their biocompatibility, flexibility, safety, low production cost, improved drug loading capacity and good colloidal stability. They also allow a versatile control of both morphology and chemical composition for surface modifications, as well as allowing the incorporation and carrying of both hydrophobic and hydrophilic drugs (Bharti *et al.*, 2015; Banik, Fattahi and Brown, 2016; Adabi *et al.*, 2017; Choi and Han, 2017; Lombardo, Kiselev and Caccamo, 2019; Martinelli, Pucci and Ciofani, 2019; Sorasitthiyanukarn *et al.*, 2019).

**Table 2.5 Types of inorganic NPs including their structure, pros, cons, uses and potential toxicities.**

| Type | Structure | Pros | Cons | Uses | Toxicity | References |
|---|---|---|---|---|---|---|
| **Silica (5nm-2µm)** | Mesoporous (rod, sphere, cube, ellipsoid, film) | High loading capacity<br>Homogenous distribution<br>Good resistance to degradation | Surface groups can cause hemolysis of red blood cells<br>Induces cellular metabolic changes that promote melanoma | Imaging agents<br>Biosensors<br>Drug delivery<br>Thermal energy storage | Biocompatible<br>Size and dose dependent cytotoxicity | (Bharti *et al.*, 2015; Murugadoss *et al.*, 2017; Manzano and Vallet-Regí, 2018; Martinelli, Pucci and Ciofani, 2019) |
| **Gold (10-200nm)** | Rod<br>Spherical<br>Star<br>Cube | Fluorescence modulation (quenching suppression)<br>Unique optical properties (plasmon resonance)<br>High conductivity<br>Catalytic properties | Weak optical signal<br>Long term cytotoxicity | Photothermic therapy<br>Imaging agents<br>Biosensors<br>POC diagnostics | Low toxicity<br>Biocompatible<br>Potential biodegradability<br><br>Gold nanorods:<br>Nephrotoxicity<br>Cardiac toxicity<br>Neural toxicity | (Alkilany *et al.*, 2009; Balasubramanian *et al.*, 2010; Brown *et al.*, 2010; Abdelhalim and Jarrar, 2011; Siddiqi *et al.*, 2012; Abadeer and Murphy, 2016; Cordeiro *et al.*, 2016; Lombardo, Kiselev and Caccamo, 2019) |
| **Iron NPs (20-30nm)** | Spherical<br>Rod<br>Cube<br>Husk<br>Flower<br>Cylinder | Good magnetic properties<br>Catalytic properties<br>Semiconductors | Can cross placenta barrier and cause fetal abnormalities | Iron-deficiency anemia<br>Imaging agents<br>Cell sorting<br>Biosensors<br>Photothermic therapy | Biodegradable<br>Nontoxic<br><br>Free Fe iron accumulation:<br>Oxidative stress<br>Inflammation | (Hanini *et al.*, 2011; Noori *et al.*, 2011; Hafner *et al.*, 2014; J. Li *et al.*, 2014; Lombardo, Kiselev and Caccamo, 2019; Martinelli, Pucci and Ciofani, 2019; Mulder *et al.*, 2019) |
| **Quantum dots (1-50nm)** | Spherical | Cost effective<br>Easy synthesis<br>High photostability<br>Semiconductors<br>Unique optical properties | Incomplete biological elimination<br>Possible quantum yield deterioration | Imaging agents | Nephrotoxicity<br>Hepatic damage<br>Reproductive toxicity<br>Vascular thrombosis<br>Carcinogenic genotoxicity | (Choi *et al.*, 2008; Geys *et al.*, 2008; Fitzpatrick *et al.*, 2009; Chu *et al.*, 2010; Sadaf *et al.*, 2012; J. Li *et al.*, 2014; Patra *et al.*, 2018) |

**Table 2.6 Types of organic NPs including their structure, pros, cons and uses.**

| Type | Structure | Pros | Cons | Uses | References |
|---|---|---|---|---|---|
| **Liposomes (30nm-several µm)** | Spherical, self-assembling, phospholipid bilayer surrounding an aqueous core | High stability<br>Increases therapeutic index of a drug<br>Minimizes drug side effects | Low encapsulation efficiency<br>Rapid drug leakage<br>High production costs | Drug delivery | (Akbarzadeh *et al.*, 2013; Bobo *et al.*, 2016; Katuwavila *et al.*, 2016; Flühmann *et al.*, 2018; Li *et al.*, 2019; Martinelli, Pucci and Ciofani, 2019) |
| **Polymeric NPs (10nm-several µm)** | Spherical analogues of liposomes made from block co-polymers | Can uniquely design co-polymers<br>Enhanced stability, elasticity, and mechanical resistance compared to liposomes<br>Encapsulates hydrophilic drugs | Reduced permeability compared to liposomes | Drug delivery<br>Encapsulate imaging agents | (Le Meins, Sandre and Lecommandoux, 2011; Zhang and Zhang, 2017; Iyisan and Landfester, 2019; Lombardo, Kiselev and Caccamo, 2019; Martinelli, Pucci and Ciofani, 2019) |
| **Micelles (<200nm)** | Spherical, self-assembling monolayer accumulates | Ability to encapsulate hydrophobic drugs<br>Drug solubility is increased by 10- to 500-fold | Possible instability in blood with drug leakage | Drug delivery (Estrasorb®; Genexol-PM®)<br>Encapsulate imaging agents (QDs) | (Doshi and Mitragotri, 2009; Yin, 2013; J. Li *et al.*, 2014; Bobo *et al.*, 2016; Ventola, 2017; Hanafy, El-Kemary and Leporatti, 2018; Lombardo, Kiselev and Caccamo, 2019) |
| **Dendrimers (1-100nm)** | Tree-like, with an atom core and terminal functional groups | Well-defined Monodispersed<br>Highly controllable architecture<br>Enhanced solubility and stability<br>Controlled release<br>Modifiable surface<br>Entraps hydrophobic and hydrophilic drugs | Immunogenicity, blood toxicity, and cytotoxicity attributed to their size and surface charge (positive) | Drug delivery | (Thiagarajan, Greish and Ghandehari, 2013; Kesharwani, Jain and Jain, 2014; Onoue, Yamada and Chan, 2014; Choi and Han, 2017; Lombardo, Kiselev and Caccamo, 2019; Martinelli, Pucci and Ciofani, 2019) |
| **Solid lipid NPs (100-400nm)** | Solid crystalline spheres | High drug stability<br>Prolonged release<br>Low cost<br>Easy scale-up | Limited drug loading capacity | Drug delivery | (Onoue, Yamada and Chan, 2014; Gordillo-Galeano and Mora-Huertas, 2018; Martinelli, Pucci and Ciofani, 2019) |
| **Protein NP conjugates (<200nm)** | Irregular | Cost-effective<br>Easy synthesisProteins reduce drug toxicity and allow better cellular uptake<br>High encapsulation efficiency (>75%) | Low yield<br>Low mechanical strength<br>Fast degradation | Drug delivery<br>Vaccinations | (Wernig *et al.*, 2008; Zhang *et al.*, 2008; Hafner *et al.*, 2014; Ventola, 2017; Jain *et al.*, 2018) |

In particular, the use of natural polymers, such as chitosan and alginate, as drug delivery systems has piqued the interest of researchers and are widely used in the pharmaceutical industry (Brezaniova *et al.*, 2017). These polymers are abundant in nature, nontoxic, excreted well by the body, and display low immunogenicity – a common issue with nanoscale particles (Douglas, Piccirillo and Tabrizian, 2006; Ibrahim *et al.*, 2013; Kumar *et al.*, 2015; Sorasitthiyanukarn *et al.*, 2019).

### 2.4.2 Chitosan

Chitosan (CS) is a cationic, linear nitrogenous polysaccharide/polymer composed of repeating units of glucosamine and *N*-acetyl-D-glucosamine, that is linked by (1→4) β-glycosidic bonds. This hydrophilic polymer is obtained from the deacetylation of amino acetyl from chitin, one of the most abundant and renewable polymers on earth (Berezina, 2016; Morin-Crini *et al.*, 2019).

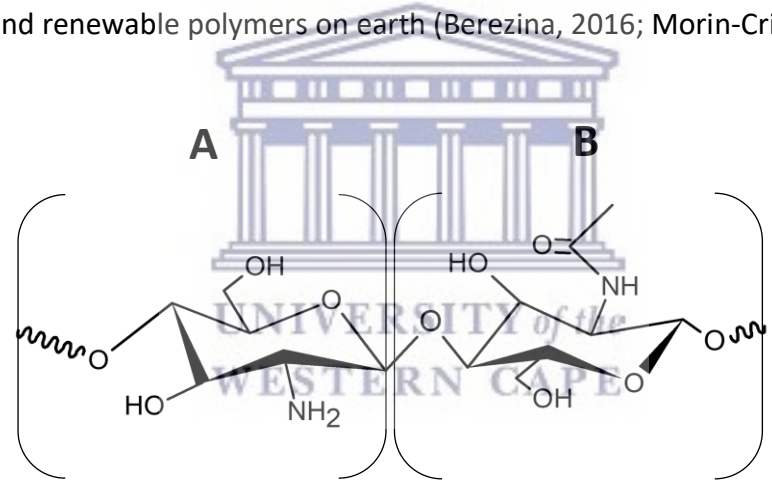


**Fig. 2.7 Structure of chitosan.** Composed of repeating units of (A) glucosamine, and (B) N-acetyl-D-glucosamine, linked together by (1→4) β-glycosidic bonds. Chitosan is a commonly used polymer in nanomedicine research due to its biodegradability, biocompatibility, low cost, and safety (Berezina, 2016)

CS is biodegradable and biocompatible in nature and has many applications across varying fields such as antimicrobial films in the food industry (Friedman and Juneja, 2010; Noorbakhsh-Soltani, Zerafat and Sabbaghi, 2018); water purification filters at water plants (Yu *et al.*, 2013; Thakur and Voicu, 2016); pesticide delivery platforms in the agricultural industry (Kashyap, Xiang and Heiden,

2015; Campos *et al.*, 2018); and as drug/vaccines carriers for biomedical purposes (Brezaniova *et al.*, 2017; Mohammed *et al.*, 2017; Ahsan *et al.*, 2018). Within the pharmaceutical field, CS has exhibited desirable properties including controlled drug release, mucoadhesive properties, transfection enhancing properties, permeation enhancing properties and ability to form NPs under mild conditions (Bagre, Jain and Jain, 2013; Katuwavila *et al.*, 2016; Brezaniova *et al.*, 2017; Morin-Crini *et al.*, 2019). The pKa of the CS amine group is approximately 6.5, and therefore CS is soluble and protonated in an acidic solution. This would enable CS to electrostatically interact with negatively charged molecules as well as polymers to form polyelectrolyte complexes (Rivera *et al.*, 2015; Brezaniova *et al.*, 2017; Mohammed *et al.*, 2017).

### 2.4.3 Alginate

Alginate (Alg) is a hydrophilic, anionic copolymer, composed of β- D-mannuronic acid and α-L-guluronic acid residues, bonded by (1→4) linkages. Alg is obtained from natural sources such as marine brown algae and bacteria (Katuwavila *et al.*, 2016; Brezaniova *et al.*, 2017; Sorasitthiyanukarn *et al.*, 2019). Alg possesses several attributes which make it a suitable polymer for use in NP formulation including biodegradability, biocompatibility, bio-adhesivity (Luo and Wang, 2014; Brezaniova *et al.*, 2017). Alg has many applications and has been used for wound healing purposes, paper and paint manufacturing, thickeners in food and beverage manufacturing and in fabric printing (Liu *et al.*, 2019; Rubio-Elizalde *et al.*, 2019).



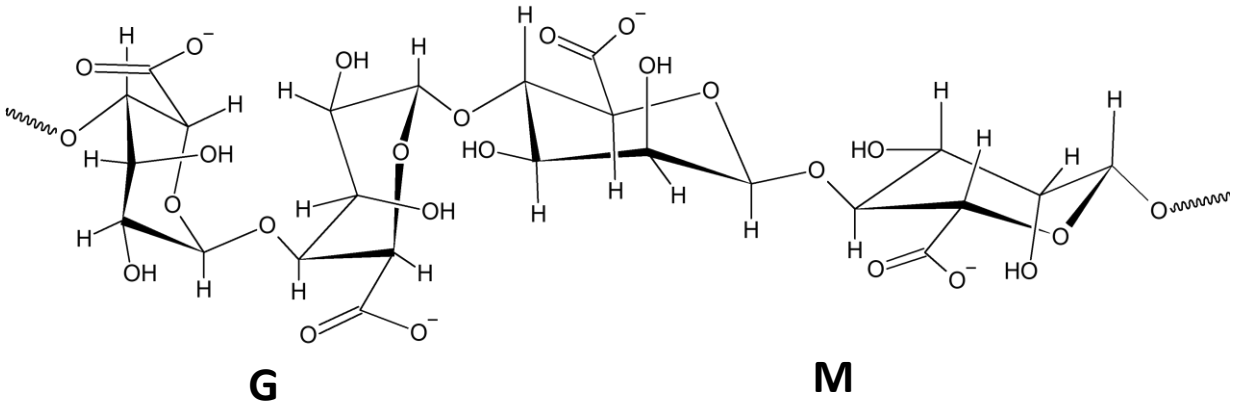


**Fig. 2.8 Structure of alginate.** Alginate consists of repeating units of α-L-guluronic acid (G) and β-D-mannuronic acid (M), connected by (1→4) linkages.

The pKa of the G and M residues of Alg are 3.4 and 3.6, respectively (Dube, 2011; Lopes *et al.*, 2016). When the pH > pKa, the carboxyl groups of the Alg are in the preferable ionized form ($COO^-$). On the other hand, when pH < pKa, these groups are in a non-ionized form (COOH or COONa) (Dube, 2011; Lima *et al.*, 2018; da Silva Fernandes *et al.*, 2019). Owing to the presence of carboxyl ($-COO^-$) groups, this anionic polymer can electrostatically interact with cationic polymers, like CS, to form gels. Alg can also electrostatically interact and cross-link with divalent cations such as $Ca^{2+}$, $Sr^{2+}$, $Zn^{2+}$ or $Ba^{2+}$, of which $Ca^{2+}$ is the most investigated. This method is known as ionotropic gelation (Luo and Wang, 2014; Kumar *et al.*, 2015; Sorasitthiyanukarn *et al.*, 2018).

The formation of NPs using the anionic Alg and cationic CS results in strong electrostatic interactions between the carboxyl groups of the Alg and the amino group of the CS (Luo and Wang, 2014; Kumar *et al.*, 2015; Brezaniova *et al.*, 2017). This suggests that, together with the properties mentioned above, that these polymers will be suitable for the preparation of NPs to be used in this study.

# Chapter 3 STUDY RATIONALE, HYPOTHESIS, AIMS AND OBJECTIVES

## 3.1 Study rationale

Having claimed over 32 million lives thus far, HIV/AIDS continues to be a major public health issue. Without a vaccine, effect HIV disease management through effective diagnosis, treatment, and further prevention is crucial. Major strides have been made in developing HIV treatment regimens, in particular HAART, enabling people to lead a long and healthy life. Although ARVs have successfully helped 54% of infected people globally in suppressing the virus, there are shortfalls. Failure of patients to adhere to life-long treatment schedules, the development of drug resistant strains and the presence of persistent viral reservoirs diminish the possibility of completely eradicating the disease. It is therefore vital to explore other avenues of HIV treatment that can contribute to the eradication of the virus.

Nanotechnology has revolutionized disease diagnostics and treatment. This is due to the unique physicochemical properties of nanomaterials and that enable biological interactions that differ from conventional agents. Additionally, the application of targeted, nanodrug therapeutics holds several pharmacokinetic advantages such as targeted drug delivery, high metabolic stability, high membrane permeability, improved bioavailability, and extended duration of drug action. Aptamers, specifically, possess many desirable benefits for targeted drug delivery such as low production cost, easy reproducibility, high stability, and large targeting range. Coupled with the desirable properties of the biodegradable polymers, CS and Alg, for nanoparticle synthesis, an attractive platform for targeted drug delivery can be achieved.

As described in section **2.2**, the study by Vocero-Akbani, *et al.* provides an effective alternative therapeutic strategy for HIV/AIDS treatment through caspase-3 induced apoptosis of HIV-1 infected cells. However, the therapeutic strategy described by Vocero-Akbani, *et al.* is not selective for HIV infected cells. The caspase-3 therpeutic drug described by Vocero-Akbani, *et al.* is also not encapsulted in a drug carrier and depending on the rout of administration, it is likely to be degraded before it reaches its intended target, making the therapy ineffective. The current study intends to utilize the advancements of nanotechnology to develop an alternative delivery

system for the caspase-3 HIV/AIDS therapeutic described by Vocero-Akbani, *et al.* Ultimately the aim is to produce Alg-CS NPs that can be used as delivery systems for the targeted delivery of the caspase-3 therapeutic protein. Since HIV mostly infects CD4 positive cells, the Alg-CS NPs will be surface functionalized with a CD4 specific DNA aptamer to facilitate the targeted delivery of caspase-3 to CD4 expressing cells. The NPs will be fluorescently labelled to be tracked and imaged by confocal microscopy. The aim of this research is to perform a preliminary study to demonstrate that protein loaded Alg-CS that are functionalized with a CD4 specific aptamer can be delivered or targeted to CD4 expressing cells. Green fluorescent protein (GFP) will be used since this protein can be easily detected with various imaging technologies. This study can provide the steppingstone for future studies to further develop the treatment described in **2.2**, whereby the caspase-3 can be encapsulated into the polymeric NPs and delivered specifically to CD4 expressing cells. This could promote the selective induction of apoptosis of HIV-1 laden CD4 positive cells only, revolutionizing personal medicine and possibly contributing to HIV eradication.

### 3.1.1 Hypothesis for this study

CS-Alg NPs containing a CD4 specific DNA aptamer are specifically taken up or bind to cells that express the CD4 receptor.



### 3.1.2 Aims of this study

To show that Alg-CS NPs that are functionalized with a CD4 specific DNA aptamer and loaded with GFP are taken up by or binds to THP-1 monocytes.

### 3.1.3 Objectives of this study

- To recombinantly express and purify GFP from bacterial cultures.
- To synthesize and characterize Alg-CS NPs.
- To synthesize and characterize Alg-CS NPs loaded with GFP and to functionalize the surface of Alg-CS NPs with a CD4 specific DNA aptamer.
- Study the uptake or binding of GFP loaded Alg-CS NPs that are functionalized with a CD4 aptamer by THP-1 monocytes .

# Chapter 4 METHODS AND MATERIALS

This chapter describes the synthesis and characterization of polymeric NPs that will be used as a carrier for a green fluorescent protein (GFP). This combination of protein and nanoparticle was conjugated to a DNA aptamer that would later be used to determine whether positive attachment to a CD4+ expressing cell-line transpired. The relevance of this study denotes the ever-evolving need for improved drug delivery systems for diseases plaguing the globe, particularly HIV/AIDS. Characterization techniques include dynamic light scattering (DLS), electrophoretic light scattering (ELS), scanning electron microscopy (SEM). Imaging was conducted using an image-based cytometer and a confocal microscope.

**Table 4.1 Reagents or materials and their suppliers**

| Reagent/Material | Supplier |
|---|---|
| 40 % Acrylamide Bis Solution (37:5:1)<br>Bromophenol blue | Bio-Rad (USA) |
| 1-Ethyl-3-(3-dimethylaminopropyl)-carbodiimide (EDC)<br>Absolute Ethanol<br>Acetic Acid<br>Chitosan (low molecular weight)<br>Calcium chloride<br>Glutathione-Agarose coated beads<br>Glutathione-Agarose column<br>Isopropyl β-d-1-thiogalactopyranoside (IPTG)<br>Lysis buffer<br>Phosphate buffered saline (PBS) pH 7.4 ready mix<br>Sodium Acetate<br>Sodium Alginate<br>Sodium Azide<br>Sodium Chloride<br>N-Hydroxysuccinimide (NHS)<br>N,N,N',N'-tetramethylethane-1,2-diamine (TEMED) | Sigma-Aldrich Co. (USA) |
| Ammonium persulfate<br>Tris(hydroxymethyl)aminomethane<br>Paraformaldehyde powder | Merck (Pty) Ltd (SA) |
| Amphotericin B | Thermo Scientific (USA) |

| | |
|---|---|
| BL21 Star™ (DE3) One Shot® *E.coli* cells<br>PageRuler™ Unstained Protein Ladder (#26614)<br>Roswell Park Memorial<br>Institute Medium (RPMI 1640) with L-glutamine<br>PreScission™ Protease<br>Smart2pure™ Distilled Water<br>UltraPure™ Distilled Water (nuclease-free water)<br>NucBlue™ Live ReadyProbes™ Reagent | |
| CD4-Aptamer:<br>/5AmMC6/ATCCAGAGTGACGCAGCACCACCACC<br>GTACAATTCGCTTTCTTTTTTCATTACC<br>TACTCTGGC | Whitehead Scientific (Pty) Ltd (SA) |

**Table 4.2 Equipment and their suppliers**

| **Equipment** | **Supplier** |
|---|---|
| Heraeus™ Biofuge13™ Centrifuge<br>Sorvall™ LYNX 6000 Centrifuge | Thermo Scientific (USA) |
| Malvern Zetasizer Nano ZS | Malvern (UK) |
| MS-H Pro Hot Plate Magnetic Stirrer | DLab (CHN) |
| Scientech™ Ultrasonic Cleaner | ScienTech (USA) |
| Vortemp™ 56 | Labnet (USA) |
| Benchmark BenchMixer™ | Benchmark Scientific (USA) |
| Adventurer® Analytical Balance | OHAUS (USA) |
| RET Basic Hot Plate Magnetic Stirrer<br>High-power T50 digital ULTRA-TURRAX® Homogeniser | IKA Laboratory (GER) |
| Eppendorf Thermomixer™ C | Merck (Pty) Ltd (SA) |
| Stuart® Block Heater | Stuart Scientific (UK) |
| Qubit® 2.0 Fluorometer<br>Tali™ Image-Based Cytometer | Invitrogen by Life Technologies (USA) |
| Synergy™ MX Microplate Reader | BioTek (USA) |
| Carl Zeiss Confocal LSM 780 Elyra PS1 | Carl Zeiss AG (GER) |
| Sonopuls Ultrasonic Homogeniser | Bandelin (GER) |

**Table 4.3 Buffers and their compositions**

| **Buffer** | **Composition** |
|---|---|
| Sample Buffer | 0.5M Tris-HCl (pH 6.8), glycerol (100%), 0.2ml of β mercaptoethanol, 0.01g of bromophenol blue and 0.2g of SDS |

| | |
|---|---|
| 1 X SDS Running Buffer | 3.03g Tris (250mM), 14.4g Glycine (1.92M) and 10g SDS (1%) |
| Coomassie Stain Solution | 50% ethanol, 10% acetic acid and 0.25% brilliant blue R-250 |
| Cleavage Buffer | PreScission™ Protease, 10 mM Tris-HCl (pH 8), 150 mM NaCl, 0.5 mM EDTA |
| De-stain Solution | 20% methanol, 10% acetic acid and 70% $dH_2O$ |
| Equilibration Buffer | 0.05 M Tris and 0.15M NaCl in $dH_2O$ (pH 8) |
| Elution Buffer | 0.05 M Tris and 0.15M NaCl (pH 8) and 0.01M reduced glutathione in $dH_2O$ |
| Lysis Buffer | 20 mM Tris-HCl, 2 Mm EDTA, 1% Triton X-100 containing 1 mg/mL lysozyme (pH 8) |
| Regeneration Buffer 1 (pH 8.5) | 0.5 M NaCl, 0.1% SDS and 0.1 M Tris (pH 8) in $dH_2O$ |
| Regeneration Buffer 2 (pH 4.5) | 0.5 M NaCl, 0.1% SDS and 0.1 M sodium acetate in $dH_2O$ |

### 4.1 Nanoparticle synthesis

Alginate and chitosan-based nanoparticles (Alg-CS NPs) were synthesized following two methods, namely polyelectrolyte complexation (Alg-CS) (Dube, 2011) and ionotropic gelation (Alg-Ca-CS) (Kumar *et al.*, 2015). The synthesis of the Alg-CS NPs was performed using the high-power T50 digital ULTRA-TURRAX® homogenizer (IKA Laboratory, Germany). The synthesis of the Alg-Ca-CS NPs was performed using the Sonopuls Ultrasonic Homogeniser (Bandelin, Germany).



#### 4.1.1 High-speed homogenization

High-speed homogenization is a mechanical process where immiscible liquids are converted through shear stress and high pressure through a very narrow chamber, into a homogenous emulsion. The higher the amount of energy applied during the homogenization process, the smaller the particle size (Pis, Islam and Hasan, 2017).

#### 4.1.2 Ultrasonic homogenization

Ultrasonic homogenization, also known as sonication, is the act of applying ultrasonic frequency (>20kHz) sound energy to a liquid media that agitates particles in a sample, for various purposes such as cell lysis or nanoparticle synthesis. The sonicator amplifies the energy through a metal

probe that moves in time with the vibration which is then transmitted into the liquid media (Peshkovsky, Peshkovsky and Bystryak, 2013).

#### 4.1.2.1 Synthesis of Alginate-Chitosan (Alg-CS) NPs by polyelectrolyte complexation

The method to synthesize the Alg-CS NPs was adapted from Dube, 2011. Alg was dissolved in $dH_20$ at a concentration of 0.1% w/v and the pH adjusted to 5.3 using 0.1M HCl. A solution of CS (0.1% w/v in 0.175% v/v acetic acid) was prepared and left stirring overnight and its pH was also adjusted to 5.3, using 0.1M NaOH. Both CS and Alg solutions were filtered through a 0.45µm syringe filter to remove any undissolved particulates before NP preparation. Furthermore, dilutions from the 0.1% Alg solution (0.02%, 0.04% and 0.06% w/v) were made up in $dH_2O$ and pH was adjusted accordingly. The same was done from the 0.1% CS solution at the same concentrations. The varying concentrations of the Alg solution were added drop-wise to varying concentrations of the CS solution under homogenization at 10 000rpm, for 2 minutes, at ambient temperature at a ratio of 2:1 (v/v), respectively. The NPs were recovered by further filtering the colloidal suspension through a 45µm syringe filter and characterized using the Malvern Zetasizer Nano ZS. The particles were unable to form a pellet after centrifugation; therefore, washes were unable to be performed (n=3). Following this, the NPs were kept at -80˚C overnight and then freeze-dried for 48hrs producing a fine, white powder.



#### 4.1.2.2 Synthesis of Alginate-Calcium-Chitosan (Alg-Ca-CS) NPs by ionotropic gelation

The method used to synthesize Alg-Ca-CS NPs was adapted from Kumar, et al. 2015. An Alg-Ca pre-gel was formed and thereafter crosslinked with CS to form hydrogel NPs. Solutions of Alg (0.06% w/v) and CS (0.1% w/v in 1% acetic acid) were separately prepared in $dH_20$ and stored overnight at 4. Thereafter, the Alg and CS solutions were filtered through a 0.45 µM filter, and their pH adjusted to 4.9 and 4.6, respectively. These pH values were chosen as CS and Alg are weak polyelectrolytes, meaning their degree of dissociation depends on the solution pH. When the pH of Alg is below its pKa value (3.4-4.4), a decrease in the ionization degree is observed, leading to insufficient surface charge. When the pH is above the pKa, deprotonation of the carboxyl groups occurs (COOH to $COO^-$ conversion). Likewise, CS is only soluble in acidic solution, where the pH value is significantly lower than its pKa (6.2-7.0). At an acidic pH, the amine groups

of CS are protonated, resulting in a sufficient surface charge ($NH_2$ to $NH_3^+$), vital for polyionic complex formation with the anionic Alg (Shafie and Fayek, 2013; Rodriguez-Lorenzo *et al.*, 2014; Rivera *et al.*, 2015; Brezaniova *et al.*, 2017; Mohammed *et al.*, 2017). The CS solution was made up to varying concentrations (0.02%, 0.05%, 0.08% w/v in $dH_20$) and the Alg solution was kept at a constant concentration (0.06%). A $CaCl_2$ solution was prepared in $dH_20$ at varying concentrations (0.04%, 0.067%, 0.1% w/v) and the pH adjusted to 4.8. The $CaCl_2$ solution (2 ml) was added dropwise to the Alg solution (10 ml) under probe sonication (50% power) for 1 minute and allowed to stand on ice for 30s; to form the pre-gel. Following this, the CS solution (1.5 ml) was added dropwise to the pre-gel solution under probe sonication (50% power) for 1 min and allowed to stand on ice for 30s. This resulted in a colloidal suspension. The NPs were recovered by centrifugation at 7,568rcf for 30 min, washed twice and stored at 4°C in $dH_20$ (pH 5) for subsequent characterization using Malvern Zetasizer Nano ZS (Malvern Instruments Limited, UK) (n=3). Following this, the NPs were kept at -80°C overnight and then freeze-dried for 48hrs producing a fine, white powder for further analysis. The weight of the powder was recorded as 20mg.

#### 4.1.2.3 Formulation of Green Fluorescent Protein (GFP)-loaded Alg-Ca-CS NPs (GFP-NPs)



It was found that ionotropic gelation produced more desirable results (smaller size and better polydispersity index (PDI)), therefore this method was adopted going forward for the encapsulation of GFP described in section and to conjugate the GFP-NPs to a CD4 specific described in section **4.4**. The synthesis of Alg-Ca-CS described in section **4.1.2.2** was modified to incorporate the GFP into the NPs. Varying concentrations of GFP (0.37%, 1.12%, 2.23% v/v) were added to the Alg solution and bath sonicated, at high frequency, for 2 min. The rest of the method was then followed as described in **4.1.2.2** to form GFP-NPs. The GFP-NPs were recovered by centrifugation at 17,568rcf for 30 min, washed twice with $dH_20$ at pH 5 and the NPs were kept at -80°C overnight and then freeze-dried for 48hrs producing a fine, white powder.

### 4.2 Characterization of the NPs

The size, polydispersity index (PDI) and the zeta potential (ZP), of the NPs, was determined, in triplicate readings, using the Malvern Zetasizer Nano ZS (Malvern Instruments Limited, UK). The diameter and morphology of the freeze-dried NPs (empty and GFP loaded) was further characterized by the Zeiss MERLIN Field Emission Scanning Electron Microscope at the Electron Microbeam Unit of Stellenbosch University's Central Analytical Facility.

#### 4.2.1 Dynamic Light Scattering (DLS) and Electrophoretic Light Scattering (ELS)

DLS is used to measure particle and molecule size. ELS is used to measure ZP. DLS is a technique wherein the size of the particles is determined based on the diffusion of particles in solution, moving under Brownian motion (Bhattacharjee, 2016). ELS is a technique wherein an electric field is applied to a suspension of particles which then move with a velocity that is measured using a laser. This measured velocity enables the calculation of electrophoretic mobility, which is translated into ZP (Berg *et al.*, 2009). Additionally, a surface ZP accessory uses tracer particles to measure electro-osmosis close to a sample surface to calculate the ZP of the surface (Berg *et al.*, 2009). Particle size (nm), size distribution (PDI), and ZP of NPs were determined (at 25°C) using a Malvern Zetasizer Nano ZS equipped with a He–Ne ion laser (λ =633 nm) at a scattering angle of 90°. The measurements (n=3) were performed in a folded capillary cell. Triplicate samples were analyzed for both size and ZP, and the average ± standard deviation of the values was calculated.



#### 4.2.2 Scanning Electron Microscope (SEM) morphology assessment

Prior to imaging, the freeze-dried NP samples were mounted on aluminum stubs with double sided carbon tape. The samples were then coated with a thin (~10 nm thick) layer of gold, using a Leica EM ACE200 Gold Sputter Coater. This is done to make the sample surface electrically conductive to avoid electron build-up on the sample surface which can cause electron charge. Beam conditions during the quantitative analysis and backscattered electron image analysis on a Zeiss MERLIN were 20 kV accelerating voltage, 16nA probe current, with a working distance of 9.5 mm and a beam current of 11nA. The counting time was 10 seconds live-time. Gold was automatically excluded from analysis due to sample coating with gold.

### 4.2.3 Determination of the stability of the Alg-Ca-CS NPs in cell culture media

The stability of the empty Alg-Ca-CS NPs was determined in Roswell Park Memorial Institute Medium 1640 (RPMI 1640) cell culture medium. The washed Alg-Ca-CS NP suspension was centrifuged at 17,568rcf for 30 min at 4 °C and the NPs were re-dispersed in 1 ml RPMI medium. The NP suspensions were incubated at 37°C and samples were analyzed at 0, 20, 30, 45 and 60 min. The size and PDI were measured using DLS with a Zetasizer Nano ZS at 25°C (Malvern Instruments, UK). Triplicate samples were analyzed and the average ± standard deviation of the values at each time point were calculated.

## 4.3 Expression and purification of green fluorescent protein (GFP)

A PGEX-6P-2/GST-GFP protein expression construct was previously constructed by Mr Darius Martin (Department of Biotechnology, University of the Western Cape) and kindly donated for the expression of GST-GFP protein in this current study. This DNA construct was designed to recombinantly express GFP protein that is tagged with Glutathione-S-transferase (GST) protein. DNA plasmids for the recombinant expression of proteins are often designed such that the protein of interest is tagged with GST to facilitate the purification of the GST tagged fusion proteins on chromatography resins coupled with glutathione (Harper and Speicher, 2011).



#### 4.3.1.1 Transformation of the BL21 Star™ (DE3) One Shot® Cells

The expression of the GST-GFP was performed in BL21 Star™ (DE3) One Shot® Cells *E. coli* strain (Thermo Scientific, USA). The pGEX-6P-2/GST-GFP plasmid DNA (5µg) was placed in a sterile 1.5 ml centrifuge tube. Competent BL21 Star™ (DE3) One Shot® *E. coli* cells (50µl) wee gently mixed with the plasmid DNA and the cells were heat-shocked in a 42 °C water bath for 30 seconds. Thereafter the tube was immediately transferred onto ice. After 5 min on ice, 950 µl Lysogeny Broth (LB), pre-warmed to 37 °C, was added to the heat shocked cells. The culture was plated onto Lysogeny agar (LA) plates (containing 100 µg/mL ampicillin), which were incubated overnight at 37 °C. The following day a single bacterial colony was removed from the plate and used for the large-scale expression of GST-GFP.

#### 4.3.1.2 Expression and purification of the GST-GFP protein

A single colony (from section **4.3.1.1**) from the LA plate was used to inoculate 10ml LB containing 100 µg/mL ampicillin. The culture was incubated overnight at 37 °C, while shaking at 300 rpm. The following day this starter culture was used to inoculate 100ml LB containing 100 µg/mL ampicillin. The cultures were cultured at 25 °C, while shaking at 300 rpm, until the optical density (measured at 600 nm) of the sample reached a density between 0.5 and 0.8, after which 1 mM Isopropyl β-d-1-thiogalactopyranoside (IPTG) was added to one of the cultures to induce the expression of GST-GFP in the bacterial cells. Several positive colonies were cultured in 10 mL LB containing 100 µg/mL ampicillin overnight at. The cultures were diluted 1:10 with fresh LB and grown for 1 h at 25 °C, shaking at 300 rpm, until the sample reached an optical density (measured at 600 nm) between 0.5 and 0.8. The cultures were then split into two 5 mL cultures and 1 mM Isopropyl β- d-1-thiogalactopyranoside (IPTG) was added to one of the cultures. IPTG triggers transcription of genes controlled by the lactose operator and is therefore used to induce the expression of specific proteins in bacterial cells that are transformed with DNA plasmids (Malakar *et al.*, 2014). Therefore, the pGEX-6P-2/GST-GFP DNA plasmid was designed such that the expression of the GST-GFP was under the control of the lactose operator. The cells were further cultured at 25 °C for 16 hours with shaking at 300 rpm. The following day, the culture was centrifuged at 4300 x *g* for 5 min to harvest the bacterial cells.



GST-GFP was purified by gravity column chromatography using a glutathione-agarose column. The bacterial cell pellet was solubilized in Lysis buffer (10 ml) and incubated at 25 °C for 10 min. The cell suspension was centrifuged for 20 min at 4300 *xg*. The supernatant containing the bacterial proteins was passed over a 10 ml glutathione-agarose column that was pre-equilibrated with Equilibrium Buffer. The GST-GFP bind to the glutathione-agarose column, while all the other proteins pass through the column. The column was washed with three column volumes of Equilibration buffer to remove proteins that are non-specifically bound to the column.

The GST-GFP was subjected to on-column cleavage using PreScission™ Protease (Thermo Scientific, USA). This enzyme separates GST and GFP by cleaving in between the GST and GFP. The column was washed with three column volumes of Cleavage buffer. One column volume (5

ml) of Cleavage Buffer containing 80 units of PreScission™ Protease was added to the column, which was incubated at 4 °C for 4 h. After 4 h, the elute containing the purified GFP was collected and dialyzed for 16 h in PBS. GST remained bound to the column. The elute containing GFP was stored at -20 °C for further use.

#### 4.3.1.3 Analysis of GFP by SDS-PAGE

The eluted GFP was analyzed on a 12% sodium dodecyl sulphate polyacrylamide gel electrophoresis (SDS-PAGE). The recipe for the 12% gel is described in **Table 4.4**. The samples obtained in **4.3.1.2** were mixed in a 1:1 ratio with 2X SDS sample buffer. The samples were boiled for 5 min at 95°C, centrifuged for 2 min at 4300 *xg* and the supernatant (10 µl) was resolved on a 12% SDS-PAGE.

**Table 4.4 Reaction mixture for SDS-PAGE**

| Reagents | 12% Separating gel | 5% Stacking gel |
|---|---|---|
| 0.5M Tris-HCl pH 6.8 | - | 0.63ml |
| 1.5M Tris-HCl, pH 8.8 | 2.5ml | - |
| 10 % SDS | 0.1ml | 0.050ml |
| Acrylamide/Bis (40 %) | 3ml | 0.4ml |
| 10 % Ammonium persulfate (APS) | 0.2ml | 0.050l |
| TEMED | 0.02ml | 0.01ml |
| Water | 4.3ml | 3.65ml |



The gel was electrophoresed with a PageRuler™ Unstained Protein Ladder (#26614) (Thermo Scientific, USA) in 1X SDS running buffer at 90 V for 30 min and thereafter the voltage was adjusted to 120V and continued to run for 60 to 90 min. The gel was stained with Coomassie Stain Solution for 30 min and de-stained in De-stain Solution overnight. The gel was visualized, and the images were captured using the Canon CanoScan LiDE 120 electronic scanner. The remaining samples were stored at -20 °C.

#### 4.3.1.4 Analysis of GFP fluorescence

Fluorescence intensity detection is a measurement of the light emitted by a fluorophore upon excitation by light at a specific wavelength. The fluorescent sample is excited by a light source

and filtered at a specific wavelength by either a filter or a monochromator. The excited sample emits light and fluoresces within microseconds upon excitation. The emitted light is filtered, collected, and measured by a detector, usually a Photo Multiplier Tube (PMT), and quantified in Relative Fluorescence Units (RFU) (Yu *et al.*, 2012).

The green fluorescence of the purified GFP sample collected in **4.3.1.2** was analyzed and confirmed with the Synergy™ MX Microplate Reader (BioTek, USA). Aliquots (20 µl) of the purified GFP were read in a Corning® 96 well black bottom plate in triplicate. Initially the excitation and emission range was set between 350 – 600 nm with the Synergy™ MX Microplate Reader. This was done to accommodate for any deviation from the expected excitation and emission spectra of the purified GFP. The expected excitation and emission of GFP is 488 nm and 510 nm, respectively (Nolles *et al.*, 2015; Cranfill *et al.*, 2016). The excitation and emission spectra were generated in a line chart and the green fluorescence of the GFP was confirmed.

#### 4.3.1.5 Quantification of GFP stock concentration

Since GFP is a fluorescent protein, it was not possible to quantify it using the Invitrogen Qubit Fluorometer that was available. The concentration of the GFP protein was thus determined by image analysis using ImageJ software. The concentration of a non-fluorescent standard protein was quantified using the Invitrogen Qubit Fluorometer. Known concentrations of this standard protein as well as specific volumes of GFP was electrophoresed on a 12% SDS-PAGE (**Fig. 4.1** (A)). The gel was stained and imaged as described in section **4.3.1.3**. The intensity of the protein bands produced for the standard protein was quantified using ImageJ Software (v1.52v available from Softonic.com) used to construct a standard curve which displayed band intensity (pixels) vs protein concentration (µg/ml) (**Fig. 4.2**). This standard curve was used to determine the concentration of the GFP sample based on the intensity of the GFP band formed on the gel. The final concentration of the GFP (808.91 µg/ml) was determined from the standard curve that had been generated.

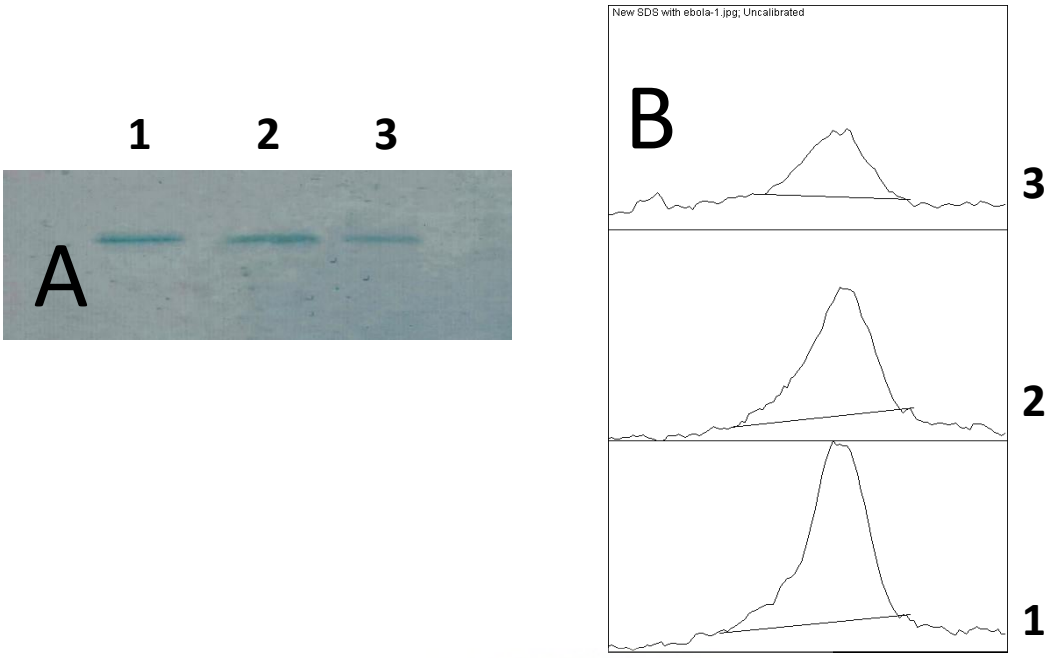


**Figure 4.1 (A) SDS-PAGE of 2-fold dilution of standard protein of known concentration; (B) Corresponding band intensities of the 2-fold dilution (1-3) of the standard protein using ImageJ software.** Initially a 2-fold dilution of the stock standard protein [434µg/ml] was conducted and prepared with SDS-PAGE from 1-3. The band intensities were then interpreted into peaks (1-3) with 1 being the starting concentration of 434µg/ml. These peaks were quantified into pixels (px) and used to generate a standard curve with the corresponding known concentrations from the two-fold dilution.



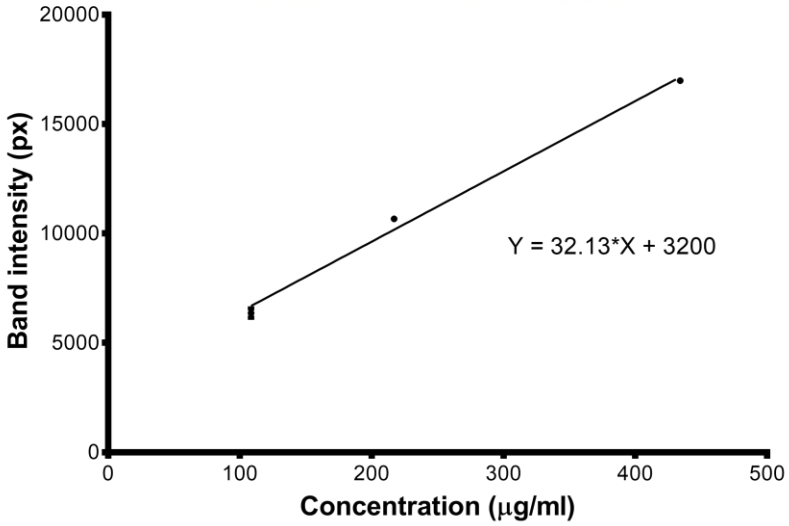


**Figure 4.2 Standard curve illustrating the relationship between pixel intensity and protein concentration -** band intensities of the standard protein were examined and quantified by ImageJ software and plotted against the corresponding concentrations (mean ± s.d., n=3, $r^2$=0.9928 )

### 4.4 Conjugation of amine-modified aptamer to the GFP loaded Alg-Ca-CS NPs (Apt-NPs)

Apt is a CD4 specific aptamer that was previously described with high specificity to the targeted CD4+ cells (Zhu *et al.*, 2012). Apt was acquired from Whitehead Scientific (Pty) Ltd (SA). The 5' end of the DNA aptamer was modified to include an amine end group ($NH^{3+}$) that could be covalently conjugated to the free carboxyl groups ($COO^-$) of the Alg on the surface of the GFP-NPs. The method described by Medley, *et al*., 2011 was used. A 250 µL aliquot of the GFP loaded NPs was washed three times with 250 µL nuclease free water. Initially 2 mg of EDC (8 mg/mL) and 5 mg of NHS (20mg/mL) were added to the NPs and incubated for 15 min at ambient temperature. A 10 µL (4 µM) aliquot of a 100 µM solution of Apt was added to the NP sample. The preparation was left at constant mixing for 2 h at ambient temperature, finishing with two final washes with nuclease free water. The Apt-NPs were stored at 4 °C before use. The Apt-NPs were characterized using Malvern Zetasizer Nano-ZS90 (Malvern, UK) (n=3) to confirm successful conjugation.

### 4.5 Statistical analysis

Statistical analysis was performed by one-way analysis of variance (ANOVA). ANOVA is used to determine whether there are statistically significant differences between the means of independent groups of data. Statistical evaluation was performed using the GraphPad Prism 6.0 software. Results are expressed as a mean ± standard deviation for every experiment. Values of $p < 0.05$ were considered statistically significant.



### 4.6 Cell culture of THP-1 cell line

#### 4.6.1.1 Cell culture

The THP-1 cell lines used in this study were obtained from the Department of Biotechnology at the University of the Western Cape. This cell line was used due to the ability of the cells to express CD4 receptors on the cell surface (Konopka and Düzgüneş, 2002; Lodge *et al.*, 2017). The respective cell lines were regularly sub-cultured in upright $25cm^2$ culture flasks at 37°C, in a 5% $CO_2$ humidified incubator, in RPMI 1640 media, enriched with 2 mM L-glutamine. The media was supplemented with 10% heat-inactivated FBS, 1% penicillin-streptomycin and 0.2% 25 µg/ml

amphotericin B. This media mix will be referred to as complete media from hereon. The complete media was changed and replaced with fresh complete media every three days. The procedures were performed in a Biological Safety Cabinet (laminar flow) using aseptic techniques and all the reagents to be used were sprayed with 70% ethanol before introducing them into the cabinet.

#### 4.6.1.2 Cell harvesting

Cells were harvested when they reached ≥70% confluency (± 7 days after seeding). As these cell lines grows predominantly in suspension, no enzyme dislodgment was required. Before harvesting, the flask was gently tapped and then scraped to encourage detachment, to dislodge any cells that may have adhered. The media containing the cells was aspirated from the flask using a 10 ml serological pipette and placed into a 15 ml conical tube. The cells were then centrifuged at 3000 rpm for 5 min. The supernatant was removed and placed into a waste beaker and the cell pellet was then re-suspended in 1 ml complete media. A cell count was performed, and an appropriate number of cells were sub-cultured.

#### 4.6.1.3 Cell counting

A cell count was performed using trypan blue exclusion assay and the Invitrogen™ Tali™ Image-Based Cytometer (Invitrogen by Life Technologies, USA). Briefly, a 10 µl aliquot of the cell suspension was mixed with 10 µl of 0.4% trypan blue dye reagent. The cells were mixed by pipetting and 20 µl of the cell-dye mixture was then loaded into an Invitrogen™ Tali Slide. Following a cell count, the data readout was given in total cells/ml of which 1.81 x $10^6$ cells/ml were sub-cultured in individual petri dishes (60 mm x 15 mm) at a concentration of 1 x $10^5$ cells/ml for 24 h, at 37 °C, in a 5% $CO_2$ humidified incubator.

### 4.7 Aptamer binding study

The THP-1 cells harvested in **4.6** were treated for 1 h, in duplicate, with Apt-NPs (synthesized as described in section **4.4**) to determine whether there is positive attachment and uptake of the fluorescent Apt-NPs into the cells. Initially the treated cells were analyzed using the Tali™ Image-Based Cytometer (Invitrogen by Life Technologies, USA) and thereafter were further analyzed

with the Carl Zeiss Confocal LSM 780 Elyra PS1 microscope (Carl Zeiss AG, Germany) at the Central Analytical Facility (Stellenbosch University, South Africa).

### 4.7.1 Image-based cytometry

Image-based cytometry utilizes the same cell-by-cell analysis principle as flow cytometry, except the samples are scanned in a visual plain, instead of in suspension. While conventional flow cytometry measures forward scattered light to estimate the relative cell size, microscopy yields the exact cell size through its bright field image (Han *et al.*, 2016). In addition to a bright-field channel, the Tali™ Image-Based Cytometer features two fluorescence channels (green and red), enabling it to count green- and red-fluorescent stained cells, which is then displayed in a graphical report (ThermoFisher, 2020).

### 4.7.2 Confocal microscopy

Confocal microscopes work on the principle of point excitation in the specimen and point detection of the resulting fluorescent signal. This microscopy enables the reconstruction of three-dimensional structures through multiple two-dimensional images at different depths in a sample (known as optical sectioning) (Pawley, 2006). Upon analysis the prepared samples were positioned within the stage incubator of the Carl Zeiss Confocal LSM 780 Elyra PS1 microscope and then excited by the Argon multiline laser (25mW) at 488 nm. The images obtained were captured through the ZEN 2011 imaging software (Carl Zeiss, Germany).

#### 4.7.2.1 Analysis of CD4-Aptamer binding of the Apt-NPs

The Apt-NPs conjugates described in section **4.4** were collected by centrifugation at 9000 rpm for 30 min and the pellet was resuspended in 250 µl RPMI 1640 medium. The sub-cultured cells within the petri dishes described in section **4.6.1.3** were treated with the Apt-NPs and incubated for 1 h at 37 °C, in a 5% $CO_2$ humidified incubator. The following controls were included: untreated cells; cells treated with empty NPs; cells treated with GFP NPs (no aptamer). The respective incubated cells were centrifuged at 3000 rpm for 5 min. The supernatant was discarded into a waste beaker and the cell pellet was re-suspended in 500 µl of PBS. The cells were further centrifuged at 3000 rpm for 5 min. The supernatant was carefully discarded into a

waste beaker and a wash with PBS was repeated. The cell pellet was then re-suspended in 200 µl of PBS and analyzed using the Tali™ Image-Based Cytometer. Moreover, the cells were examined by fluorescent microscopy. Shortly after incubation with the NPs, NucBlue™ fluorescent nucleus dye (Thermo Scientific, USA) was added to the samples. The cells were washed as above and were then fixed with 4% paraformaldehyde and analyzed with the Carl Zeiss Confocal LSM 780 Elyra S1 microscope.

# Chapter 5 RESULTS AND DISCUSSION

NPs consisting of the polymers Alg and CS were prepared using two different methods, namely the polyelectrolyte complexation (Alg-CS NPs), and ionotropic gelation (Alg-Ca-CS NPs) methods. The freshly prepared nanodispersions were evaluated for particle size, PDI and ZP using DLS and particle morphology using scanning electron microscopy (SEM). The Alg-Ca-CS NPs were loaded with GFP to produce GFP-NPs which were surface functionalized with a CD4 specific DNA aptamer to produce Apt-NPs. The Apt-NPs were used to study the uptake/binding of these NPs in THP-1 monocytes by image-based cytometry and confocal microscopy.

## 5.1 Synthesis and characterization of empty Alg-CS NPs

### 5.1.1 Characterization of Alg-CS NPs synthesized by polyelectrolyte complexation

Particles composed Alg and CS (without $Ca^{2+}$) were synthesized using the polyelectrolyte complexation method by varying Alg-CS mass ratios (see **Table 5.1**). NPs are formed when the anionic Alg forms cross-linked complexes with the cationic CS (Luo and Wang, 2014; Aluani *et al.*, 2017).



**Table 5.1** Characteristics of Alg-CS NPs in terms of concentration ratio, mass ratio, average particle size, PDI and ZP (mean ± s.d., n=3, size $p<0.0001$; PDI $p<0.0001$; ZP $p<0.0001$)

| % w/v Alg | % w/v CS | Mass Ratio (Alg-CS) | Size (nm) | PDI | ZP (mV) |
|---|---|---|---|---|---|
| 0.06 | 0.02 | 1:0.167 | 2035.25 ± 305.79 | 0.170 ± 0.063 | -43.23 ± 1.01 |
| 0.04 | 0.02 | 1:0.250 | 1206.75 ± 222.89 | 0.552 ± 0.132 | -38.87 ± 0.74 |
| 0.06 | 0.04 | 1:0.333 | 1565.25 ± 174.40 | 0.424 ± 0.046 | -33.93 ±1.20 |
| 0.02 | 0.02 | 1:0.500 (a) | 1468.50 ± 138.25 | 0.343 ± 0.052 | -36.15 ± 1.23 |
| 0.04 | 0.04 | 1:0.500 (b) | 1670.50 ± 133.28 | 0.332 ± 0.107 | -33.77 ± 1.19 |
| 0.06 | 0.06 | 1:0.500 (c) | 9555.7 ± 1705.5 | 1.000 ± 0 | -36.50 ± 0.50 |
| 0.04 | 0.06 | 1:0.750 | 1808.00 ± 131.41 | 0.503 ± 0.206 | -29.43 ± 0.06 |
| 0.02 | 0.04 | 1:1 | 1518.67 ± 174.91 | 0.794 ± 0.047 | 7.69 ± 2.76 |
| 0.02 | 0.06 | 1:1.500 | 878.00 ± 44.86 | 1.000 ± 0 | 26.53 ± 1.19 |

The ratios were established according to varying concentrations of the Alg (0.02%, 0.04%, 0.06% w/v) that were added dropwise to varying concentrations of CS (0.02%, 0.04%, 0.06% w/v). This was all done at fixed Alg and CS volumes of 5ml and 2.5ml, respectively.

The opalescent suspensions of NPs were optimized based on the particle size, polydispersity index (PDI) and zeta potentials (ZP). The DLS results from this method demonstrate trends in the particle size, PDI and ZP as a function of the Alg-CS mass ratio (**Table 5.1**, **Fig. 5.1**, and **Fig. 5.2**). According to the % w/v, there was no apparent trend in size as the mass ratio changes however, the results show large particle sizes, mostly in the micron range. A distinctive increase in PDI can be noted from mass ratio 1:0.500 (b) onwards. It was noted that the Alg-CS mass ratio of 1:0.500 (c) formed NPs that were several microns in size (9555.7 $\pm$ 1705.5 nm) and had a PDI of 1. Due to these unfavorable findings, this formulation was not pursued further.

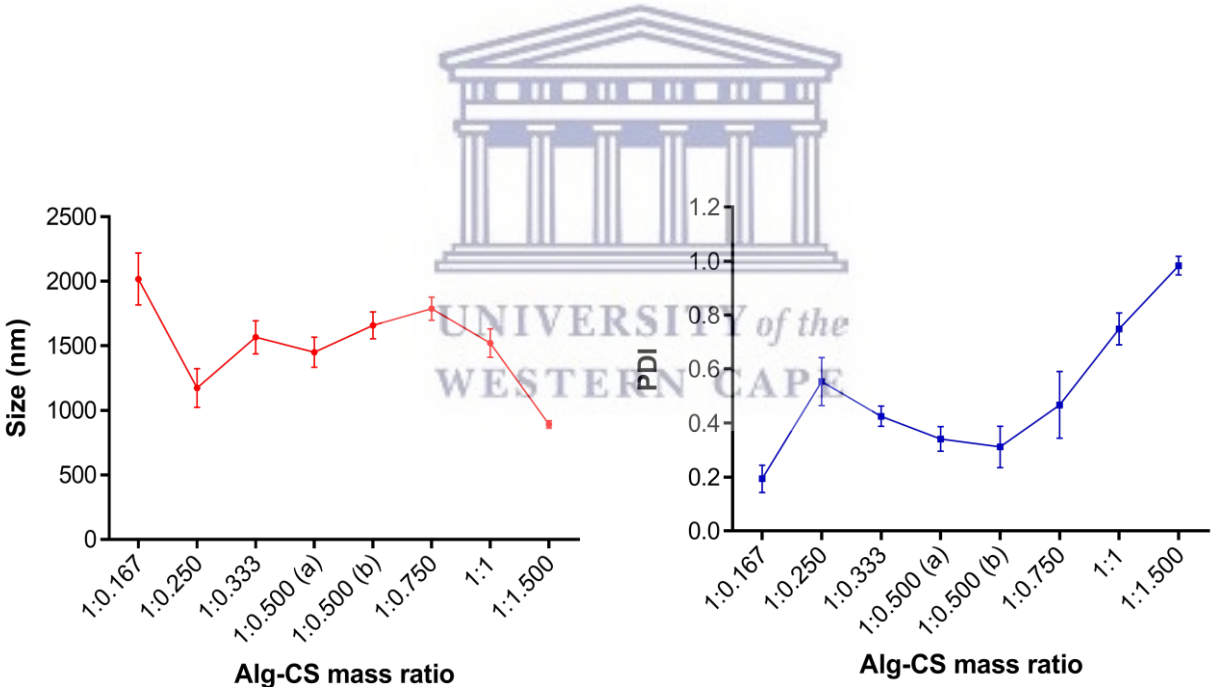


**Fig. 5.1** Trends in size distribution (red) and PDI (blue) of Alg-CS NPs with varying Alg-CS mass ratios (mean ± s.d., n=3, size $p<0.0001$ and PDI $p<0.0001$)

A PDI value <0.5 is ideal for colloidal suspension as it portrays that the suspension has homogenous size distribution. The PDI can range from 0 – 1 with an upper limit of 1 representing an overly broad particle size distribution (Dube, 2011; Kumar *et al.*, 2015). Upon analysis, four readings depicted the optimum PDI at mass ratios 1:0.500 (a) (0.343 $\pm$ 0.052), 1:0.500 (b) (0.332 $\pm$ 0.107), 1:0.167 (0.170 $\pm$ 0.063), and 1:0.333 (0.424 $\pm$ 0.046).

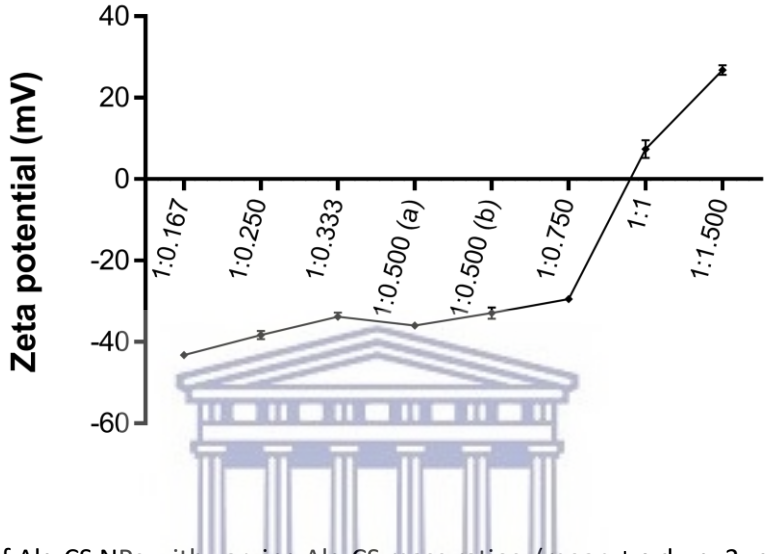


**Fig. 5.2** Trends in ZP of Alg-CS NPs with varying Alg-CS mass ratios (mean ± s.d., n=3, p<0.0001)



The overall ZP readings were considered stable, except for a mass ratio of 1:1 (7.69 $\pm$ 2.76 mV). This is due to the fact that ZP readings of ±20-30 mV are assumed to be good for suspension, as these charges result in repulsion of the formed particles, thereby preventing aggregation (Kumar *et al.*, 2015; Haji *et al.*, 2018; Sorasitthiyanukarn *et al.*, 2018; Rinaudo and Goycoolea, 2019). The NPs in this study portrayed a strongly negative ZP, owing to the presence of more carboxyl ($COO^-$) groups on the NP surface. The carboxyl groups present on Alg form complexes with the amino ($NH_3^+$) groups of CS, but due to the higher concentration of Alg, there remains free carboxyl groups, rendering the ZP negative (Bagre, Jain and Jain, 2013; Kumar *et al.*, 2015; Sorasitthiyanukarn *et al.*, 2019).

Statistical analysis demonstrated p<0.0001 for Alg-CS particle size. This indicated that the mean sizes of the particle were statistically different across the range of Alg-CS mass ratios (1:0.167 to

1:1.500) (ANOVA). Statistical analysis of the PDI demonstrated $p<0.0001$, indicating a statistical difference in the PDI means across the range of Alg-CS mass ratios (1:0.167 to 1:1.500) (ANOVA). Statistical analysis of the ZP also demonstrated $p<0.0001$, indicating that the means were statistically different across the range of Alg-CS mass ratios (1:0.167 to 1:1.500) (ANOVA). This can be attributed to the noteworthy changes in the size, PDI and ZP associated with the change in the concentration of the polymers. The trend in PDI showed that upon increasing the concentration of CS, the PDI would follow a general increase too, from mass ratio 1:0.500 (b) to 1:1.500. From this, it can be noted that the higher CS concentration would result in a higher PDI and therefore, a less homogenous suspension. The sizes were considerably larger with the higher concentrations of polymer. This can be expected as higher polymer concentration is accompanied by a higher amount of polymer forming the core of the particle resulting in larger particle formation (Morsi *et al.*, 2015).

The results obtained in this study denoted the exploration of another synthesis method, therefore ionotropic gelation was investigated.

### 5.1.2 Characterization of Alg-Ca-CS NPs synthesized by ionotropic gelation

The opalescent suspensions of the Alg-Ca-CS NPs, prepared by the ionotropic gelation method, were comprised of varying Alg-Ca-CS mass ratios. The ionotropic gelation method incorporates calcium chloride into the synthesis method to form NPs with an Alg-Ca pre-gel core. The addition of CS to the solution forms polyelectrolyte complexes with the pre-gel core, which stabilizes the core into separate sponge-like NPs with a resultant core/shell structure (Bagre, Jain and Jain, 2013; Kumar *et al.*, 2015; Morsi *et al.*, 2015). For this study, the Alg concentration was kept constant at 0.06% w/v. This was done because, the results described in section **5.1.1** indicated that the NPs synthesized at an Alg-CS mass ratio of 1:0.167, were stable (-43.23 $\pm$ 1.01 mV) and homogenous (0.170 $\pm$ 0.063) in suspension. The mass ratios were calculated with the inclusion of calcium chloride.

**Table 5.2** Characteristics of Alg-Ca-CS NPs in terms of mass ratio, average particle size, PDI and ZP. Formulation codes were assigned to the varying mass ratios of Alg, Ca and CS (mean ± s.d., n=3, size $p<0.0001$; PDI $p<0.0001$; ZP $p<0.0001$).

| Mass Ratio Code | (% w/v) Alg | CS | Ca | Mass Ratio (Alg-Ca-CS) | Size (nm) | PDI | ZP (mV) |
|---|---|---|---|---|---|---|---|
| $A_1$ | 0.06 | 0.02 | 0.04 | 1:0.133:0.050 | 275.62 $\pm$ 14.40 | 0.308 $\pm$ 0.05 | -26.94 $\pm$ 2.67 |
| $A_2$ | 0.06 | 0.02 | 0.067 | 1:0.223:0.050 | 312.57 $\pm$ 10.38 | 0.319 $\pm$ 0.07 | -24.46 $\pm$ 1.83 |
| $A_3$ | 0.06 | 0.02 | 0.1 | 1:0.333:0.050 | 557.50 $\pm$ 12.95 | 0.359 $\pm$ 0.03 | -22.60 $\pm$ 0.85 |
| $B_1$ | 0.06 | 0.05 | 0.04 | 1:0.133:0.125 | 337.79 $\pm$ 7.99 | 0.230 $\pm$ 0.04 | -31.87 $\pm$ 1.62 |
| $B_2$ | 0.06 | 0.05 | 0.067 | 1:0.223:0.125 | 411.69 $\pm$ 19.04 | 0.235 $\pm$ 0.03 | -26.54 $\pm$ 0.58 |
| $B_3$ | 0.06 | 0.05 | 0.1 | 1:0.333:0.125 | 529.82 $\pm$ 24.97 | 0.312 $\pm$ 0.05 | -24.27 $\pm$ 0.57 |
| $C_1$ | 0.06 | 0.08 | 0.04 | 1:0.133:0.200 | 393.29 $\pm$ 9.88 | 0.228 $\pm$ 0.03 | -28.87 $\pm$ 1.16 |
| $C_2$ | 0.06 | 0.08 | 0.067 | 1:0.223:0.200 | 475.01 $\pm$ 22.57 | 0.228 $\pm$ 0.02 | -26.51 $\pm$ 1.22 |
| $C_3$ | 0.06 | 0.08 | 0.1 | 1:0.333:0.200 | 607.09 $\pm$ 45.09 | 0.308 $\pm$ 0.05 | -23.46 $\pm$ 3.46 |

DLS results revealed the optimum formulation was $A_1$ at an Alg-Ca-CS mass ratio of 1:0.133:0.050 (**Table 5.2** and **Fig. 5.3**). The NP size was 275.62 ± 14.40 nm, with a PDI of 0.308 ± 0.05, and a ZP of -26.94 ± 2.67 mV. The size of $A_1$ was the final determinant for the optimum ratio, despite obtaining desirable PDI and ZP readings for the rest of the formulas. From these results it is apparent that this method, with the inclusion of calcium chloride, produces NPs of a suitable size that are homogenous and stable in suspension, whereas in the absence of calcium chloride, microparticles were formed. For example, at an Alg-CS mass ratio of 1:0.250, particles of sizes 1206.75 ± 222.89 nm were obtained however, with the inclusion of calcium chloride at a similar Alg-Ca-CS mass ratio ($C_1$-$C_3$), NPs with sizes between 393 nm and 610 nm were formed.

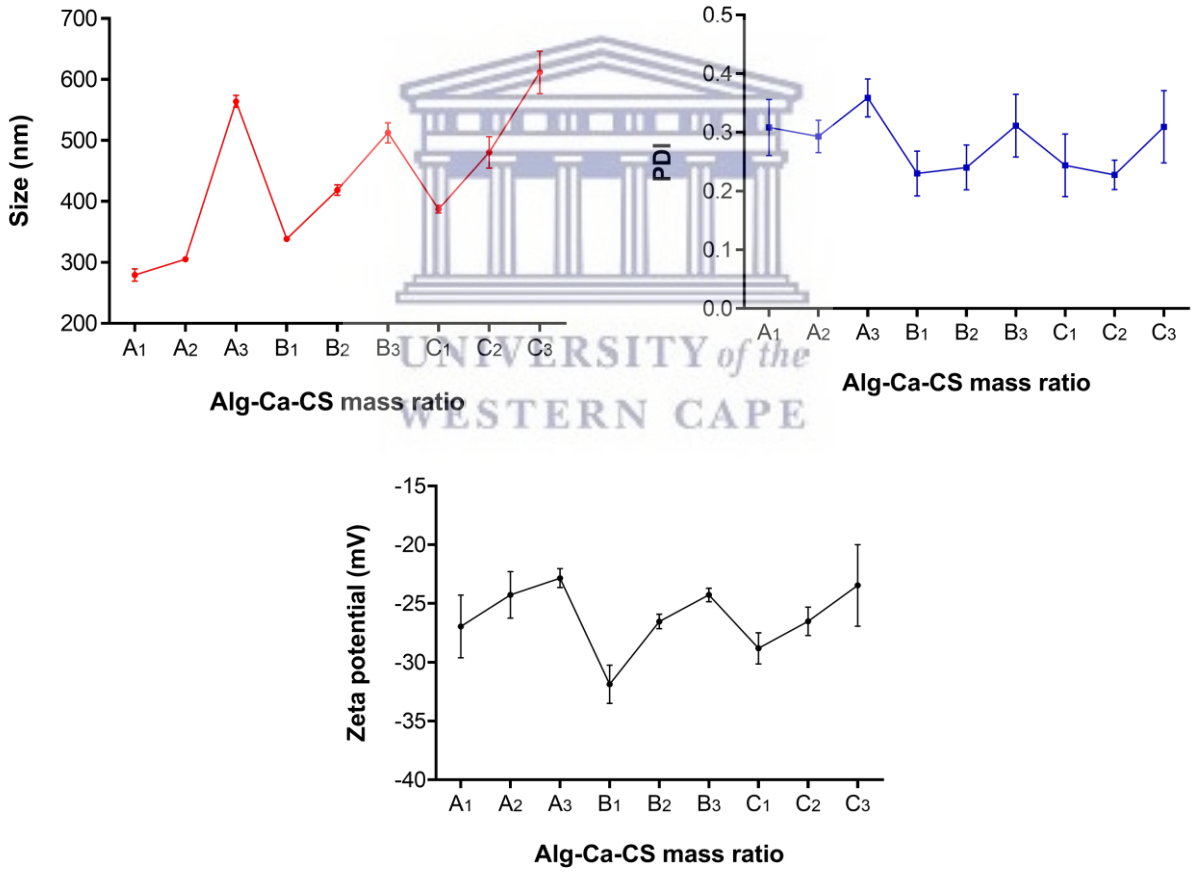




**Fig. 5.3** Trends in size distribution (red), PDI (blue) and ZP (black) of Alg-Ca-CS NPs with varying Alg-Ca-CS mass ratios (mean ± s.d., n=3, size p<0.0001; PDI p<0.0001; ZP p<0.0001)

The PDI for these ratios also improved from 0.552 $\pm$ 0.132 (Alg-CS mass ratio 1:0.250) to between 0.228 and 0.308 ($C_1$ -$C_3$). This would suggest that the inclusion of calcium chloride into the synthesis method promoted a homogenous size distribution in suspension.

Statistical analysis demonstrated $p<0.0001$ for Alg-Ca-CS particle size. This indicated that the mean particle size of the NPs were statistically different across the range of Alg-Ca-CS mass ratios ($A_1$ to $C_3$) (ANOVA). Statistical analysis of the PDI demonstrated $p<0.0001$, indicating a statistical difference in the PDI means across the range of Alg-CS mass ratios ($A_1$ to $C_3$) (ANOVA). Statistical analysis of the ZP also demonstrated $p<0.0001$, indicating that the means were statistically different across the range of Alg-CS mass ratios ($A_1$ to $C_3$) (ANOVA). The statistical significance amongst the size, PDI and ZP can be attributed to the noteworthy changes associated with the change in the concentration of the calcium chloride and the polymers.

Due to the incorporation of $Ca^{2+}$ ions the NP size is considerably smaller for this method when compared to polyelectrolyte complexation. The most likely explanation could be credited to the formation of the pre-gel phase between the $Ca^{2+}$ ions and Alg, allowing the formation of NPs with an increased compact structure (Morsi *et al.*, 2015). There appears to be a general trend in size increase with the higher calcium chloride concentrations, possibly attributed to the increase in core size associated with the presence of more $Ca^{2+}$ ions. This has been observed in previous studies, whereby the increase of calcium chloride concentration resulted in larger particle sizes. These studies suggest that the bulk of the NP matrix is composed of $Ca^{2+}$, thereby signifying larger particles (Shafie and Fayek, 2013; Morsi *et al.*, 2015). Previous literature also describes the ability of free $Ca^{2+}$ ions to bind to any free $COO^-$ groups on the surface of the NPs, reducing the overall NP charge, weakening the strength of interparticle repulsions, allowing for an increase in particle collisions and consequently resulting in increased average particle sizes (Zhu *et al.*, 2014; Son, Vavra and Forbes, 2015; Miao *et al.*, 2016; Haji *et al.*, 2018). Previous literature also explains the impact CS has NP size in relation to its molecular weight.

The concentration of CS appeared to have no effect on the size of the NPs during synthesis when compared to the apparent trend Ca created. This is suggested to be due to the molecular weight of the CS. High molecular weight CS has a longer chain structure with more $NH_3^+$ end groups

which allows increased bonding to occur between the polymers. This has shown to increase NP size by increasing the hydrodynamic diameter on the surface of the NP (Loquercio *et al.*, 2015; Yu, Nguyen and Hadinoto, 2018; Song *et al.*, 2020; Villegas-Peralta *et al.*, 2020). For this study, low molecular weight CS was utilized which therefore, resulted in smaller particle sizes due to less $NH_3^+$ end groups on the CS, resulting in a smaller hydrodynamic diameter.

There was no apparent trend in the PDI as it remained relatively constant over the range of ratios investigated, with values between 0.2-0.4. This indicates that the suspensions had homogenous size distribution for all the mass ratios investigated (Dube, 2011; Kumar *et al.*, 2015) and that the range of mass ratios did not affect the overall PDI. The ZP for each formulation was negative, owing to the higher Alg concentrations as expected. The values of ZP are highly influenced by the Alg or CS concentrations, as discussed earlier, because of the availability of total protonated $NH_3^+$ groups on CS and their neutralization with $COO^-$ groups of Alg (Bagre, Jain and Jain, 2013; Morsi *et al.*, 2015).

Although size is often the parameter of most concern, charge plays an equally important role. Some studies have shown that cationic nanoparticles show higher uptake due to the interaction with anionic cell membranes however, cationic particles are more likely to induce haemolysis and platelet aggregation than neutral or anionic particles (Foged *et al.*, 2005; Huang, Cavalcante and Townley, 2020). The ZP values from this study were strongly negative, more so in the polyelectrolyte complexation method than with the ionotropic gelation method. For example, at Alg-CS mass ratio 1:0.167 for polyelectrolyte complexation, the ZP was -43.23 $\pm$ 1.01 mV, whereas at a similar Alg-Ca-CS mass ratio of 1:0.333:0.200 ($C_3$) for ionotropic gelation, the ZP was -23.46 $\pm$ 3.46 mV. This is because the latter incorporates cationic $Ca^{2+}$ ions into the NP synthesis and any excess $Ca^{2+}$ not incorporated into the core is segregated to the outer shell of the NP, forming an ion shield therefore, increasing the overall charge of the NPs (Morsi *et al.*, 2015; Miao *et al.*, 2016).

Following this study, the ionotropic gelation method, using formulation $A_1$ at Alg-Ca-CS mass ratio 1:0.113:0.05, was adopted for the rest of the study.

### 5.1.3 SEM morphology assessment of Alg-Ca-CS NPs

The Alg-Ca-CS NPs at mass ratio 1:0.133:0.050 (formulation $A_1$), were further characterized with SEM to determine the surface morphology of the NPs. After synthesis, the NPs were lyophilized, and the powder was examined. SEM analysis revealed a rough, grainy appearance on the surface of the powder (see **Fig. 5.4** (A)), and the presence of aggregated, poorly defined NPs with estimated sizes between 200-300 nm (see **Fig. 5.4** (B), red circles). There are also aggregates larger than 200-300 nm. These images suggest that upon lyophilization, the NP matrix was disrupted and the electrostatic bonds between the polymers collapsed, causing a grainy, flocculated appearance (Suopajärvi, 2015; Villegas-Peralta *et al.*, 2020).


**Fig. 5.4** SEM images of lyophilized, empty Alg-Ca-CS NPs. The images reveal a rough, grainy appearance on the surface of the lyophilized powder (A) with poorly defined, irregular NP aggregates (B). NPs with sizes between 200-300nm were visible (red circles), as well confirming DLS results .

It is possible that water from the gelation medium was retained within the NPs and upon dehydration the retained water was lost, leading to the collapse of the polymer network. This then created depressions in the emptied spaces and the resultant polymer aggregation (Masalova *et al.*, 2013; Jiang *et al.*, 2014; Patel *et al.*, 2016; Villegas-Peralta *et al.*, 2020). This collapse could be due to the disruption of hydrogen bonds between the $NH_3^+$ groups of CS and the water, which usually aids the stability of NPs in suspension. Upon lyophilization, the samples are dehydrated which diminishes water content, resulting in a loss of hydrogen bonding, reducing

NP stability via the collapse of the polymer network and thus, resulting in NP agglomeration (see **Fig. 5.5**) (Villegas-Peralta *et al.*, 2020).

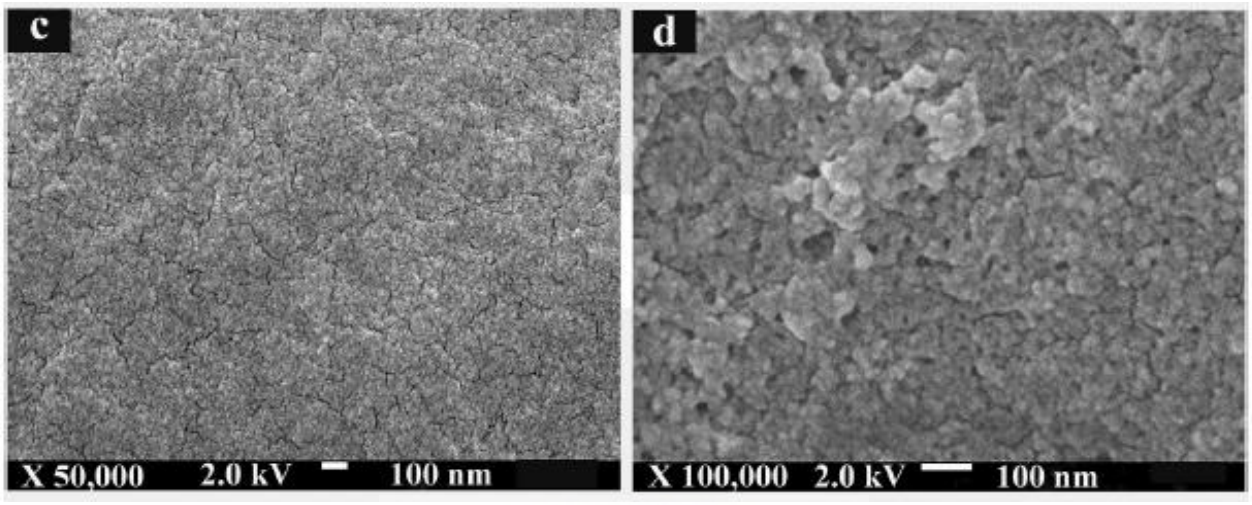


**Fig. 5.5 SEM analysis of CS NPs**. Agglomeration of the NPs was apparent due to the collapse of the hydrogen bonds between the amino end groups of CS and the water after lyophilization of the sample (Villegas-Paralta *et al.* 2020).

Furthermore, the molecular weight of CS plays a vital role in the stability of NPs in suspension. The higher the molecular weight, the more $NH_3^+$ groups are present in CS, therefore more hydrogen bonds can form, resulting in increased stability in suspension (Villegas-Peralta *et al.*, 2020). For this study, low molecular weight CS was utilized to coat the Alg-Ca NPs. Therefore, a possible explanation for the collapsed polymer network could be attributed to the lack of $NH_3^+$ groups present, resulting in higher instability in suspension and thus, after lyophilization. Other literature explains that the concentration of polyelectrolytes could have been too low for the NPs to maintain their three dimensional structure to form continuous NPs (Jiang *et al.*, 2014).

Using similar synthesis methods, previous studies demonstrated strongly the formation of spherical NPs after synthesis (empty or drug-loaded) (Bagre, Jain and Jain, 2013; Rivera *et al.*, 2015; Sorasitthiyanukarn *et al.*, 2019), however aggregation and clumping of the empty NPs had been observed (Rivera *et al.*, 2015; Lopes *et al.*, 2016; Miao *et al.*, 2016; Villegas-Peralta *et al.*, 2020). The dominant polymer also plays a role in the morphology of the NPs. For example, in a study whereby Alg/CS NPs were synthesized and compared, the surface of Alg-coated NPs were

rough in comparison to CS-coated NPs, which were spherical and smooth (Bagre, Jain and Jain, 2013). This finding would suggest that Alg could be the reason behind the grainy, flocculated appearance of the Alg-Ca-CS NPs synthesized in this study.

Moreover, aggregation can occur due to van der Waal's forces between atoms or molecules in a colloidal suspension (see **Fig. 5.6** (a)) (Moore *et al.*, 2015; Suopajärvi, 2015). Although these interactions are weak, the induced electrical interaction can lead to aggregation of NPs through the interaction of induced, instantaneous, or permanent dipoles (i.e. the separation of charges in atoms – electrons vs protons) in the interatomic bonds of NPs, which destabilize a colloidal system (Gebauer *et al.*, 2012; Moore *et al.*, 2015). These forces occur due to either of the following: : i) the electronegativity of some atoms is higher than for others in the same molecule, ii) vibration of charges within one atom creates a rapidly fluctuating dipole or iii) approaching particles induce vibrations in phase with each other, resulting in an attractive force between the two oppositely oriented dipoles (Suopajärvi, 2015). Essentially, the closer the particles are, the greater the attractive force experienced between the particles and thus the higher chance of adherence (Gebauer *et al.*, 2012; Moore *et al.*, 2015; Suopajärvi, 2015; Aftab *et al.*, 2020).

In addition, Ca is known to produce aggregation of Alg molecules, due to the complexation of the carboxylic groups with divalent, cationic $Ca^{2+}$ ions. This complexation bridges the molecules in the Alg network (β-D-mannuronate and α-L-guluronate) to form gel-like aggregates (Gallego-Urrea, Perez-Holmberga and Hassellöv, 2012; Kloster and Avena, 2015; Son, Vavra and Forbes, 2015; Miao *et al.*, 2016). For example, previous studies described how the interaction between humic acid and $Ca^{2+}$ enhanced the agglomeration of NPs by forming a bridge between carboxyl ($COO^-$) groups of the humic acid and cationic $Ca^{2+}$ ions (Zhu *et al.*, 2014; Son, Vavra and Forbes, 2015). Therefore, a plausible reason for the NP aggregation observed with SEM analysis could be due to the bridging between the $Ca^{2+}$ ions with the free carboxyl ($COO^-$) groups of the Alg molecules, resulting in the clumping of the NPs.

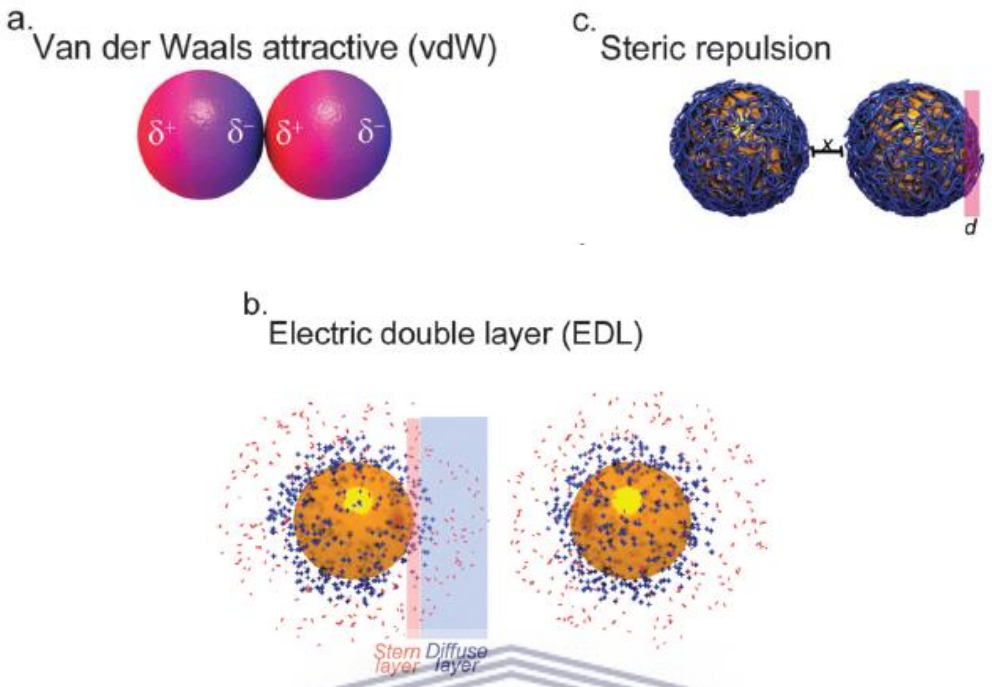


**Fig. 5.6 Colloidal interactions of NPs in suspension.** (a) At the most basic level, NP aggregation is governed by van der Waals interactions. Permanent or induced dipoles within the NP can result in net attractive forces between NPs and subsequent aggregation. (b) Macromolecules, such as proteins, surfactants (TWEEN 80) or polymers (PEG), can physically stabilize NPs, resulting in steric repulsion. (c) The inherent surface charge of NPs, caused by surface ions or functional groups, results in the formation of the electric double layer (EDL) consisting of the charge at the surface of the particle (stern layer) and electrostatically attracted oppositely charged ions (diffuse layer). The EDL forms a net charge, and when two like-particles are in close proximity the EDL repels the two (Moore, *et al*., 2015).



Previous studies also describe the ability of $Ca^{2+}$ ions to compress the electrostatic double layer (EDL) around the formed NPs in solution, leading to enhanced NP agglomeration (Zhu *et al.*, 2014; Son, Vavra and Forbes, 2015; Miao *et al.*, 2016). The EDL is a structure that appears on the surface of an object when it is exposed to a fluid (see **Fig. 5.6** (c)). The first layer is the actual surface charge of the NP (stern layer) and the second layer is composed of ions electrostatically attracted to the surface charge of the NPs in suspension (diffuse layer) (Schmickler, 2014; Moore *et al.*, 2015; Suopajärvi, 2015). Therefore, free $Ca^{2+}$ ions could potentially bind electrostatically to the NP surface, decreasing the surface charge on the NPs, resulting in the decline of the interparticle repulsions, compressing the EDL, leading to a decrease in the energy barrier between particles and therefore, promoting NP agglomeration.

NP aggregation due to colloidal instability in water has been previously reported with Alg and CS NPs (Masalova *et al.*, 2013). In the reported study, the separately prepared Alg-Ca and CS NPs displayed instability in water and collapsed after one day due to possible separation of the colloids. However, upon synthesizing the NPs with stabilizers, TWEEN 80 and polyethylene glycol (PEG), the colloidal suspension remained stable for up to 30 days. The lyophilized samples also showed the presence of stable, spherical NPs. It was proposed that the interaction between TWEEN 80 and PEG was responsible for the improved stability (Masalova *et al.*, 2013). TWEEN 80 is a nonionogenic surfactant that can modify the surface of NPs and prevent aggregation through steric repulsion (rather than electrostatic repulsion) (see **Fig. 5.6** (b)) (Masalova *et al.*, 2013; Zhu *et al.*, 2019; Aftab *et al.*, 2020). Steric repulsion is the process by which adsorbed nonionogenic surfactants or polymers produce strong repulsion between particles in dispersion due to overlapping electron clouds (Tadros, 2013). PEG played a role in the prevention of NP aggregation due to its ability to adsorb onto the NP surface through hydrogen bonding, forming a barrier between the NPs and resulting in less 'sticking' of NPs in concentrated colloids (Masalova *et al.*, 2013). Exploring the use of stabilizers such as TWEEN 80 and PEG should be explored to stabilize the NPs in solution and after lyophilization for more accurate SEM analysis.

Another method that can improve NP stability is through covalently linking the polymers instead of allowing spontaneous electrostatic interactions to occur. Covalently cross-linking the polymers using carboxylic acids, such as citric acid, has been shown to provide another way in which to improve the stability and mechanic properties of the NPs (Lombardo, Kiselev and Caccamo, 2019).

## 5.2 Synthesis and characterization of GFP loaded NPs (GFP-NPS)

### 5.2.1 Expression and purification GST-GFP

GST-GFP that was expressed in BL21Star™ *E.coli* cells and subsequently isolated from the bacterial cells as described in section **4.3.** The protein lysate was passed over a glutathione column, the flow through was collected. The GST-GFP fusion protein was captured on the column and subsequently cleaved (on-column) with PreScission™ Protease and the GFP was separated from GST. **Fig. 5.7** represents a polyacrylamide gel of the purified GFP used for this study.

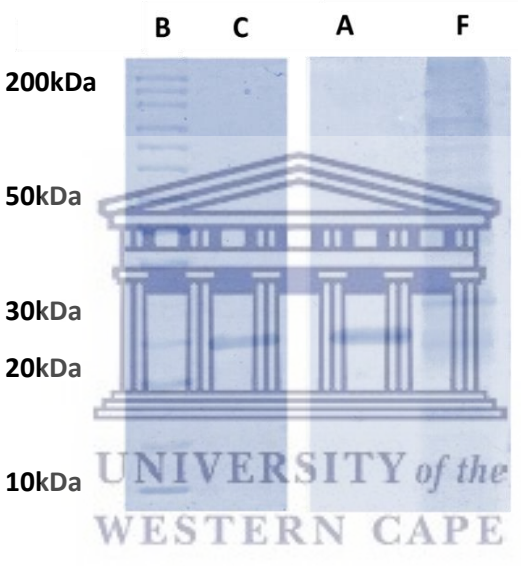



**Fig. 5.7 SDS-PAGE of large-scale expression and purification of the GST-tagged GFP**. The recombinant GST-GFP was successfully expressed in the BL21™ Star *E.coli* cells and purified GFP was attained by affinity chromatography. The figure above denotes (lane A) purified GFP eluted from a glutathione column; (lane B) PageRuler Unstained Protein Ladder; (lane C) small-scaled purified protein as a control and (lane F) flow through.

GFP is a 26.9 kDa protein (dos Santos, 2012; Laber *et al.*, 2017), which corresponds to the size of the purified GFP in **Fig. 5.7**. The protein was dialyzed for 16 h and then quantified by the Image J software™ as described in **4.3.1.5**. and the concentration from GFP was calculated to be 808.91 µg/ml. The sample was stored at -20˚C until ready for downstream applications.

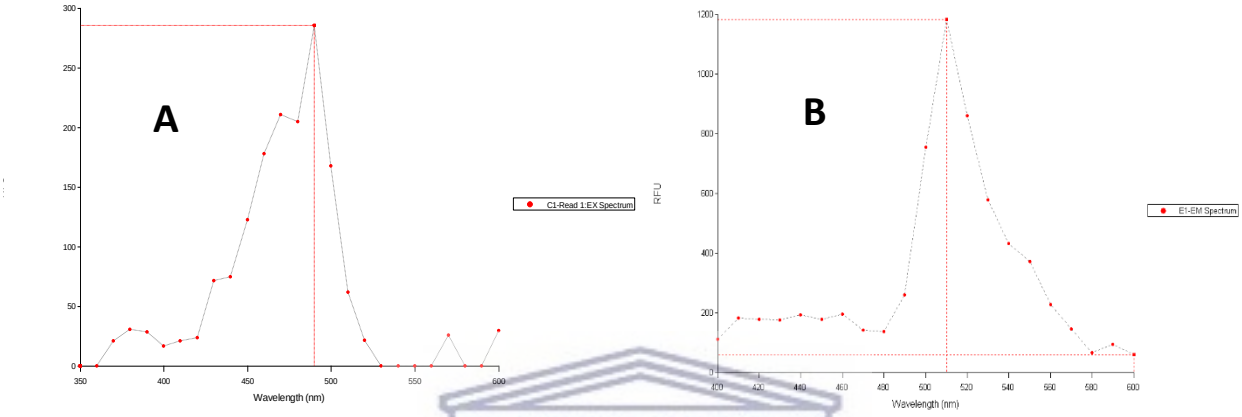


**Fig. 5.8 Excitation (A) and emission (B) spectra of the GFP used in this study.** The confirmed excitation was at around 490 nm and the emission was around 510 nm. This is the expected spectra of GFP, further confirming the presence of the required protein.

GFP has an excitation and emission usually at 488 nm and 510 nm, respectively (Nolles *et al.*, 2015; Cranfill *et al.*, 2016). The excitation and emission spectra of the purified GFP was determined using the Synergy™ MX Microplate Reader (**Fig. 5.8**), which confirmed that the purified protein is GFP.

### 5.2.2 Preparation and characterization of GFP-loaded NPs (GFP-NPs)

Alg-Ca-CS NPs at mass ratio 1:0.133:0.05 (formulation $A_1$) were synthesized in the presence of GFP at increasing GFP concentrations (98.77, 111.3 and 139 µg/ml). DLS results, shown in **Table 5.3**, indicated that as GFP concentrations increased from 98.77 µg/ml to 139 µg/ml the particles were stable (ZP) and homogenous is size dispersity (PDI). A noticeable size increase, of around 100 nm, was observed for GFP concentrations 111.3 µg/ml (362.09 $\pm$ 29.89) and 98.77 µg/ml (358.25 $\pm$ 54.91) when compared to the highest GFP concentration at 139 µg/ml (273.54 $\pm$ 23.43), which showed no increase in size from the unloaded NPs $A_1$ (275.62 $\pm$ 14.40). The PDI of

$A_1$ (0.308 $\pm$ 0.05) was lower when compared to the GFP-NPs (0.323, 0.408, 0.397) and the ZP of the GFP-NPs remained stable and within ~1-2 mV of $A_1$ (-26.94 $\pm$ 2.67). Statistical analysis amongst the three formulations indicated that the size and ZP displayed statistical significance (both with p<0.0001) due to the observed changes in readings for each formulation, while the PDI indicated no statistical significance (p=0.0729) and remained relatively unchanged throughout.

**Table 5.3** Characteristics of GFP-loaded Alg-Ca-CS NPs in terms of concentration of GFP, average size, PDI and ZP (mean ± s.d., n=5, size p<0.0001; PDI p=0.0721; ZP p<0.0001)

| Concentration (µg/ml) | Size (nm) | PDI | ZP (mV) |
|---|---|---|---|
| **139** | 273.54 $\pm$ 23.43 | 0.323 $\pm$ 0.06 | -24.99 $\pm$ 2.57 |
| **111.3** | 362.09 $\pm$ 29.89 | 0.408 $\pm$ 0.14 | -29.04 $\pm$ 2.43 |
| **98.77** | 358.25 $\pm$ 54.91 | 0.397 $\pm$ 0.12 | -25.93 $\pm$ 3.72 |

The size of the GFP-NPs displayed statistical significance (p<0.0001) when compared to the unloaded NPs at $A_1$. When comparing the size at 139 µg/ml to $A_1$ p=0.4939, indicating no statistical significance due to no apparent change in the readings. This could be attributed to the general increase in the NP size with increasing GFP concentration, excluding NPs formed with GFP concentration 139 µg/ml. These findings would suggest protein encapsulation/incorporation into the NPs due to the increased content of protein in the nanoparticles (Sorasitthiyanukarn *et al.*, 2019). However, previous studies have reported no change in NP size, despite having confirmed protein encapsulation. This was suggested to be due to a low amount of protein actually encapsulated into the NPs (Haji *et al.*, 2018), which could be the rationale for the unchanged size exhibited for GFP concentration 139 µg/ml. Moreover, at higher concentrations, such as that of 139 µg/ml, proteins can form networks mediated by weak, nonspecific protein−protein interactions that increase viscosity and aggregation, and possibly decrease encapsulation (J. Li *et al.*, 2014; Arora *et al.*, 2016; Laber *et al.*, 2017). It should be noted that

although DLS can determine the size distribution of the NPs, it does not provide direct information on the number of protein molecules incorporated (Nolles *et al.*, 2015). Therefore, further encapsulation studies would be needed to confirm exact encapsulation efficiencies for these NPs.

In a previous study encapsulation efficiency of bovine serum albumin (BSA) was determined for either CS or Alg NPs. When applying a fourfold increase of the BSA protein concentration, there was a noticeable decrease in encapsulation efficiency by 15% for the Alg NPs. However, when the same fourfold increase was applied to the CS NPs, the BSA encapsulation efficiency was doubled (Masalova *et al.*, 2013). From the results obtained, a possible reason for the unchanged size of the GFP-NPs when compared to the empty NPs could be attributed to the Alg polymer that was utilized, resulting in a loss of protein encapsulation. Further investigations should be explored to confirm the effect of different polymers on encapsulation efficiencies.

The PDI remained comparatively the same for each formulation, displaying a stable and homogenous NP size distribution, thereby denoting no statistical significance between each formulation ($p=0.0729$). However, when compared to the unloaded NPs, the PDI increased slightly for the GFP-NPs, thereby displaying statistical significance ($p=0.0397$). The increased PDI is perhaps indicative of the addition of the GFP to each formulation, thus altering the size dispersity slightly.



There was an observed decrease, of ~3-4 mV in the ZP when the GFP concentration was 111.3 µg/ml ($-29.04 \pm 2.43$) when compared to the other formulations. The ZP of the GFP-NPs showed statistical significance ($p<0.0001$) when compared to the unloaded NPs at $A_1$, therefore suggesting that the change in ZP was likely influenced by the incorporation of the protein. From previous literature, it can be noted that upon protein encapsulation, some proteins may be located close to the NP surface (Haji *et al.*, 2018). Therefore, suggesting that the varying ZPs, from varying GFP concentrations, could be attributed to protein on the NP surface. This could also influence the NP size, as observed at GFP concentrations 111.3 µg/ml and 98.77 µg/ml, respectively.

Prior to synthesis, varying concentrations of GFP were added to the Alg solution, with the intention of altering the net charge of the GFP to maximize encapsulation. This is possible as both the Alg polymer and the protein possess ionizable groups, influenced by pH, that could play a major role in encapsulation efficiency of the GFP (Laber *et al.*, 2017; Lima *et al.*, 2018). An important factor with protein solubility in solution is the isoelectric point (pI), which is the point at which a protein has a net neutral charge. Protein molecules have smaller net electrical charge and thus lower aqueous solubility when the pH is buffered near the protein's pI. When the pH>pI, the protein carries a net negative charge, and therefore when the pH<pI, the protein carries a net positive charge (Bekale, Agudelo and Tajmir-Riahi, 2015; Zou *et al.*, 2016; Laber *et al.*, 2017; Haji *et al.*, 2018).

The GFP used in this study had a net charge of -5.7 mV (Malvern Zetasizer Nano ZS) and a theoretical pI of 5.8 (dos Santos, 2012), therefore by adding the protein to the Alg solution (pH 4.9), the net charge of the GFP should have, theoretically, increased and become positive. Proteins are generally more soluble at pH values 1−2 units away from their pI, and with an increased net surface charge proteins are expected to increase long-range electrostatic repulsive forces and prevent protein−protein interactions (Kramer *et al.*, 2012; Zou *et al.*, 2016; Laber *et al.*, 2017). Therefore, by adding the GFP to the Alg solution with a pH of 4.9, the protein should have sufficient repulsive forces and not aggregate.



Previous literature demonstrated a reduction in protein loss through electrostatic bonding between the negatively-charged $COO^-$ groups of the polymer and the positively-charged basic proteins upon encapsulation (Haji *et al.*, 2018). The addition of the GFP to the acidic Alg solution should have thus increased the protein's net charge and possibly encouraged electrostatic bonding between the negatively-charged Alg polymer and the more positively-charged GFP protein – although further confirmation of the change in GFP charge would be needed to confirm this. Additionally, and contrary to this, enhanced encapsulation has been observed when the pH is buffered closer to the protein's pI, because it is likely that the smaller net charge attenuates the electrostatic repulsions between protein molecules and therefore allows the protein load to be compacted, which can facilitate its entrapment within the NPs (Santander-Ortega *et al.*, 2009;

Haji *et al.*, 2018). To definitively determine which method resulted in a higher encapsulation of the protein into the NPs, encapsulation efficiency studies would need to be conducted.

For the rest of the study, the NPs were synthesized with GFP concentration 139 µg/ml, due to the favorable size obtained (273.54 $\pm$ 23.43).

### 5.2.3 SEM analysis of GFP-NPs

The GFP-NPs, with GFP concentration 139 µg/ml and Alg-Ca-CS mass ratio 1:0.133:0.05 (formulation $A_1$), were further characterized with SEM to analyze the surface morphology of the NPs. After synthesis, the NPs were lyophilized, and the powder was examined. SEM analysis revealed irregular, solid cuboid NPs with sizes between 200-300 nm, confirming DLS findings.

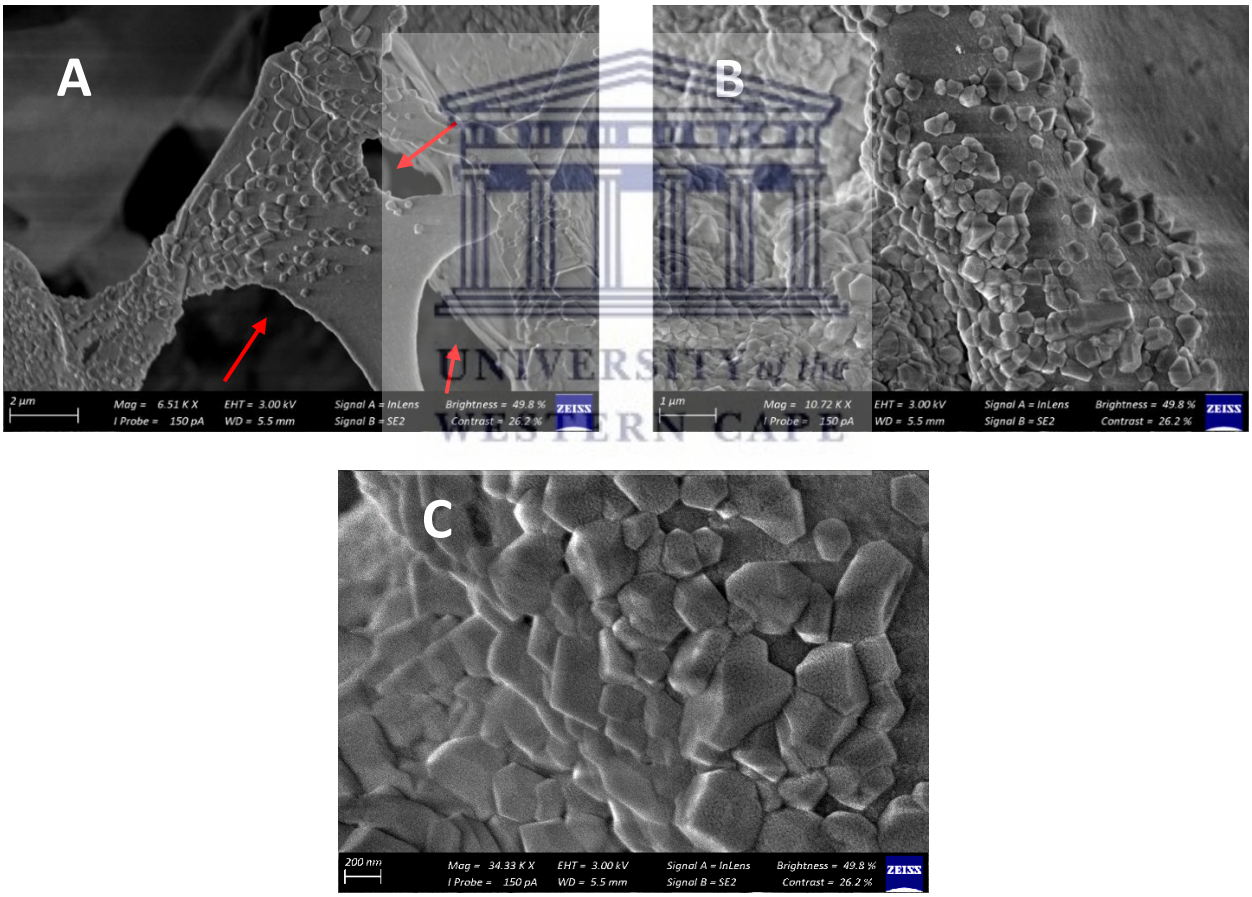


**Fig. 5.9 SEM images of GFP-NPs Alg-Ca-CS NPs**; low to high magnification (A-C). The images demonstrate irregular, solid cuboid NPs embedded on a micron-sized structure with large pores (red arrows). These large pores could be indicative of the formation of an Alg hydrogel, onto which the NPs have attached.

The NPs are also attached to what appears to be a smooth structure with micron-sized pores (see **Fig. 5.9** (A) – red arrows).

Previous studies have demonstrated predominantly smooth, spherical NPs for similar synthesis methods of Alg/CS NPs after drug encapsulation (Kumar *et al.*, 2015; Morsi *et al.*, 2015; Rivera *et al.*, 2015; Sorasitthiyanukarn *et al.*, 2018). This would contrast with the SEM images obtained for this study, whereby NPs with irregular shapes were obtained. A possible explanation could be due to the uneven crosslinking and coating of the polymers during synthesis, creating an uneven, irregular surface morphology (Ling *et al.*, 2019). With regards to the structure onto which the NPs are embedded, previous literature has demonstrated that Alg can create a porous hydrogel that is formed from masses of Alg (see **Fig. 5.10** (A)) (Lima *et al.*, 2018; Ling *et al.*, 2019) and these hydrogels can cause NPs to cluster and embed onto the surface (see **Fig. 5.10** (B)) (Miao *et al.*, 2016). Therefore, the SEM images from this study suggest that the formed NPs are embedded onto Alg hydrogel matrices.

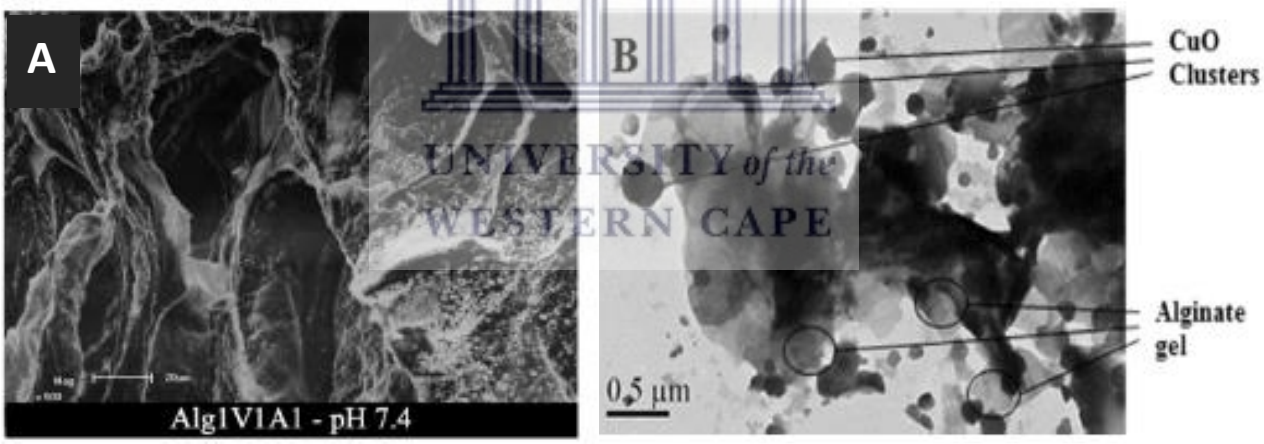


**Fig. 5.10** SEM analysis of lyophilized Alg hydrogel (A) (Lima *et al.*, 2018); TEM image of copper oxide NP clusters embedded on an Alg-Ca gel formed through the aggregation of Alg residues (B) (Miao *et al.*, 2016).

A reason for the formed hydrogels could be explained by possible competition between the Ca and CS for Alg binding sites, resulting in abnormalities in the NP surface morphology (Lopes *et al.*, 2016; Ling *et al.*, 2019). Due to the competitive binding, CS is unable to efficiently coat and separate the Alg-Ca hydrogel in sponge-like NPs therefore, resulting in the formation of fully-

formed hydrogels with irregularly shaped NPs embedded onto the surface (Kumar *et al.*, 2015; Morsi *et al.*, 2015; Ling *et al.*, 2019). A suggested improvement in this method involves a 1-step simultaneous CS and Ca cross-linking process. This would lead to equal competition of Ca and CS for Alg binding sites, and increase the amount of CS incorporated into the NP matrix therefore, increasing the likelihood of forming more regularly shaped NPs (Ling *et al.*, 2019). Alternatively, exploration of stabilizing agents in the synthesis method could be explored as mentioned above in **5.1.3**.

The SEM images do reveal possible encapsulation/loading of the protein due to the appearance of physical NPs, when compared to the SEM images of the empty or pre-loaded NPs (**Fig. 5.4**). This could suggest that the protein-polymer interactions resulted in the formation of NPs that were able to maintain their 3D structure without the polymer network collapsing after lyophilization. This was corroborated in a study whereby the effects of protein encapsulation on NP shape was observed and confirmed. This occurred through a tightly bound complex between the polymer and protein which changed the shape of the polymer in favor of the protein (Bekale, Agudelo and Tajmir-Riahi, 2015). Therefore, the SEM images obtained may be depictive of the NPs formed from the actual protein shape. Further studies would be required to confirm the effects of polymer–protein complexation on the shapes of these Alg-Ca-CS nanocarriers.



**5.3 Nanoparticle stability test in RPMI media**

The stability of the Alg-Ca-CS NPs were assessed in RPMI media according to the method described in **4.2.3**. The physical characteristic measured was the size distribution of the NPs within the media. ZP could not be measured due to the fact that the proteins found in the medium will influence the overall charge. The size distribution of the NPs was recorded at time intervals 0, 20, 30, 45 and 60 minutes after NPs were placed into RPMI media. It was apparent at 0 minutes (immediate read), that the NPs were uniform in size (see **Fig. 5.11** (A)). After 20 min the size distribution remained relatively unchanged, although it was moderately broader (see **Fig. 5.11** (B)). However, between 30 and 60 min there appears to be substantial aggregation of the NPs. The NPs aggregate into particles of micron scale after 30 min (see **Fig. 5.11** (C)). This

aggregation appears to be time dependent and the size gets larger as the time increases. These results indicated that the NPs were still relatively stable after 20 minutes within the media (see **Fig. 5.11** (B)), which is significant as this could be indicative of how well the NPs would maintain their structure *in vivo* for downstream applications (Moore *et al.*, 2015).

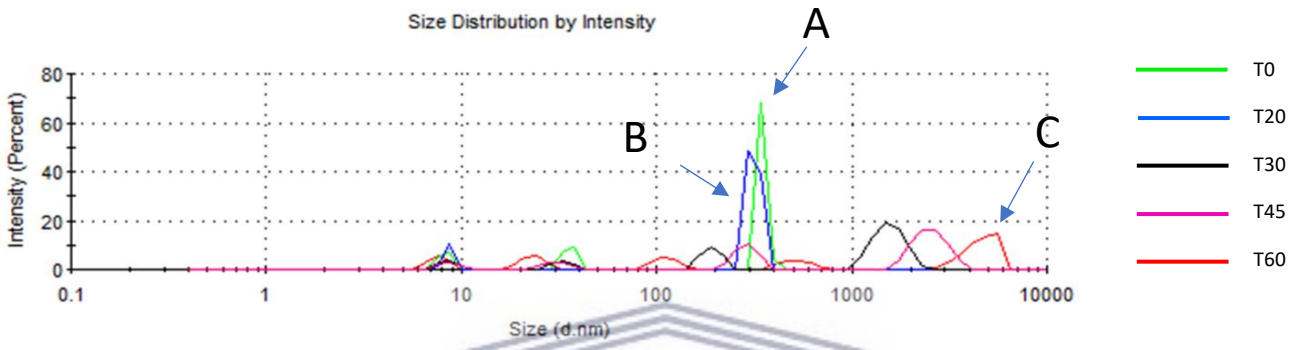


**Fig. 5.11 Nanoparticle stability test conducted in RPMI media at time intervals T0, T20, T30, T45 and T60.** The NPs which show mostly uniform size distribution at T0 (A) and T20 (B). From T30 onwards the NPs undergo aggregation to form larger NPs (C). The increase in size is also observed at T45 and T60 and appears to be time dependent.



NPs intended for use in biological environments will inevitably come into contact with physiological fluids that contain a wide range of biomolecules, that can potentially bind to the NP surface, altering the physicochemical properties of the NPs (Nel *et al.*, 2009; Gebauer *et al.*, 2012; Moore *et al.*, 2015). Cell culture medium is a buffered heterogenous solution that is primarily comprised of proteins such as serum albumin or globulins, and a number of other biomolecules including amino acids, and ionic salts (Moore *et al.*, 2015). In this complex environment NPs can aggregate, due to this colloidal instability. This is a common phenomenon, caused by irreversible inter-particular adherence, that leads to the formation of large and irregularly shaped clusters (Rausch *et al.*, 2010; Sabuncu *et al.*, 2012; Moore *et al.*, 2015; Aluani *et al.*, 2017). Even NPs that were proven to be stable during the design and development phase, can be unstable in biological environments due to molecule/protein adsorption resulting in the loss of unique physicochemical

properties of the NPs, which may have been designed into the NP (Moore *et al.*, 2015). Furthermore, electrostatically stabilized NPs have generally shown poor stability in cellular media and the formation of a stable adsorbed protein corona upon incubation seems to be the singular factor for maintaining colloidal stability, which can further influence the *in vivo* behavior and significantly alter NP mobility (Onoue, Yamada and Chan, 2014; Moore *et al.*, 2015).

The constituents of cell culture medium influence the hydrodynamic behavior of NPs through various intermolecular forces that affect the electrostatic double layer (EDL) of the NP surface (Moore *et al.*, 2015; Suopajärvi, 2015; Miao *et al.*, 2016). This occurs due to the ability of the surface charges of colloids to influence the distribution of the nearby ions in a liquid, so that counter-ions accumulate on the surfaces of the suspended particles. When the ion concentration is high, the EDL is compressed, resulting is the collapse of the colloidal system (Edwards and Williams, 2004; Zhu *et al.*, 2014; Son, Vavra and Forbes, 2015; Suopajärvi, 2015). This collapse occurs when these counter ions accumulate onto the surface, a change in the charge of the particles in experienced and thus, the forces that once repelled, no longer exist, leading to colloidal instability (Sabuncu *et al.*, 2012; Aluani *et al.*, 2017). This effect was reported in a study whereby the influence of $Na^+$ ions on the NP surface charge was studied. Initially the NPs had a ZP reading of -37 mV however, after incubation in NaCl for 2 h, the colloidal ZP were reduce to -10 mV indicating adsorption of the $Na^+$ ions onto the NP surface, reducing the overall charge and promoting NP aggregation (Liu *et al.*, 2020). It is suggested to be a cause of counter-ions/molecules/proteins accumulating onto the NP surface thus, suppressing the EDL and reducing overall charge (Moore *et al.*, 2015; Suopajärvi, 2015; Miao *et al.*, 2016).

Previous studies have reported agglomeration of similar Alg/CS NPs caused by an apparent decrease in overall ZP (Aluani *et al.*, 2017). Similar reduction in ZP and subsequent agglomeration of gold nanoparticles upon incubation in cell culture medium has also been reported (Sabuncu *et al.*, 2012). Therefore, a potential cause of the agglomeration in this current study could be attributed to change in overall ZP from highly negative to more neutral from the surrounding proteins/molecules/ions in the media. Furthermore, it has been found that NPs which had a negative ZP in water tended to form larger aggregates in media supplemented with 10% FBS

compared to unsupplemented RPMI (Moore *et al.*, 2015). Further studies would be needed to confirm these findings however, owing to varying charges in cell culture media, this may prove difficult with DLS.

A protein corona is formed when proteins in biological fluid adsorbs onto the surface of the NPs and this typically happens within seconds to minutes after exposure (Gebauer *et al.*, 2012; Sabuncu *et al.*, 2012; Martin *et al.*, 2014; Moore *et al.*, 2015). The presence of proteins in the colloidal suspension can stabilize NPs against agglomeration even in the presence of physiological electrolyte concentrations by steric or electrosteric effect (Gebauer *et al.*, 2012; Larson, Joshi and Sokolov, 2012; Lesniak *et al.*, 2012). This finding was confirmed in a previous study wherein it was reported that gold NPs, electrostatically stabilized with a tris(sodium-m-sulfonatophenyl)phosphine (TPPTS) coating, exhibited a considerable increase in size, from 25 nm to 750 nm, once dispersed in RPMI media without FBS. However, once the media was supplemented with BSA, there was a slight increase in NP size to 50 nm (Mahl *et al.*, 2010). In relation to this study, a possible reason the NPs remained stable for up to 20 minutes, could be due to the presence of a protein corona formed from the proteins present the culture medium. However, this must be confirmed by further characterization of the NPs. It has been noted however, that destabilization of the colloidal NP systems is significantly related to the protein–NP interaction (Moore *et al.*, 2015).



Another factor that could affect the colloidal stability of the NPs is the pH of the media which has shown to affect the surface charge of polyelectrolytes due to protonation or deprotonation of the functional groups (Ghosh *et al.*, 2011; Rodriguez-Lorenzo *et al.*, 2014; Moore *et al.*, 2015). As mentioned previously in **4.1.2.2**, Alg and CS are weak polyelectrolytes therefore, their degree of dissociation depends on the solution pH. When the pH of Alg is below its pKa value (3.4-4.4), a decrease in the degree of ionization is observed, leading to insufficient surface charge. When the pH is above the pKa, deprotonation of the carboxyl groups occurs to gain an overall negative charge (COOH to $COO^-$). Likewise, CS is only soluble in acidic solution, where the pH value is significantly lower than its pKa (6.2-7.0). At an acidic pH, the amine groups of CS are protonated, resulting in a sufficient positive surface charge ($NH_2$ to $NH_3^+$), vital for polyionic complex

formation with the anionic Alg (Shafie and Fayek, 2013; Rodriguez-Lorenzo *et al.*, 2014; Moore *et al.*, 2015; Rivera *et al.*, 2015; Brezaniova *et al.*, 2017; Mohammed *et al.*, 2017). Alg is also stable under acidic environments, but swells and slowly dissolves in alkaline conditions (Sorasitthiyanukarn *et al.*, 2019). Therefore, with a pH between 7 to 7.4, RPMI media could induce unwanted deprotonation ($NH_3^+$ to $NH_2$) of the CS or swelling and dissolution of Alg, resulting in a breakdown of the electrostatic interactions between the NPs (Rodriguez-Lorenzo *et al.*, 2014; Moore *et al.*, 2015).

The observed NP aggregation would prove undesirable for drug delivery as it leads to opsonization and therefore, rapid clearance in the liver and RES, thereby limiting the probability of reaching the anticipated therapeutic target (Onoue, Yamada and Chan, 2014; Moore *et al.*, 2015). Additionally, previous literature has indicated a higher cellular uptake of Alg/CS NPs after 4 hours of incubation with a significant increase after 24 hours (Sorasitthiyanukarn *et al.*, 2019; Zhang *et al.*, 2019). This finding would suggest improvements to the NPs would need to be implemented to increase stability and circulatory time for effective delivery of a therapeutic agent.

Surface modification of NPs is one of the most widely accepted methods to improve colloidal stability (Albanese and Chan, 2011; Moore *et al.*, 2015). Typically, steric stabilization is the most commonly used approach to increase the stability of NPs in suspension, and is generally accomplished via natural (e.g. dextran, alginate, chitosan) or a synthetic polymer coating (e.g. PEG; poly(vinyl alcohol) (PVA); poly(vinyl pyrrolidone) (PVP)) (Li *et al.*, 2014; Moore *et al.*, 2015; Nasir, Kausar and Younus, 2015; Banik, Fattahi and Brown, 2016; Lombardo, Kiselev and Caccamo, 2019). Steric stabilization provides a powerful tool to enhance the dispersion state of NPs under otherwise harsh conditions by preventing two particles from forming attractive van der Waal's interactions. Steric stabilization also allows for increased circulatory time of NPs (Gallego-Urrea, Perez-Holmberga and Hassellöv, 2012; Gebauer *et al.*, 2012; Masalova *et al.*, 2013; Moore *et al.*, 2015).

It has also been shown that by using charged macromolecules or proteins, the stabilization of colloidal systems could be improved due to the combined electrosteric repulsion (Domingos *et*

*al.*, 2009; Masalova *et al.*, 2013). This was confirmed in a study exploring the enhanced delivery of insulin using CS/Alg NPs, albumin was used to efficiently stabilize the NPs and prevent premature release of the loaded insulin cargo through enzymatic degradation (Lopes *et al.*, 2016). This is due to albumin's ability to avoid protease degradation of the NPs in the gastrointestinal tract (GIT) (Woitiski *et al.*, 2011; Lopes *et al.*, 2016). Therefore, albumin could also be explored to stabilize the NPs, particularly for further down-stream applications with cell lines or in simulated GIT studies.

Unfortunately, the stability of GFP-NPs was not assessed. Stability assessment of the loaded NPs would have been vital as SEM analysis indicated the maintenance of structure of the GFP-NPs after lyophilization. As mentioned above, certain proteins can protect NPs from degradation, therefore it would have been of interest to explore the stability of the loaded NPs in RPMI media and report on the possible effect the GFP could have had in maintaining colloidal stability.

**5.4 Characterization of aptamer-conjugated GFP-NPs (Apt-NPs)**

Amine-modified CD4 aptamers (Apt) (4 µM) were conjugated to GFP-NPs at mass ratio 1:0.133:0.05 (formulation $A_1$). The GFP-NPs were synthesized with varying GFP concentrations (98.77, 111.3 and 139 µg/ml) as described in **4.4**. For this study DNA aptamers were utilized as they are more stable compared to RNA aptamers, since RNA has a 20-hydroxyl group that make it susceptible to hydrolysis (Zhu *et al.*, 2012). Although the GFP concentration 139 µg/ml was used in the synthesized NPs for the rest of the study, the comparison of the DLS results after Apt conjugation was still of interest. DLS results, shown in **Table 5.4**, exhibited uniformity in all three formulations for size, PDI and ZP, indicating that protein encapsulation did not affect the Apt conjugation. The results indicated an apparent increase in size (~200-300 nm) for all three formulations of the Apt-NPs when compared to the unconjugated GFP-NPs (273.54 $\pm$ 23.43 nm; 362.09$\pm$ 29.89 nm; 358.25 $\pm$ 54.91 nm). There was a slight increase in the PDI of the Apt-NPs, with GFP concentration 139 µg/ml, from 0.323 $\pm$ 0.06 to 0.467 ± 0.109, and as well as at 98.77 µg/ml from 0.397 $\pm$ 0.12 to 0.420 ± 0.106. Interestingly, there was a decrease in PDI at GFP concentration 111.3 µg/ml, from 0.408 $\pm$ 0.14 to 0.364 ± 0.050. For all three Apt-NPs

formulations, the ZP exhibited a positive increase of ~8-11 mV. This suggests changes on the surface of the NPs and possible conjugation of the Apt to the GFP-NPs Alg-Ca-CS NPs.

**Table 5.4 Trends in ZP of aptamer-conjugated GFP-NPs Alg-Ca-CS.** An observed increase in the overall ZP from the unconjugated NPs to the aptamer-conjugated NPs was apparent, indicating positive aptamer conjugation to the available carboxyl end groups on the surface of the NP (mean ± s.d., n=3).

| GFP concentration (µg/ml) | Size (nm) | PDI | ZP (mV) | ZP (mV) unconjugated NPs |
|---|---|---|---|---|
| **139** | 556.00 ± 42.41 | 0.467 ± 0.109 | -16.90 ± 0.70 | -24.99 ± 2.57 |
| **111.3** | 567.67 ± 27.49 | 0.364 ± 0.050 | -17.67 ± 0.76 | -29.04 ± 2.43 |
| **98.77** | 510.10 ± 24.72 | 0.420 ± 0.106 | -15.23 ± 0.76 | -25.93 ± 3.72 |

Similar increases in NP size after aptamer conjugation have previously been reported, and it was proposed to indicate APTAMER conjugation (Guo *et al.*, 2011; Yu *et al.*, 2011; Alibolandi *et al.*, 2015). Changes in particle ZP have also been reported (Guo *et al.*, 2011; Li *et al.*, 2014). Therefore, the changes observed after the addition of the Apt to the GFP-NPs suggest positive conjugation. Statistical analysis demonstrated $p<0.0001$ when comparing the size of the Apt-NPs to the GFP-NPs, indicating statistical significance. This is due to the expected increase in size observed after Apt conjugation. Statistical analysis also demonstrated $p<0.0001$ when comparing the ZP between the conjugated and unconjugated NPs, showing statistical significance owing to the increase in ZP observed after Apt conjugation. Lastly, the PDI showed statistical significance ($p=0.0008$) due to the general increase in PDI, suggested to be caused by the size increase, thereby affecting the size dispersity.



The conjugation of the Apt, described in more detail in section **4.4**, was achieved by covalently linking the 5'-$NH_2$ of the Apt to the free carboxyl groups on the NPs through EDC/NHS chemistry. 1-Ethyl-3-(3-Dimethylaminopropyl) Carbodiimide (EDC) is a water soluble crosslinker which used to couple carboxyl groups to primary amines. EDC first forms an unstable, active ester intermediate which is then stabilized with the addition of N-Hydroxysuccinimide (NHS) to form semi-stable, amine-reactive ester (Yu *et al.*, 2011; Aravind *et al.*, 2012; Alibolandi *et al.*, 2015; Wickramathilaka and Tao, 2019). This ester then covalently links with the amine groups of the

functionalized Apt. The linking of the amine-functionalized Apt to the free carboxyl groups from the Alg on the NPs could explain the increase in ZP observed as more carboxyl groups would be occupied, thereby rendering the NPs less negative.

### 5.5 Assessing the binding of Apt-NPs to THP-1 cells

The THP-1 cell-line is an immortalized monocyte-like cell line (average size of 21 µm) that can be differentiated into macrophage-like cells (Konopka and Düzgüneş, 2002; Huang, Cavalcante and Townley, 2020). In this study, the THP-1 cell line was used due to the ability of the cells to express CD4 receptors on the cell surface (Konopka and Düzgüneş, 2002; Lodge *et al.*, 2017). This cell line to assess the targeting of GFP loaded NPs that are functionalized with a CD4 specific DNA aptamer to CD4 expressing cells. As described in section **4.7.2.1**, the binding of the Apt-NPs to the THP-1 cells was assessed by quantifying the percentage of fluorescently tagged cells using the Tali™ Image-Based Cytometer. After exposing the cells to the NPs (GFP-NPs and Apt-NPs), the samples were loaded onto a Tali™ slide and the cells were analyzed. The following controls were included: untreated cells and empty NPs. The empty cells showed no green fluorescence, suggesting no polymer-related fluorescence. . This can be confirmed by previous literature, that demonstrated that these polymers (Alg and CS) exhibit no green fluorescence when treating cells under confocal microscopy (Sorasitthiyanukarn *et al.*, 2018).

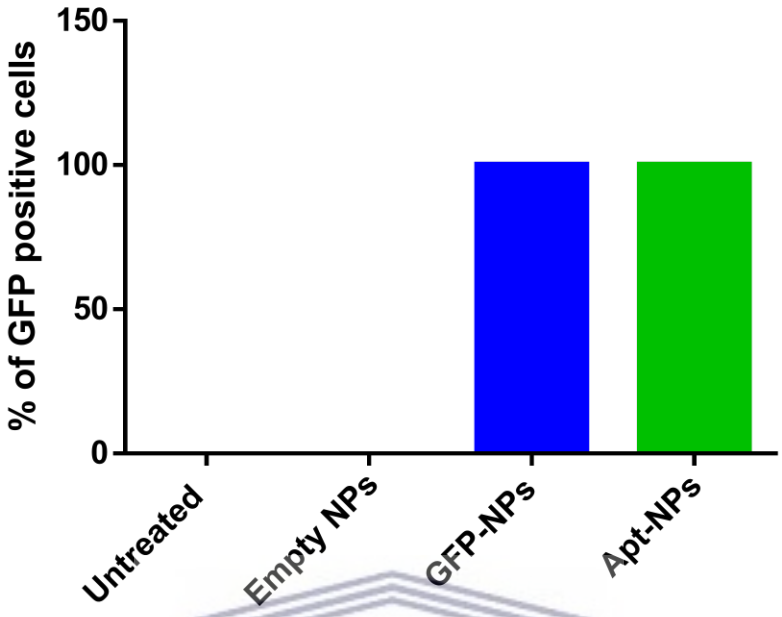


**Figure 5.12 Percentage of GFP positive cells determined by the Tali™ Image-Based Cytometer.** The results showed 100% green fluorescence in both GFP samples. (n=2)

The results from the image-based cytometer demonstrated the presence of green fluorescence in cells treated with GFP-NPs and the Apt-NPs (see **Fig. 5.12**). It is not known if the NPs were internalized by the cells or whether the NPs simply attached to the surface of the cells. All the cells (i.e. 100%) were positive for green fluorescence after being treated with the GFP-NPs and the Apt-NPs. This suggests that binding or uptake of GFP loaded NPs was independent of the presence of the CD4 specific aptamer (Apt) and that GFP-NPs without the aptamer can also bind to or be internalized by THP-1 cells. The expectation was that Apt-NPs will be targeted to THP-1 cells more efficiently than GFP-NPs which do not contain the aptamer. However, the data does not support this. Previous studies suggested cellular uptake is due to the small size of Alg/CS NPs and uptake can occur without the use of a target ligand (Morsi *et al.*, 2015; Ling *et al.*, 2019). This suggests that the GFP-NPs can be taken up regardless of the presence of an Apt however, the rate of uptake could differ. Even though this study shows that both GFP-NPs and the Apt-NPs bind to or are taken up by THP-1 cells, it is possible that there is a difference between the rate

these NPs bind to THP-1 cells. I.e. Apt-NPs may be taken up faster than GFP-NPs. Since this study only investigated a 24 h exposure period, it is not known if this is indeed the case and further studies investigating uptake or binding between 0 and 24 h is needed.

**5.6 Cellular uptake of Apt-NPs**

The THP-1 cells harvested in **4.6** were treated for 1 h, in duplicate, with Apt-NPs (synthesized as described in section **4.4**) to determine whether there was uptake of the fluorescent Apt-NPs into the cells. The treated cells were analyzed using the Carl Zeiss Confocal LSM 780 Elyra PS1 microscope (Carl Zeiss AG, Germany) to determine the location of the Apt-NPs. The images were separated into fixed and live samples. The fixed samples were fixed after 1 h of exposure and the live samples were read after 2-3 h of exposure to the NPs. The images obtained are shown in **Fig. 5.13** and **Fig. 5.14**. The images show the apparent presence of green fluorescence from GFP (**Fig. 5.13** and **Fig. 5.14**) with sizes corresponding with those obtained in **5.4** (500-600 nm), however it is unclear whether the green staining is in the cells, on the surface of the cells or perhaps that the protein was released from the NPs and scattered on the surface of the slide.

When considering the desired application of aptamers, one should also consider the selectivity and sensitivity of the aptamers. Selectivity refers to the ability of the aptamer to identify the target in a complex mixture without interference from other components (Vessman *et al.*, 2001; Jeong and Rhee Paeng, 2012; Kalra *et al.*, 2018). Sensitivity refers to the lowest concentration at which the aptamer can detect the target of interest (Kalra *et al.*, 2018). For clinical applications, the more selective aptamer-NP sets would be more attractive for a more “universal” targeting of therapeutic agents, whereas the more sensitive aptamer-NP sets could be more attractive for diagnosis applications (Medley *et al.*, 2011). For this study, it is suggested that the aptamers should have higher selectivity to ensure positive delivery of the load within the NPs. Aptamers enhance the binding and uptake of NPs, drugs, proteins, etc., through receptor mediated

transport called endocytosis (Aravind *et al.*, 2012; Ho *et al.*, 2015). Therefore, the assumed uptake, if any for this study, would be through endocytosis.

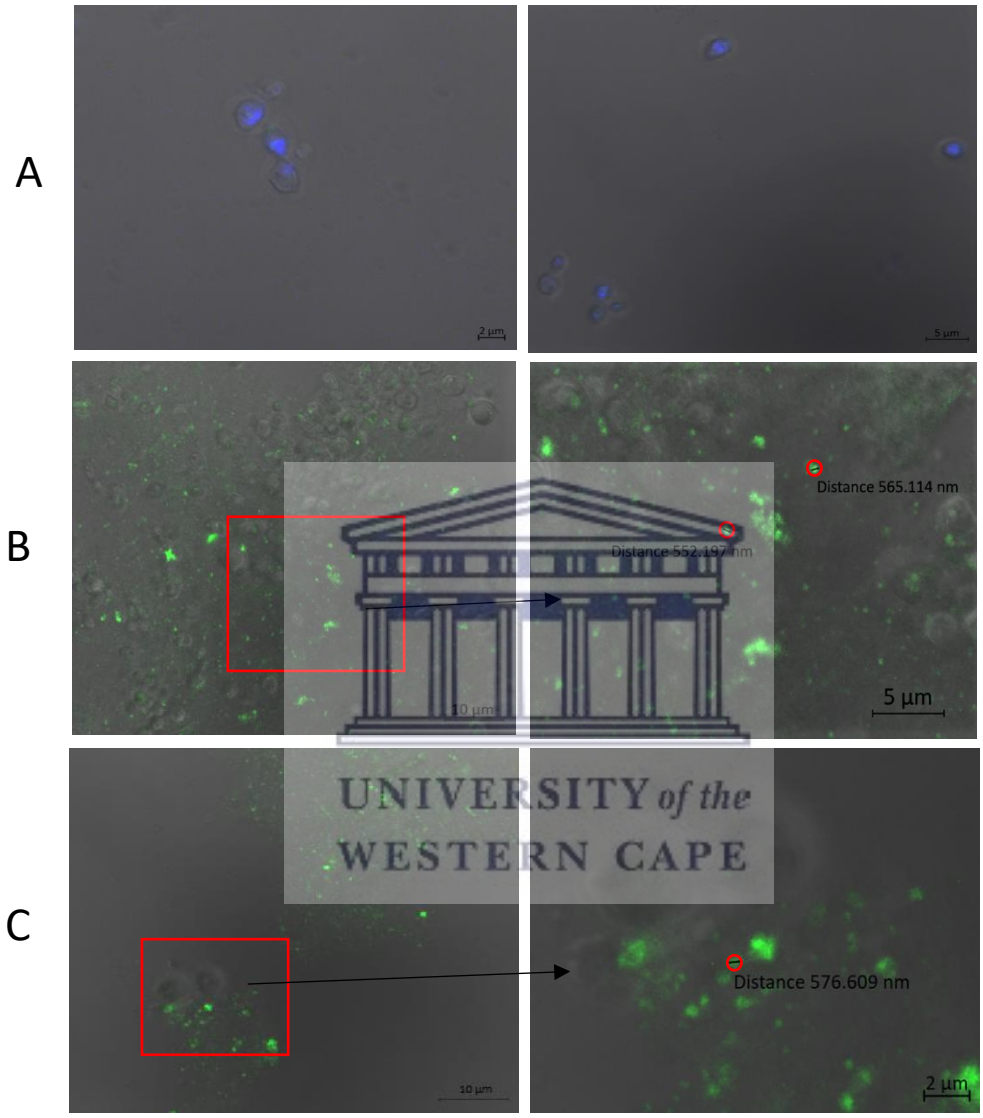




**Fig. 5.13 Confocal microscopy analysis of GFP-NPs.** The images represent a (A) control containing NucBlue nucleus dye only; (B) GFP-NPs (fixed after 1 h); (C) GFP-NPs (live sample 2-3 h of incubation). These images confirm the presence of green fluorescence, however cellular binding and uptake could not be confirmed.

Upon inspection, there appears to be guided accumulation of the what seems to be the Apt-NPs towards the cell membrane (see **Fig. 5.14** (E)), whereas random accumulation of the

unconjugated GFP-NPs or free GFP is depicted (see **Fig. 5.13** (B) and (C)). The accumulation could be explained as the aptamers bound to the NPs probably promoted the interaction between the NPs and the THP-1 cells via ligand-receptor recognition, which then acts as an anchor, pulling the NPs closer to the vicinity of the cell (see **Fig. 5.14** (E)) (Yu *et al.*, 2011; Xiao *et al.*, 2012; Xie *et al.*, 2016). Moreover, the fluorescence seen in **Fig. 5.14** (F) could be indicative of cellular autofluorescence and not internalized Apt-NPs. Further studies would be needed to confirm these findings.

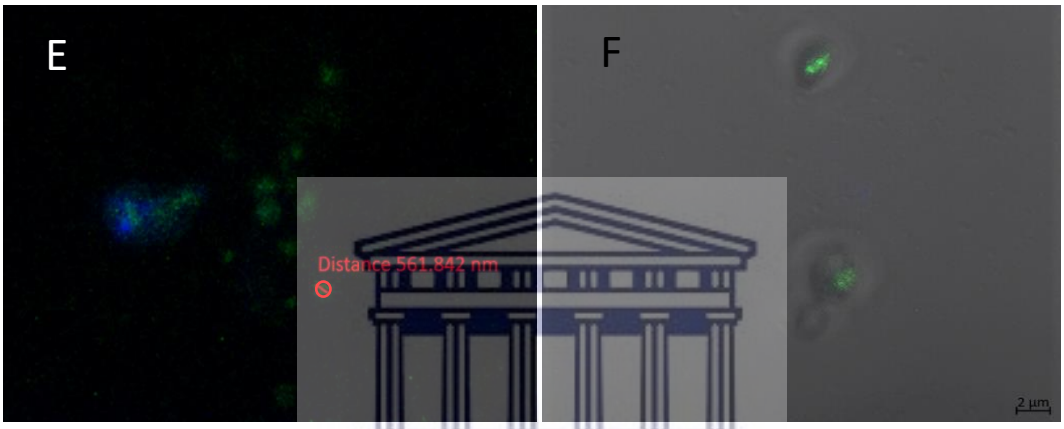


**Fig. 5.14 Confocal microscopy analysis of Apt-NPs cellular uptake.** The images represent (E) fixed Apt-NPs (fixed after 1 h) and (F) live Apt-NPs (live sample 2-3 h of incubation). The images suggest the presence of green fluorescence, although it is unclear if there are NPs present or free GFP molecules.



A possible reason for the inconclusive uptake images could be explained by the steric hinderance aptamers can cause due to their small size. The steric hinderance allows for aptamers to approach analytes more easily, promoting weak interactions between cations and the negatively charged phosphate backbone of the aptamer. Thus, this may lead to the conformational changes of binding site and cause aptamer's lower affinity to their target (Jeong and Rhee Paeng, 2012). This was shown in a previous study whereby a higher concentration of $Mg^{2+}$ ions resulted in decreased sensitivity of the aptamer to its target (Jeong and Rhee Paeng, 2012). Therefore, there is a possibility that the free $Ca^{2+}$ ions on the NP matrix, or the cations in the culture media, may induce these weak interactions with the aptamer, decreasing the affinity towards the CD4

receptor. It should be noted however, that negatively charged particles usually minimize the non-specific interaction with the negatively charged nucleic acid aptamers, thus preserving aptamer conformation and binding characteristics (Aravind *et al.*, 2012). Therefore, the strongly negative charge on the Apt-NPs may have attenuated these possible interactions. UV-Vis spectroscopy could be utilized, along with flow cytometry to further determine positive cellular internalization to reach more conclusive findings. Additionally, the approach of PEGylation could be explored to not only prolong the circulation half-life, and minimize nanoparticle aggregation, but also for reducing the interaction between the conjugated aptamers with the cations present on the NP surface (Guo *et al.*, 2011; Aravind *et al.*, 2012; Li *et al.*, 2014).

Incubation time of the NPs with the target cells could play a potential role in the uptake. Previous literature has indicated incubation of aptamer-conjugated NPs for at least 2-4 h to allow for cellular uptake (Xiao *et al.*, 2012; Alibolandi *et al.*, 2015; Venkatesan *et al.*, 2016), whereas in this current study the incubation (before fixing) was 1 h and for the live samples, 2-3 h. This could explain why the difference between the live and fixed images, as the live images had more time to allow for cellular uptake. Longer incubation time would also allow for a better understanding of the release kinetics of the Apt-NPs. Previous studies have shown the release of loaded drugs was usually after a few hours. Xing *et al*. developed CS/Alg NPs by an emulsion method to incorporate 5-FU - a pyrimidine analog drug that has been used to treat cancer for several decades. A drug release of 50% was observed at 12 h *in vitro* (Xing, Deng and Dong, 2010). Another study reported the binding of aptamer-conjugated curcumin NPs within 5 minutes of incubation, while internalization only became markedly pronounced after 60 minutes and the release of the curcumin from the NPs occurred after 8 h (Li *et al.*, 2014). This shows that although the aptamer may enhance delivery to the cells, internalization may only occur long after with an even longer release time thereafter.

The changing pH between the culture media and the cellular endosome should also be considered for the uptake and release profile of the Apt-NPs. The culture media has a pH of around 7.4, whereas the endosome has an acidic pH of around 5 (Kim *et al.*, 2010). As mentioned in **5.3**, the pH plays a vital role in the protonation ($NH_2$ to $NH_3^+$) and the deprotonation (COOH to

$COO^-$) of the weak polyelectrolytes Alg and CS (Shafie and Fayek, 2013; Rodriguez-Lorenzo *et al.*, 2014; Moore *et al.*, 2015; Rivera *et al.*, 2015; Brezaniova *et al.*, 2017; Mohammed *et al.*, 2017). In an acidic environment (pH 5), CS is protonated and Alg is deprotonated, encouraging a more compacted NP structure through electrostatic repulsion between the NPs. Therefore, uptake may be affected due to NP conformation changes in the culture media and release kinetics may be altered due to increased electrostatic repulsion in an acidic environment in the endosome. pH can also affect the fluorescent intensity of the GFP through tight packing of the protein in a compact NP matrix when the pH is acidic therefore, visibility of the protein within the cell may be decreased (Ho *et al.*, 2015).

# Conclusion and Recommendations

The aim of the study was to synthesize and characterize fluorescently labelled polymeric NPs that have the ability to be targeted to CD4 expressing cells in the hope that these NPs could be used in the future for the development of an HIV treatment. When reviewing the aims of the study, it is apparent that empty and GFP-loaded Alg-Ca-CS NPs were successfully synthesized and further characterized with DLS and SEM. Two synthesis methods were investigated, namely polyelectrolyte complexation and ionotropic gelation, of which the latter was shown to be the better method. The apparent difference in shape and structure of the NPs was observed when comparing the empty and loaded NPs. The GFP-loaded NPs indicated more defined, cuboid shaped NPs whereas, the empty NPs showed apparent structure loss. These images confirmed the loading of the GFP into the NPs. The loading of GFP was also confirmed through confocal microscopy which clearly showed the NPs fluorescing green in cell culture. The most promising finding was the Tali™ Image-Based Cytometer data, which suggested the binding or uptake of the fluorescent NPs to the THP-1 cells. DLS was used to confirm the conjugation of the Apt to the NPs whereby an increase in the overall ZP was observed after covalent linking of the Apt to the NPs. Cellular delivery of the Apt-NPs could not be confirmed as the confocal imaging was inconclusive and therefore, would need further studies to confirm positive cellular delivery and binding. Coupled with the findings and recommendations of this study, it is discernible that nanomedicine holds promise and high significance in future infectious disease management.

After reviewing the results of this study, it was apparent that various improvements could be implemented in future. Encapsulation efficiency studies could be explored to determine positive encapsulation of the protein/drug as well as to determine the maximum loading capacity of the NPs. It was evident that improved NP stability in culture media is required and could be achieved through utilizing higher polymer concentrations, using stabilizers such as TWEEN 80 or PEG and exploring alternative, stronger chemical bonds, such as covalent bonding (Masalova *et al.*, 2013; Lombardo, Kiselev and Caccamo, 2019; Zhu *et al.*, 2019; Aftab *et al.*, 2020). It would also be recommended for future studies that further characterization of aptamer conjugation be explored. Examples used in previous studies include flow cytometry, UV-vis spectroscopy (Yu *et*

*al.*, 2011; Aravind *et al.*, 2012), agarose gel electrophoresis, X-ray photoelectron spectroscopy (XPS) (Aravind *et al.*, 2012; Li *et al.*, 2014) and polyacrylamide gel electrophoresis (Xie *et al.*, 2016). Future studies should also explore the use of flow cytometry analysis for a more accurate and powerful fluorescent reading. This analysis method can detect the fluorescence of each single cell, giving more information about individual cellular uptake (Ho *et al.*, 2015). To accurately determine the binding of the aptamer conjugated NPs to the target CD4 protein, future studies could use surface plasmin resonance (SPR) and/or MicroScale Thermophoresis (MST) (Kalra *et al.*, 2018; Iyisan and Landfester, 2019). Future studies could also further explore the addition of different aptamer sequences on the NP surface to allow for enhanced cellular delivery and uptake (Ho *et al.*, 2015). Additionally, future studies should explore the inclusion of a negative control cell line that does not express CD4 receptors.

# References


Abadeer, N. S. and Murphy, C. J. (2016) 'Recent Progress in Cancer Thermal Therapy Using Gold Nanoparticles', *Journal of Physical Chemistry C*, 120(9), pp. 4691–4716. doi: 10.1021/acs.jpcc.5b11232.

Abdelhalim, M. A. K. and Jarrar, B. M. (2011) 'Renal tissue alterations were size-dependent with smaller ones induced more effects and related with time exposure of gold nanoparticles', *Journal of Cancer Science and Therapy*, 10, p. 163. doi: 10.4172/1948-5956.1000135.

Adabi, Mahdi *et al.* (2017) 'Biocompatibility and nanostructured materials: applications in nanomedicine', *Artificial Cells, Nanomedicine and Biotechnology*, 45(4), pp. 833–842. doi: 10.1080/21691401.2016.1178134.

Adamson, B. *et al.* (2017) 'The Potential Cost-Effectiveness of HIV Vaccines: A Systematic Review', *PharmacoEconomics - Open*. Springer International Publishing, 1(1), pp. 1–12. doi: 10.1007/s41669-016-0009-9.

Aftab, A. *et al.* (2020) 'Environmental Friendliness and High Performance of Multifunctional Tween 80/ZnO-Nanoparticles-Added Water-Based Drilling Fluid: An Experimental Approach', *ACS Sustainable Chemistry and Engineering*, 8, pp. 11224–11243. doi: 10.1021/acssuschemeng.0c02661.

Ahsan, S. M. *et al.* (2018) 'Chitosan as biomaterial in drug delivery and tissue engineering', *International Journal of Biological Macromolecules*. Elsevier B.V., 110, pp. 97–109. doi: 10.1016/j.ijbiomac.2017.08.140.

Akbarzadeh, A. *et al.* (2013) 'Liposome : classification , preparation , and applications', *Nanoscale Research Letters*, 8(102), pp. 1–9. doi: 10.1038/4710.

Albanese, A. and Chan, W. C. W. (2011) 'Effect of Gold Nanoparticle Aggregation on Cell Uptake and Toxicity', *ACS Nano*. American Chemical Society, 5(7), pp. 5478–5489. doi: 10.1021/nn2007496.

Alibolandi, M. *et al.* (2015) 'Epithelial cell adhesion molecule aptamer conjugated PEG-PLGA nanopolymersomes for targeted delivery of doxorubicin to human breast adenocarcinoma cell line in vitro', *International Journal of Pharmaceutics*. Elsevier B.V., 479(1), pp. 241–251. doi: 10.1016/j.ijpharm.2014.12.035.

Alkilany, A. M. *et al.* (2009) 'Cellular uptake and cytotoxicity of gold nanorods: Molecular origin of cytotoxicity and surface effects', *Small*, 5(6), pp. 701–708. doi: 10.1002/smll.200801546.

Allen, T. M. (2002) 'Ligand-targeted therapeutics in anticancer therapy', *Nature Reviews Cancer*, 2(10), pp. 750–763. doi: 10.1038/nrc903.

Aluani, D. *et al.* (2017) 'Evaluation of Biocompatibility and Antioxidant Efficiency of Chitosan-Alginate Nanoparticles Loaded With Quercetin', *International Journal of Biological Macromolecules*. Elsevier B.V., 103, pp. 771–782. doi: 10.1016/j.ijbiomac.2017.05.062.

Ananworanich, J. *et al.* (2016) 'HIV DNA Set Point is Rapidly Established in Acute HIV Infection and Dramatically Reduced by Early ART', *EBioMedicine*. The Authors, 11, pp. 68–72. doi: 10.1016/j.ebiom.2016.07.024.

Andersen, M. *et al.* (2005) 'Cytotoxic T Cells', *Comprehensive Toxicology, Second Edition*. Elsevier Masson SAS, 5(126), pp. 32–41. doi: 10.1016/B978-0-08-046884-6.00606-0.

Anthony, H. *et al.* (2019) 'Bridging the gap between HIV epidemiology and antiretroviral resistance evolution : Modelling the spread of resistance in South Africa', *Computational Biology*, 15(6), pp. 1–17.

Aravind, A. *et al.* (2012) 'Aptamer-conjugated polymeric nanoparticles for targeted cancer therapy', *Drug Delivery and Translational Research*, 2(6), pp. 418–436. doi: 10.1007/s13346-012-0104-0.

Arora, J. *et al.* (2016) 'Charge-mediated Fab-Fc interactions in an IgG1 antibody induce reversible self-association, cluster formation, and elevated viscosity', *mAbs*. Taylor & Francis, 8(8), pp. 1561–1574. doi: 10.1080/19420862.2016.1222342.

Arts, E. J. and Hazuda, D. J. (2012) 'HIV-1 antiretroviral drug therapy', *Cold Spring Harbor*

*Perspectives in Medicine*, 2(4). doi: 10.1101/cshperspect.a007161.

Avert (2019) *HIV strains and types*. Available at: https://www.avert.org/professionals/hiv-science/types-strains.

Avert (2020) *HIV and AIDS in South Africa*. Available at: https://www.avert.org/professionals/hiv-around-world/sub-saharan-africa/south-africa.

Azam, M. *et al.* (2014) 'Trends of drug-resistance-associated mutations in the reverse transcriptase gene of HIV type 1 isolates from North India', *Archives of Virology*, 159(4), pp. 719–725. doi: 10.1007/s00705-013-1889-y.

Bagre, A. P., Jain, K. and Jain, N. K. (2013) 'Alginate coated chitosan core shell nanoparticles for oral delivery of enoxaparin: in vitro and in vivo assessment.', *International journal of pharmaceutics*. Elsevier B.V., 456(1), pp. 31–40. doi: 10.1016/j.ijpharm.2013.08.037.

Balasubramanian, S. K. *et al.* (2010) 'Biodistribution of gold nanoparticles and gene expression changes in the liver and spleen after intravenous administration in rats', *Biomaterials*. Elsevier Ltd, 31(8), pp. 2034–2042. doi: 10.1016/j.biomaterials.2009.11.079.

Bandera, A. *et al.* (2019) 'Phylogenies in ART: HIV reservoirs, HIV latency and drug resistance', *Current Opinion in Pharmacology*. Elsevier Ltd, 48, pp. 24–32. doi: 10.1016/j.coph.2019.03.003.

Banik, B. L., Fattahi, P. and Brown, J. L. (2016) 'Polymeric nanoparticles: The future of nanomedicine', *Wiley Interdisciplinary Reviews: Nanomedicine and Nanobiotechnology*, 8(2), pp. 271–299. doi: 10.1002/wnan.1364.

Bauer, M. *et al.* (2019) 'Anything you can do, i can do better: Can aptamers replace antibodies in clinical diagnostic applications?', *Molecules*, 24(23), pp. 1–13. doi: 10.3390/molecules24234377.

Bekale, L., Agudelo, D. and Tajmir-Riahi, H. A. (2015) 'Effect of polymer molecular weight on chitosan-protein interaction', *Colloids and Surfaces B: Biointerfaces*. Elsevier B.V., 125, pp. 309–317. doi: 10.1016/j.colsurfb.2014.11.037.

Berezina, N. (2016) 'Production and application of chitin', *Physical Sciences Reviews*, 1(9), pp. 1–

8. doi: 10.1515/psr-2016-0048.

Berg, J. M. *et al.* (2009) 'The relationship between pH and zeta potential of ∼ 30 nm metal oxide nanoparticle suspensions relevant to in vitro toxicological evaluations', *Nanotoxicology*. Taylor & Francis, 3(4), pp. 276–283. doi: 10.3109/17435390903276941.

Bhargava, M. *et al.* (2014) 'Do HIV-1 non-B subtypes differentially impact resistance mutations and clinical disease progression in treated populations? Evidence from a systematic review', *Journal of the International AIDS Society*, 17(18944), pp. 1–6. doi: 10.7448/IAS.17.1.18944.

Bharti, C. *et al.* (2015) 'Mesoporous silica nanoparticles in target drug delivery system: A review', *International Journal of Pharmaceutical Investigation*, 5(3), pp. 124–133.

Bhattacharjee, S. (2016) 'DLS and zeta potential - What they are and what they are not?', *Journal of Controlled Release*. Elsevier B.V., 235, pp. 337–351. doi: 10.1016/j.jconrel.2016.06.017.

Bobo, D. *et al.* (2016) 'Nanoparticle-Based Medicines: A Review of FDA-Approved Materials and Clinical Trials to Date', *Pharmaceutical Research*, 33(10), pp. 2373–2387. doi: 10.1007/s11095-016-1958-5.

Brady, M. T. *et al.* (2010) 'Declines in mortality rates and changes in causes of death in HIV-1-infected children during the haart era', *Journal of Acquired Immune Deficiency Syndromes*, 53(1), pp. 86–94. doi: 10.1097/QAI.0b013e3181b9869f.

Brenchley, J. M. and Douek, D. C. (2008) 'HIV infection and the gastrointestinal immune system', *Mucosal Immunology*, 1(1), pp. 23–30. doi: 10.1038/mi.2007.1.

Brezaniova, I. *et al.* (2017) 'Self-assembled chitosan-alginate polyplex nanoparticles containing temoporfin', *Colloid and Polymer Science*. Colloid and Polymer Science, 295(8), pp. 1259–1270. doi: 10.1007/s00396-016-3992-6.

Brown, S. D. *et al.* (2010) 'Gold nanoparticles for the improved anticancer drug delivery of the active component of oxaliplatin', *Journal of the American Chemical Society*, 132(13), pp. 4678–4684. doi: 10.1021/ja908117a.

Caballero-George, C., Marin and Briceño (2013) 'Critical evaluation of biodegradable polymers used in nanodrugs', *International Journal of Nanomedicine*, p. 3071. doi: 10.2147/ijn.s47186.

Campos, E. V. R. *et al.* (2018) 'Chitosan nanoparticles functionalized with β-cyclodextrin: A promising carrier for botanical pesticides', *Scientific Reports*, 8(1), pp. 1–15. doi: 10.1038/s41598-018-20602-y.

Chavez, L., Calvanese, V. and Verdin, E. (2015) 'HIV Latency Is Established Directly and Early in Both Resting and Activated Primary CD4 T Cells', *PLoS Pathogens*, 11(6), pp. 1–21. doi: 10.1371/journal.ppat.1004955.

Chen, A. and Yang, S. (2015) 'Replacing antibodies with aptamers in lateral flow immunoassay', *Biosensors and Bioelectronics*. Elsevier, 71, pp. 230–242. doi: 10.1016/j.bios.2015.04.041.

Chen, J., Wang, F. and Liu, J. P. (2016) 'HIV Genome wide protein associations', *Microbiology and Molecular Bilogy Reviews*, 80(3), pp. 679–731. doi: 10.1128/MMBR.00065-15.Address.

Cheng, Y., Zhang, F. and Zhao, M. (2019) 'A stochastic model of HIV infection incorporating combined therapy of HAART driven by Lévy jumps', *Advances in Difference Equations*. The Author(s), 2019(1). doi: 10.1186/s13662-019-2108-2.

Choi, A. O. *et al.* (2008) 'Quantum dot-induced epigenetic and genotoxic changes in human breast cancer cells', *Journal of Molecular Medicine*, 86(3), pp. 291–302. doi: 10.1007/s00109-007-0274-2.

Choi, Y. H. and Han, H. K. (2017) 'Nanomedicines: current status and future perspectives in aspect of drug delivery and pharmacokinetics', *Journal of Pharmaceutical Investigation*. Springer Netherlands, 48(1), pp. 43–60. doi: 10.1007/s40005-017-0370-4.

Chu, M. *et al.* (2010) 'Transfer of quantum dots from pregnant mice to pups across the placental barrier', *Small*, 6(5), pp. 670–678. doi: 10.1002/smll.200902049.

Clutter, D. S. *et al.* (2017) 'HHS Public Access', *Infect Genet Evol*, (46), pp. 292–307. doi: 10.1016/j.meegid.2016.08.031.HIV-1.

Collier, A. C. *et al.* (1996) 'Treatment of human immunodeficiency virus infection with saquinavir, zidovudine, and zalcitabine', *New England Journal of Medicine*, 334(16), pp. 1011–1017. doi: 10.1056/NEJM199604183341602.

Conde, J. *et al.* (2014) 'Revisiting 30 years of biofunctionalization and surface chemistry of inorganic nanoparticles for nanomedicine', *Frontiers in Chemistry*, 2(JUL), pp. 1–27. doi: 10.3389/fchem.2014.00048.

Cordeiro, M. *et al.* (2016) 'Gold nanoparticles for diagnostics: Advances towards points of care', *Diagnostics*, 6(4). doi: 10.3390/diagnostics6040043.

Couturier, J. and Lewis, D. E. (2018) 'HIV Persistence in Adipose Tissue Reservoirs', *Current HIV/AIDS Reports*, 15(1), pp. 60–71. doi: 10.1007/s11904-018-0378-z.

Cranfill, P. J. *et al.* (2016) 'Quantitative assessment of fluorescent proteins', *Nature Methods*, 13(7), pp. 557–562. doi: 10.1038/nmeth.3891.

Cullen, B. and Greene, W. C. (1989) 'Regulatroy pathways governing HIV-1 replication', *Cell*, 58(3), pp. 423–426.

D'Aquila, R. *et al.* (1996) 'Nevirapine, zidovudine, and didanosine compared with zidovudine and didanosine in patients with HIV-1 infection a randomized, double-blind, placebo-controlled trial', *Annals of Internal Medicine*, 124(12), pp. 1019–1030.

D'Mello, S. R. *et al.* (2017) 'The evolving landscape of drug products containing nanomaterials in the United States', *Nature Nanotechnology*. Nature Publishing Group, 12(6), pp. 523–529. doi: 10.1038/nnano.2017.67.

Di, Y. *et al.* (2019) 'Fundus manifestations and HIV viral loads of AIDS patients before and after HAART', *International Journal of Ophthalmology*, 12(9), pp. 1438–1443. doi: 10.18240/ijo.2019.09.11.

Doitsh, G. and Greene, W. C. (2016) 'Dissecting How CD4 T Cells Are Lost during HIV Infection', *Cell Host and Microbe*. Elsevier Inc., 19(3), pp. 280–291. doi: 10.1016/j.chom.2016.02.012.

Domingos, R. F. *et al.* (2009) 'Characterizing manufactured nanoparticles in the environment: Multimethod determination of particle sizes', *Environmental Science and Technology*, 43(19), pp. 7277–7284. doi: 10.1021/es900249m.

Doshi, N. and Mitragotri, S. (2009) 'Designer biomaterials for nanomedicine', *Advanced Functional Materials*, 19(24), pp. 3843–3854. doi: 10.1002/adfm.200901538.

Douek, D. C., Picker, L. J. and Koup, R. A. (2003) 'T Cell Dynamics in HIV-1 Infection', *Annual Review of Immunology*. Annual Reviews, 21(1), pp. 265–304. doi: 10.1146/annurev.immunol.21.120601.141053.

Douglas, K. L., Piccirillo, C. A. and Tabrizian, M. (2006) 'Effects of alginate inclusion on the vector properties of chitosan-based nanoparticles', *Journal of Controlled Release*, 115(3), pp. 354–361. doi: 10.1016/j.jconrel.2006.08.021.

Dube, A. (2011) *Assessment of the impact of biopolymeric nanoparticles on the oral absorption of green tea catechins*.

Edwards, S. A. and Williams, D. R. M. (2004) 'Double Layers and Interparticle Forces in Colloid Science and Biology: Analytic Results for the Effect of Ionic Dispersion Forces', *Physical Review Letters*. American Physical Society, 92(24), p. 248303. doi: 10.1103/PhysRevLett.92.248303.

Ellington, A. D. and Szostak, J. W. (1990) 'In vitro selection of RNA molecules that bind specific ligands', *Nature*, 346(6287), pp. 818–822. doi: 10.1038/346818a0.

EMEA (2006) 'Reflection Paper on Nanotechnology-Based Medicinal Products for Human Use', *European Medicines Agency*, (June), p. s. 3. Available at: http://www.emea.eu.inthttp//www.emea.eu.int/htms/human/itf/itfguide.htm.

Engelman, A. and Cherepanov, P. (2013) 'The structural biology of HIV-1: mechanistic and therapeutic insights', *Nature reviews. Microbiology*, 10(4), pp. 279–290. doi: 10.1038/nrmicro2747.The.

Fitzpatrick, J. A. J. *et al.* (2009) 'Long-term persistence and spectral blue shifting of quantum dots in vivo', *Nano Letters*, 9(7), pp. 2736–2741. doi: 10.1021/nl901534q.

Flühmann, B. *et al.* (2018) 'Nanomedicines: The magic bullets reaching their target?', *European Journal of Pharmaceutical Sciences*. Elsevier, 128(2019), pp. 73–80. doi: 10.1016/j.ejps.2018.11.019.

Foged, C. *et al.* (2005) 'Particle size and surface charge affect particle uptake by human dendritic cells in an in vitro model', 298, pp. 315–322. doi: 10.1016/j.ijpharm.2005.03.035.

Freed, E. O. (2016) 'HIV-1 assembly, release and maturation', *Nature reviews. Microbiology*, 13(8), pp. 484–496. doi: 10.1016/j.physbeh.2017.03.040.

Friedman, M. and Juneja, V. (2010) 'Review of Antimicrobial and Antioxidative Activities of Chitosans in Food', *Journal of Food Protection*, 73(9), pp. 1737–1761.

Gallego-Urrea, J. A., Perez-Holmberga, J. and Hassellöv, M. (2012) 'Influence of different types of natural organic matter on titania nanoparticles stability: effects of counter ion concentration and pH', *Royal Society of Chemsitry*, 12(00), pp. 731–738. doi: 10.1039/x0xx00000x.

Galvis, A. E. (2014) 'An RNA Lariat Intermediate in HIV-1 cDNA Synthesis', *Research Gate*, (November). Available at: https://www.researchgate.net/publication/284360827.

Gauthier, M. and Klok, H.-A. (2010) 'Polymer-protein conjugates: an enzymatic activity perspective', *Polymer Chemistry*, 1, pp. 1352–1373.

Gebauer, J. S. *et al.* (2012) 'Impact of the nanoparticle-protein corona on colloidal stability and protein structure', *Langmuir*, 28(25), pp. 9673–9679. doi: 10.1021/la301104a.

Geys, J. *et al.* (2008) 'Acute toxicity and prothrombotic effects of Quantum dots: Impact of surface charge', *Environmental Health Perspectives*, 116(12), pp. 1607–1613. doi: 10.1289/ehp.11566.

Ghosh, S. *et al.* (2011) 'Colloidal Stability of Magnetic Iron Oxide Nanoparticles: Influence of Natural Organic Matter and Synthetic Polyelectrolytes', *Langmuir*. American Chemical Society, 27(13), pp. 8036–8043. doi: 10.1021/la200772e.

Giner-Casares, J. J. *et al.* (2016) 'Inorganic nanoparticles for biomedicine: Where materials scientists meet medical research', *Materials Today*, 19(1), pp. 19–28. doi:

10.1016/j.mattod.2015.07.004.

Glowicz (2015) 'Role of myeloid cells in HIV-1- host interplay', *Physiology & behavior*, 21(3), pp. 242–248. doi: 10.1016/j.physbeh.2017.03.040.

Gordillo-Galeano, A. and Mora-Huertas, C. E. (2018) 'Solid lipid nanoparticles and nanostructured lipid carriers: A review emphasizing on particle structure and drug release', *European Journal of Pharmaceutics and Biopharmaceutics*. Elsevier, 133(August), pp. 285–308. doi: 10.1016/j.ejpb.2018.10.017.

Gray, G. E. *et al.* (2016) 'Approaches to preventative and therapeutic HIV vaccines', *Current Opinion in Virology*. Elsevier B.V., 17(li), pp. 104–109. doi: 10.1016/j.coviro.2016.02.010.

Gulick, R. *et al.* (1997) 'With Human Immunodeficiency Virus Infection and Prior Antiretroviral Therapy', *The New England Journal of Medicine*, 337(11), pp. 734–739.

Guo, J. *et al.* (2011) 'Aptamer-functionalized PEG-PLGA nanoparticles for enhanced anti-glioma drug delivery', *Biomaterials*. Elsevier Ltd, 32(31), pp. 8010–8020. doi: 10.1016/j.biomaterials.2011.07.004.

Hafner, A. *et al.* (2014) 'Nanotherapeutics in the EU: An overview on current state and future directions', *International Journal of Nanomedicine*, 9(1), pp. 1005–1023. doi: 10.2147/IJN.S55359.

Haji, M. *et al.* (2018) 'European Journal of Pharmaceutics and Biopharmaceutics Development of a non-toxic and non-denaturing formulation process for encapsulation of SDF-1 α into PLGA / PEG-PLGA nanoparticles to achieve sustained release', *European Journal of Pharmaceutics and Biopharmaceutics*. Elsevier, 125(January), pp. 38–50. doi: 10.1016/j.ejpb.2017.12.020.

Han, Y. *et al.* (2016) 'Review: Imaging technologies for flow cytometry', *Lab on a Chip*, 16(24), pp. 4639–4647. doi: 10.1039/c6lc01063f.

Hanafy, N. A. N., El-Kemary, M. and Leporatti, S. (2018) 'Micelles structure development as a strategy to improve smart cancer therapy', *Cancers*, 10(7), pp. 1–14. doi: 10.3390/cancers10070238.

Hanini, A. *et al.* (2011) 'Evaluation of iron oxide nanoparticle biocompatibility', *International Journal of Nanomedicine*, (6), p. 787. doi: 10.2147/ijn.s17574.

Harper, S. and Speicher, D. (2011) 'Purification of proteins fused to glutathione S-tranferase', *Methods in molecular biology*, 681(3), pp. 259–280. doi: 10.1007/978-1-60761-913-0.

Henrich, T. J. *et al.* (2017) 'HIV-1 persistence following extremely early initiation of antiretroviral therapy (ART) during acute HIV-1 infection: An observational study', *PLoS Medicine*, 14(11), pp. 1–22. doi: 10.1371/journal.pmed.1002417.

HHS (2014) *Guide for HIV/AIDS clinical care*.

Ho, L. C. *et al.* (2015) 'Aptamer-conjugated polymeric nanoparticles for the detection of cancer cells through "turn-On" retro-self-quenched fluorescence', *Analytical Chemistry*, 87(9), pp. 4925–4932. doi: 10.1021/acs.analchem.5b00569.

Huang, X., Cavalcante, D. P. and Townley, H. E. (2020) 'Macrophage-like THP-1 cells show effective uptake of silica nanoparticles carrying inactivated diphtheria toxoid for vaccination', *Journal of Nanoparticle Research*, 22(1), pp. 1–23. doi: 10.1007/s11051-019-4720-1.

Huang, Y. *et al.* (2019) 'A framework for identification of on- and off-target transcriptional responses to drug treatment', *Scientific Reports*. Springer US, 9(1), pp. 1–9. doi: 10.1038/s41598-019-54180-4.

Iacob, S. A., Iacob, D. G. and Jugulete, G. (2017) 'Improving the adherence to antiretroviral therapy, a difficult but essential task for a successful HIV treatment-clinical points of view and practical considerations', *Frontiers in Pharmacology*, 8(831), pp. 1–12. doi: 10.3389/fphar.2017.00831.

Ibrahim, M. M. *et al.* (2013) 'Natural bioadhesive biodegradable nanoparticles-based topical ophthalmic formulations for sustained celecoxib release: in vitro study', *journal of Pharmaceutical Technology and Drug Research*, 2(1), p. 7. doi: 10.7243/2050-120x-2-7.

Iyisan, B. and Landfester, K. (2019) 'Modular Approach for the Design of Smart Polymeric Nanocapsules', *Macromolecular Rapid Communications*, 40(1). doi: 10.1002/marc.201800577.

Jain, A. *et al.* (2018) 'Protein Nanoparticles: Promising Platforms for Drug Delivery Applications', *ACS Biomaterials Science and Engineering*, 4(12), pp. 3939–3961. doi: 10.1021/acsbiomaterials.8b01098.

Jakobsen, M. R. *et al.* (2013) 'IFI16 senses DNA forms of the lentiviral replication cycle and controls HIV-1 replication', *Proceedings of the National Academy of Sciences of the United States of America*, 110(48). doi: 10.1073/pnas.1311669110.

Jeong, S. and Rhee Paeng, I. (2012) 'Sensitivity and selectivity on aptamer-based assay: The determination of tetracycline residue in bovine milk', *The Scientific World Journal*, pp. 1–10. doi: 10.1100/2012/159456.

Jiang, C. *et al.* (2014) 'Crosslinked polyelectrolyte complex fiber membrane based on chitosan-sodium alginate by freeze-drying', *RCS Advances*, 4, pp. 41551–41560. doi: 10.1039/C6LC01362G.

Kalra, P. *et al.* (2018) 'Simple methods and rational design for enhancing aptamer sensitivity and specificity', *Frontiers in Molecular Biosciences*, 5(MAY), pp. 1–16. doi: 10.3389/fmolb.2018.00041.

Kashyap, P. L., Xiang, X. and Heiden, P. (2015) 'Chitosan nanoparticle based delivery systems for sustainable agriculture', *International Journal of Biological Macromolecules*. Elsevier B.V., 77, pp. 36–51. doi: 10.1016/j.ijbiomac.2015.02.039.

Katuwavila, N. P. *et al.* (2016) 'Chitosan-Alginate Nanoparticle System Efficiently Delivers Doxorubicin to MCF-7 Cells', *Journal of Nanomaterials*, 2016, p. 12.

Kawai, T. and Akira, S. (2010) 'The role of pattern-recognition receptors in innate immunity: Update on toll-like receptors', *Nature Immunology*. Nature Publishing Group, 11(5), pp. 373–384. doi: 10.1038/ni.1863.

Kesharwani, P., Jain, K. and Jain, N. K. (2014) 'Dendrimer as nanocarrier for drug delivery', *Progress in Polymer Science*. Elsevier Ltd, 39(2), pp. 268–307. doi: 10.1016/j.progpolymsci.2013.07.005.

Kim, D. *et al.* (2016) 'Predicting unintended effects of drugs based on off-target tissue effects',

*Biochemical and Biophysical Research Communications*. Elsevier Ltd, 469(3), pp. 399–404. doi: 10.1016/j.bbrc.2015.11.095.

Kim, E. *et al.* (2010) 'Prostate cancer cell death produced by the co-delivery of Bcl-xL shRNA and doxorubicin using an aptamer-conjugated polyplex', *Biomaterials*. Elsevier Ltd, 31(16), pp. 4592–4599. doi: 10.1016/j.biomaterials.2010.02.030.

Kiptoo, M. *et al.* (2013) 'HIV-1 drug resistance-associated mutations among HIV-1 infected drug-naïve antenatal clinic attendees in rural Kenya', *BMC Infectious Diseases*, 13(1), pp. 2–5. doi: 10.1186/1471-2334-13-517.

Klatt, E. C. (2019) 'PATHOLOGY OF HIV / AIDS', pp. 1–336.

Klatt, N. R., Funderburg, N. T. and Brenchley, J. M. (2013) 'Microbial translocation, immune activation, and HIV disease', *Trends in Microbiology*. doi: 10.1016/j.tim.2012.09.001.

Kloster, N. and Avena, M. (2015) 'Interaction of humic acids with soil minerals: adsorption and surface aggregation induced by Ca2+', *Environmental Chemistry*, 12(6), pp. 731–738. Available at: https://doi.org/10.1071/EN14157.

Knyazhanskaya, E. S. *et al.* (2016) 'Role of DNA-dependent protein kinase in the HIV-1 replication cycle', *Molecular Biology*, 50(4), pp. 567–579. doi: 10.1134/S0026893316040075.

Konopka, K. and Düzgüneş, N. (2002) 'Expression of CD4 controls the susceptibility of THP-1 cells to infection by R5 and X4 HIV type 1 isolates', *AIDS Research and Human Retroviruses*, 18(2), pp. 123–131. doi: 10.1089/08892220252779665.

Kramer, R. M. *et al.* (2012) 'Toward a molecular understanding of protein solubility: Increased negative surface charge correlates with increased solubility', *Biophysical Journal*. Biophysical Society, 102(8), pp. 1907–1915. doi: 10.1016/j.bpj.2012.01.060.

Kumar, S. *et al.* (2015) 'Development and evaluation of alginate-chitosan nanocapsules for controlled release of acetamiprid', *International Journal of Biological Macromolecules*. Elsevier B.V., 81, pp. 631–637. doi: 10.1016/j.ijbiomac.2015.08.062.

Laber, J. R. *et al.* (2017) 'Charge Shielding Prevents Aggregation of Supercharged GFP Variants at High Protein Concentration', *Molecular Pharmaceutics*, 14(10), pp. 3269–3280. doi: 10.1021/acs.molpharmaceut.7b00322.

Lambotin, M. *et al.* (2010) 'A look behind closed doors: Interaction of persistent viruses with dendritic cells', *Nature Reviews Microbiology*. Nature Publishing Group, 8(5), pp. 350–360. doi: 10.1038/nrmicro2332.

Larson, T. A., Joshi, P. P. and Sokolov, K. (2012) 'Preventing protein adsorption and macrophage uptake of gold nanoparticles via a hydrophobic shield', *ACS Nano*, 6(10), pp. 9182–9190. doi: 10.1021/nn3035155.

Laws, M. B. *et al.* (2019) 'An instrument to assess HIV-related knowledge and adjustment to HIV+ status, and their association with anti-retroviral adherence'.

Legrice, S. and Gotte, M. (2013) *Immunode ciency Virus Reverse Transcriptase*. Springer.

Lesniak, A. *et al.* (2012) 'Effects of the presence or absence of a protein corona on silica nanoparticle uptake and impact on cells', *ACS Nano*, 6(7), pp. 5845–5857. doi: 10.1021/nn300223w.



Li *et al.* (2014) 'Epithelial cell adhesion molecule aptamer functionalized PLGA-lecithin-curcumin-PEG nanoparticles for targeted drug delivery to human colorectal adenocarcinoma cells', *International Journal of Nanomedicine*, 9, pp. 1083–1096.

Li, J. *et al.* (2014) 'Toxicity of inorganic nanomaterials in biomedical imaging', *Biotechnology Advances*. Elsevier Inc., 32(4), pp. 727–743. doi: 10.1016/j.biotechadv.2013.12.009.

Li, M. *et al.* (2019) 'Composition design and medical application of liposomes', *European Journal of Medicinal Chemistry*, 164, pp. 640–653. doi: 10.1016/j.ejmech.2019.01.007.

Lima, D. S. *et al.* (2018) 'pH-responsive alginate-based hydrogels for protein delivery', *Journal of Molecular Liquids*. Elsevier B.V., 262, pp. 29–36. doi: 10.1016/j.molliq.2018.04.002.

Ling, K. *et al.* (2019) 'Alginate/chitosan microparticles for gastric passage and intestinal release

of therapeutic protein nanoparticles', *Journal of Controlled Release*. Elsevier, 295, pp. 174–186. doi: 10.1016/j.jconrel.2018.12.017.

Liu, J. *et al.* (2019) 'Alginate Oligosaccharides: Production, Biological Activities, and Potential Applications', *Comprehensive Reviews in Food Science and Food Safety*, 18(6), pp. 1859–1881. doi: 10.1111/1541-4337.12494.

Liu, Q. *et al.* (2020) 'Fabrication of curcumin-loaded zein nanoparticles stabilized by sodium caseinate/sodium alginate: Curcumin solubility, thermal properties, rheology, and stability', *Process Biochemistry*. Elsevier, 94(November 2019), pp. 30–38. doi: 10.1016/j.procbio.2020.03.017.

Lodge, R. *et al.* (2017) 'Regulation of CD4 receptor and HIV-1 entry by microRNAs-221 and -222 during differentiation of THP-1 cells', *Viruses*, 10(1), pp. 1–18. doi: 10.3390/v10010013.

Lombardo, D., Kiselev, M. A. and Caccamo, M. T. (2019) 'Smart Nanoparticles for Drug Delivery Application: Development of Versatile Nanocarrier Platforms in Biotechnology and Nanomedicine', *Journal of Nanomaterials*, 2019, p. 26. doi: 10.1155/2019/3702518.

Lopes, M. *et al.* (2016) 'Dual chitosan/albumin-coated alginate/dextran sulfate nanoparticles for enhanced oral delivery of insulin', *Journal of Controlled Release*. Elsevier B.V., 232, pp. 29–41. doi: 10.1016/j.jconrel.2016.04.012.

Loquercio, A. *et al.* (2015) 'Preparation of Chitosan-Alginate Nanoparticles for Trans-cinnamaldehyde Entrapment', *Journal of Food Science*, 80(10), pp. N2305–N2315. doi: 10.1111/1750-3841.12997.

Lorenzo-Redondo, R. *et al.* (2016) 'Persistent HIV-1 replication maintains the tissue reservoir during therapy', *Nature*, 530(7588), pp. 51–56. doi: 10.1016/j.physbeh.2017.03.040.

Luo, X. lu *et al.* (2019) 'Incidence and types of HIV-1 drug resistance mutation among patients failing first-line antiretroviral therapy', *Journal of Pharmacological Sciences*, 139(4), pp. 275–279. doi: 10.1016/j.jphs.2018.11.016.

Luo, Y. and Wang, Q. (2014) 'Recent development of chitosan-based polyelectrolyte complexes

with natural polysaccharides for drug delivery', *International Journal of Biological Macromolecules*. Elsevier B.V., 64, pp. 353–367. doi: 10.1016/j.ijbiomac.2013.12.017.

Mahl, D. *et al.* (2010) 'Gold nanoparticles: dispersibility in biological media and cell-biological effect', *Journal of Materials Chemistry*. The Royal Society of Chemistry, 20(29), pp. 6176–6181. doi: 10.1039/C0JM01071E.

Malakar, P. *et al.* (2014) 'Effect on β-galactosidase synthesis and burden on growth of osmotic stress in Escherichia coli', *SpringerPlus*, 3(1), pp. 1–10. doi: 10.1186/2193-1801-3-748.

Manzano, M. and Vallet-Regí, M. (2018) 'Mesoporous silica nanoparticles in nanomedicine applications', *Journal of Materials Science: Materials in Medicine*. Springer US, 29(5), p. 65. doi: 10.1007/s10856-018-6069-x.

Martin, D. R. (2018) 'The identification of aptamers against serum biomarkers of human tuberculosis'.

Martin, M. N. *et al.* (2014) 'Dissolution, agglomerate morphology, and stability limits of protein-coated silver nanoparticles', *Langmuir*, 30(38), pp. 11442–11452. doi: 10.1021/la502973z.

Martinelli, C., Pucci, C. and Ciofani, G. (2019) 'Nanostructured carriers as innovative tools for cancer diagnosis and therapy', *APL Bioengineering*, 3(1), pp. 011502-1–13. doi: 10.1063/1.5079943.

Masalova, O. *et al.* (2013) 'Alginate and chitosan gel nanoparticles for efficient protein entrapment', *Physics Procedia*. Elsevier B.V., 40, pp. 69–75. doi: 10.1016/j.phpro.2012.12.010.

Maso, K. *et al.* (2019) 'Molecular platforms for targeted drug delivery', in *International Review of Cell and Molecular Biology*, pp. 1–36.

Mbunkah, H. A. *et al.* (2019) 'Low-Abundance Drug-Resistant HIV-1 Variants in Antiretroviral Drug-Naive Individuals: A Systematic Review of Detection Methods, Prevalence, and Clinical Impact', *The Journal of Infectious Diseases*, (December). doi: 10.1093/infdis/jiz650.

Medley, C. D. *et al.* (2011) 'Aptamer-conjugated nanoparticles for cancer cell detection',

*Analytical Chemistry*, 83(3), pp. 727–734. doi: 10.1021/ac102263v.

Medzhitov, R. (2007) 'Recognition of microorganisms and activation of the immune response', *Nature*, 449(7164), pp. 819–826. doi: 10.1038/nature06246.

Le Meins, J. F., Sandre, O. and Lecommandoux, S. (2011) 'Recent trends in the tuning of polymersomes' membrane properties', *European Physical Journal E*, 34(14), pp. 3–17. doi: 10.1140/epje/i2011-11014-y.

van der Merwe, C. (2019) 'The association between fracture risk and bone mineral density in black postmenopausal HIV-positive women on HAART C van der Merwe Supervisor ':, (May).

Miao, L. *et al.* (2016) 'Effect of alginate on the aggregation kinetics of copper oxide nanoparticles (CuO NPs): bridging interaction and hetero-aggregation induced by Ca2+', *Environmental Science and Pollution Research*, 23(12), pp. 11611–11619. doi: 10.1007/s11356-016-6358-1.

Mohammed, M. A. *et al.* (2017) 'An overview of chitosan nanoparticles and its application in non-parenteral drug delivery', *Pharmaceutics*, 9(4). doi: 10.3390/pharmaceutics9040053.

Mongo-delis, A. *et al.* (2019) 'Factors associated with adherence to ARV treatment in people living with HIV / AIDS in a rural area ( Koula-Moutou ) in East Gabon Factors associated with adherence to ARV treatment in people living with', *African Journal of AIDS Research*, 18(1), pp. 51–57. doi: 10.2989/16085906.2018.1552878.

Monroe, K. M. *et al.* (2014) 'IFI16 DNA Sensor Is Required for', *Science (New York, N.Y.)*, 343(January), pp. 428–432. doi: 10.1126/science.1243640.

Moore, T. L. *et al.* (2015) 'Nanoparticle colloidal stability in cell culture media and impact on cellular interactions', *Chemical Society Reviews*. Royal Society of Chemistry, 44(17), pp. 6287–6305. doi: 10.1039/c4cs00487f.

Morin-Crini, N. *et al.* (2019) 'Applications of chitosan in food, pharmaceuticals, medicine, cosmetics, agriculture, textiles, pulp and paper, biotechnology, and environmental chemistry', *Environmental Chemistry Letters*. Springer International Publishing, 17(4), pp. 1667–1692. doi: 10.1007/s10311-019-00904-x.

Morsi, N. *et al.* (2015) 'Preparation and evaluation of alginate/chitosan nanodispersions for ocular delivery', *International Journal of Pharmacy and Pharmaceutical Sciences*, 7(7), pp. 234–240.

Mulder, M. B. *et al.* (2019) 'Comparison of hypersensitivity reactions of intravenous iron: iron isomaltoside-1000 (Monofer ® ) versus ferric carboxy-maltose (Ferinject ® ). A single center, cohort study', *British Journal of Clinical Pharmacology*, 85(2), pp. 385–392. doi: 10.1111/bcp.13805.

Murugadoss, S. *et al.* (2017) 'Toxicology of silica nanoparticles: an update', *Archives of Toxicology*. Springer Berlin Heidelberg, 91(9), pp. 2967–3010. doi: 10.1007/s00204-017-1993-y.

Nasir, A., Kausar, A. and Younus, A. (2015) 'A Review on Preparation, Properties and Applications of Polymeric Nanoparticle-Based Materials', *Polymer - Plastics Technology and Engineering*. 2015, 54(4), pp. 325–341. doi: 10.1080/03602559.2014.958780.

Nel, A. E. *et al.* (2009) 'Understanding biophysicochemical interactions at the nano–bio interface', *Nature Materials*, 8(7), pp. 543–557. doi: 10.1038/nmat2442.

Nezlin, R. (2016) 'Use of aptamers in immunoassays', *Molecular Immunology*. Elsevier Ltd, 70, pp. 149–154. doi: 10.1016/j.molimm.2015.12.009.

NIH (2020) *List of Approved HIV Antiretroviral Drugs*, *US National Library of Medicine*. Available at: https://aidsinfo.nih.gov/understanding-hiv-aids/fact-sheets/21/58/fda-approved-hiv-medicines.

Nimjee, S. *et al.* (2017) 'Aptamers as Therapeutics', *Annual Review of Pharmacological Toxicology*, 57, pp. 61–79. doi: 10.1016/j.physbeh.2017.03.040.

Nissen, S. K. *et al.* (2014) 'Innate DNA sensing is impaired in HIV patients and IFI16 expression correlates with chronic immune activation', *Clinical and Experimental Immunology*, 177(1), pp. 295–309. doi: 10.1111/cei.12317.

Nolles, A. *et al.* (2015) 'Encapsulation of GFP in complex coacervate core micelles', *Biomacromolecules*, 16(5), pp. 1542–1549. doi: 10.1021/acs.biomac.5b00092.

Noorbakhsh-Soltani, S. M., Zerafat, M. M. and Sabbaghi, S. (2018) 'A comparative study of gelatin and starch-based nano-composite films modified by nano-cellulose and chitosan for food packaging applications', *Carbohydrate Polymers*. Elsevier, 189(February), pp. 48–55. doi: 10.1016/j.carbpol.2018.02.012.

Noori, A. *et al.* (2011) 'Effect of magnetic iron oxide nanoparticles on pregnancy and testicular development of mice', *African Journal of Biotechnology*, 10(7), pp. 1221–1227. doi: 10.1016/j.clinbiochem.2011.08.796.

Nurfalah, F., Yona, S. and Waluyo, A. (2019) 'The relationship between HIV stigma and adherence to antiretroviral (ARV) drug therapy among women with HIV in Lampung, Indonesia', *Elsevier*, 29(2), pp. 234–237.

Onoue, S., Yamada, S. and Chan, H. K. (2014) 'Nanodrugs: Pharmacokinetics and safety', *International Journal of Nanomedicine*, 9(1), pp. 1025–1037. doi: 10.2147/IJN.S38378.

Paliwal, R., Babu, R. J. and Palakurthi, S. (2014) 'Nanomedicine Scale-up Technologies: Feasibilities and Challenges', *Ageing International*, 15(6), pp. 1527–1534. doi: 10.1208/s12249-014-0177-9.

Palve, V. *et al.* (2020) 'Turning liabilities into opportunities: Off-target based drug repurposing in cancer', *Seminars in Cancer Biology*. Elsevier, pp. 1–21. doi: 10.1016/j.semcancer.2020.02.003.

Patel, N. *et al.* (2016) 'Development and evaluation of a calcium alginate based oral ceftriaxone sodium formulation', *Progress in Biomaterials*. Springer Berlin Heidelberg, 5(2), pp. 117–133. doi: 10.1007/s40204-016-0051-9.

Patra, J. K. *et al.* (2018) 'Nano based drug delivery systems: Recent developments and future prospects 10 Technology 1007 Nanotechnology 03 Chemical Sciences 0306 Physical Chemistry (incl. Structural) 03 Chemical Sciences 0303 Macromolecular and Materials Chemistry 11 Medical and He', *Journal of Nanobiotechnology*. BioMed Central, 16(1), pp. 1–33. doi: 10.1186/s12951-018-0392-8.

Pawley, J. (2006) *Confocal Handbook.Pdf*.

Pennock, N. D. *et al.* (2013) 'T cell responses: Naïve to memory and everything in between', *American Journal of Physiology - Advances in Physiology Education*, 37(4), pp. 273–283. doi: 10.1152/advan.00066.2013.

Peshkovsky, A. S., Peshkovsky, S. L. and Bystryak, S. (2013) 'Scalable high-power ultrasonic technology for the production of translucent nanoemulsions', *Chemical Engineering and Processing: Process Intensification*. Elsevier B.V., 69, pp. 77–82. doi: 10.1016/j.cep.2013.02.010.

Pis, A., Islam, M. A. and Hasan, N. (2017) 'Effect of pressure on homogenization', *Research Gate*, 35, pp. 1–22.

Quinones-Mateu, M. and Arts, E. (2001) 'HIV1 Fitness: Implications for Drug Resistance, Disease Progression, and Global Epidemic Evolution', *HIV Sequence Compendium*.

Quiñones-Mateu, M. and Arts, E. (2001) 'HIV-1 fitness: implications for drug resistance, disease progression, and global epidemic evolution', *HIV sequence compendium*, 2001(January), pp. 134–170.

Rausch, K. *et al.* (2010) 'Evaluation of Nanoparticle Aggregation in Human Blood Serum', *Biomacromolecules*. American Chemical Society, 11(11), pp. 2836–2839. doi: 10.1021/bm100971q.



Rinaudo, M. and Goycoolea, F. M. (2019) *Advances in Chitin/Chitosan Characterization and Applications*, *Advances in Chitin/Chitosan Characterization and Applications*. doi: 10.3390/books978-3-03897-803-9.

Rivera, M. C. *et al.* (2015) 'Hollow chitosan/alginate nanocapsules for bioactive compound delivery', *International Journal of Biological Macromolecules*. Elsevier B.V., 79, pp. 95–102. doi: 10.1016/j.ijbiomac.2015.03.003.

Rodriguez-Lorenzo, L. *et al.* (2014) 'Fluorescence-encoded gold nanoparticles: Library design and modulation of cellular uptake into dendritic cells', *Small*, 10(7), pp. 1341–1350. doi: 10.1002/smll.201302889.

Rubio-Elizalde, I. *et al.* (2019) 'Scaffolds based on alginate-PEG methyl ether methacrylate-

Moringa oleifera-Aloe vera for wound healing applications', *Carbohydrate Polymers*. Elsevier, 206(3918), pp. 455–467. doi: 10.1016/j.carbpol.2018.11.027.

Rudmann, D. G. (2013) 'On-target and off-target-based toxicologic effects', *Toxicologic Pathology*, 41(2), pp. 310–314. doi: 10.1177/0192623312464311.

Sabuncu, A. C. *et al.* (2012) 'Probing nanoparticle interactions in cell culture media', *Colloids and Surfaces B: Biointerfaces*. Elsevier B.V., 95, pp. 96–102. doi: 10.1016/j.colsurfb.2012.02.022.

Sadaf, A. *et al.* (2012) 'Toxicity Evaluation of Hydrophilic CdTe Quantum Dots and CdTe@SiO2 Nanoparticles in Mice', *Journal of Nanoscience and Nanotechnology*, 12(11), pp. 8287–8292.

Saini, S. *et al.* (2012) 'Resistance-associated mutations in HIV-1 among patients failing first-line antiretroviral therapy', *Journal of the International Association of Physicians in AIDS Care*, 11(3), pp. 203–209. doi: 10.1177/1545109711421217.

Sainski, A. M. *et al.* (2011) 'The HIV-1-Specific Protein Casp8p41 Induces Death of Infected Cells through Bax/Bak', *Journal of Virology*, 85(16), pp. 7965–7975. doi: 10.1128/jvi.02515-10.

Santander-Ortega, M. J. *et al.* (2009) 'Protein-loaded PLGA-PEO blend nanoparticles: Encapsulation, release and degradation characteristics', *Colloid and Polymer Science*, 288(2), pp. 141–150. doi: 10.1007/s00396-009-2131-z.

dos Santos, A. M. (2012) 'Thermal effect on Aequorea green fluorescent protein anionic and neutral chromophore forms fluorescence', *Journal of Fluorescence*, 22(1), pp. 151–154. doi: 10.1007/s10895-011-0941-0.

Sattentau, Q. J. and Stevenson, M. (2016) 'Macrophages and HIV-1: An Unhealthy Constellation', *Cell Host and Microbe*. doi: 10.1016/j.chom.2016.02.013.

Schmickler, W. (2014) 'Electrochemical Theory: Double Layer', in *Molecular Sciences and Chemical Engineering*. Elsevier. doi: https://doi.org/10.1016/B978-0-12-409547-2.11149-7.

Schütze, T. *et al.* (2011) 'Probing the SELEX process with next-generation sequencing', *PLoS ONE*, 6(12), pp. 1–10. doi: 10.1371/journal.pone.0029604.

Shafie, M. and Fayek, H. H. (2013) 'Formulation and Evaluation of Betamethasone Sodium Phosphate Loaded Nanoparticles for Ophthalmic Delivery', *Journal of Clinical & Experimental Ophthalmology*, 04(02). doi: 10.4172/2155-9570.1000273.

Shaw, G. M. and Hunter, E. (2012) 'HIV transmission', *Cold Spring Harb Perspect Med*, (2). doi: 10.1101/cshperspect.a006965.

Shigdar, S. *et al.* (2011) 'Clinical applications of aptamers and nucleic acid therapeutics in haematological malignancies', *British Journal of Haematology*, 155(1), pp. 3–13. doi: 10.1111/j.1365-2141.2011.08807.x.

Shigdar, S. *et al.* (2013) 'The Use of Sensitive Chemical Antibodies for Diagnosis: Detection of Low Levels of Epcam in Breast Cancer', *PLoS ONE*, 8(2). doi: 10.1371/journal.pone.0057613.

Siddiqi, N. J. *et al.* (2012) 'Identification of potential biomarkers of gold nanoparticle toxicity in rat brains', *Journal of Neuroinflammation*, 9, pp. 1–7. doi: 10.1186/1742-2094-9-123.

Siliciano, R. F. and Greene, W. C. (2011) 'HIV latency', *Cold Spring Harbor Perspectives in Medicine*, 1(1), pp. 1–20. doi: 10.1101/cshperspect.a007096.

da Silva Fernandes, R. *et al.* (2019) 'Development of alginate/starch-based hydrogels crosslinked with different ions: Hydrophilic, kinetic and spectroscopic properties', *Materials Today Communications*. Elsevier, 21, pp. 1–9. doi: 10.1016/j.mtcomm.2019.100636.

Son, J., Vavra, J. and Forbes, V. E. (2015) 'Effects of water quality parameters on agglomeration and dissolution of copper oxide nanoparticles (CuO-NPs) using a central composite circumscribed design', *Science of The Total Environment*, 521–522, pp. 183–190. doi: https://doi.org/10.1016/j.scitotenv.2015.03.093.

Song, K. M., Lee, S. and Ban, C. (2012) 'Aptamers and their biological applications', *Sensors*, 12(1), pp. 612–631. doi: 10.3390/s120100612.

Song, X. *et al.* (2020) 'Effect of molecular weight of chitosan and its oligosaccharides on antitumor activities of chitosan-selenium nanoparticles', *Carbohydrate Polymers*. Elsevier, 231(September 2019), p. 115689. doi: 10.1016/j.carbpol.2019.115689.

Sorasitthiyanukarn, F. N. *et al.* (2018) 'Chitosan/alginate nanoparticles as a promising approach for oral delivery of curcumin diglutaric acid for cancer treatment', *Materials Science and Engineering C*, 93, pp. 178–190. doi: 10.1016/j.msec.2018.07.069.

Sorasitthiyanukarn, F. N. *et al.* (2019) 'Chitosan/alginate nanoparticles as a promising carrier of novel curcumin diethyl diglutarate', *International Journal of Biological Macromolecules*. Elsevier B.V., 131, pp. 1125–1136. doi: 10.1016/j.ijbiomac.2019.03.120.

Stevenson, M. (2015) 'Role of myeloid cells in HIV-1-host interplay', *Journal of NeuroVirology*, 21(3), pp. 242–248. doi: 10.1007/s13365-014-0281-3.

Suopajärvi, T. (2015) *Functionalized nanocelluloses in wastewater treatment applications*.

Swanstrom, R. and Coffin, J. (2012) 'HIV-1 Pathogenesis : The Virus', *Cold Spring Harb Perspect Med*, 2.

Tadros, T. (2013) 'Steric Stabilization', in Tadros, T. (ed.) *Encyclopedia of Colloid and Interface Science*. Berlin, Heidelberg: Springer Berlin Heidelberg, pp. 1048–1049. doi: 10.1007/978-3-642-20665-8_146.

Talam, N. C. *et al.* (2008) 'Factors affecting antiretroviral drug adherence among HIV/AIDS adult patients attending HIV/AIDS clinic at Moi Teaching and Referral Hospital, Eldoret, Kenya.', *East African journal of public health*, 5(2), pp. 74–78.

Tebit, D. M. *et al.* (2010) 'Divergent Evolution in Reverse Transcriptase ( RT ) of HIV-1 Group O and M Lineages : Impact on Structure , Fitness , and Sensitivity to', 84(19), pp. 9817–9830. doi: 10.1128/JVI.00991-10.

Thakur, V. K. and Voicu, S. I. (2016) 'Recent advances in cellulose and chitosan based membranes for water purification: A concise review', *Carbohydrate Polymers*. Elsevier Ltd., 146, pp. 148–165. doi: 10.1016/j.carbpol.2016.03.030.

ThermoFisher (2020) *Invitrogen Tali - Image Based Cytometer*. Available at: http://www.hylandscientific.com/product.aspx?itemid=1383&prodid=13935&pagetitle=-Invitrogen-Tali---Image-Based-Cytometer-.

Thiagarajan, G., Greish, K. and Ghandehari, H. (2013) 'Charge affects the oral toxicity of poly(amidoamine) dendrimers', *European Journal of Pharmaceutics and Biopharmaceutics*. Elsevier B.V., 84(2), pp. 330–334. doi: 10.1016/j.ejpb.2013.01.019.

Tuerk, C. and Gold, L. (1990) 'Systematic evolution of ligands by exponential enrichment: RNA ligands to bacteriophage T4 DNA polymerase', *Science*, 249(4968), pp. 505–510. doi: 10.1126/science.2200121.

Turner, B. G. and Summers, M. F. (1999) 'Structural biology of HIV', *Journal of Molecular Biology*, (285), pp. 1–32. doi: 10.1042/BST0301001.

Uhlen, M. *et al.* (2010) 'Towards a knowledge-based Human Protein Atlas', *Nature Biotechnology*, 28(12), pp. 1248–1250. doi: 10.1038/nbt1210-1248.

UNAIDS (2019) *Global HIV & AIDS statistics - 2019 fact sheet*.

Venkatesan, J. *et al.* (2016) 'Seaweed polysaccharide-based nanoparticles: Preparation and applications for drug delivery', *Polymers*, 8(2), pp. 1–25. doi: 10.3390/polym8020030.

Ventola, C. L. (2017) 'Progress in nanomedicine: Approved and investigational nanodrugs', *P and T*, 42(12), pp. 742–755.

Vessman, J. *et al.* (2001) 'Selectivity in analytical chemistry', *Revue Roumaine de Chimie*, 73(8), pp. 1381–1386.

Villegas-Peralta, Y. *et al.* (2020) 'Impact of the molecular weight on the size of chitosan nanoparticles: characterization and its solid-state application', *Polymer Bulletin*. Springer Berlin Heidelberg. doi: 10.1007/s00289-020-03139-x.

Vocero-Akbani, A. M. *et al.* (1999) 'Killing HIV-infected cells by transduction with an HIV protease-activated caspase-3 protein', *Nature Medicine*, 5(1), pp. 29–33. doi: 10.1038/4710.

Wacleche, V. S. *et al.* (2018) 'The biology of monocytes and dendritic cells: Contribution to HIV pathogenesis', *Viruses*, 10(2), pp. 1–31. doi: 10.3390/v10020065.

Walter, J. G., Stahl, F. and Scheper, T. (2012) 'Aptamers as affinity ligands for downstream

processing', *Engineering in Life Sciences*, 12(5), pp. 496–506. doi: 10.1002/elsc.201100197.

Wang, Z. *et al.* (2018) 'Expanded cellular clones carrying replication-competent HIV-1 persist, wax, and wane', *Proceedings of the National Academy of Sciences of the United States of America*, 115(11), pp. E2575–E2584. doi: 10.1073/pnas.1720665115.

Wernig, K. *et al.* (2008) 'Depot formulation of vasoactive intestinal peptide by protamine-based biodegradable nanoparticles', *Journal of Controlled Release*. Elsevier B.V., 130(2), pp. 192–198. doi: 10.1016/j.jconrel.2008.06.005.

WHO (2019a) *HIV/AIDS*. Available at: https://www.who.int/news-room/fact-sheets/detail/hiv-aids.

WHO (2019b) *Hiv drug resistance report 2019*. Available at: https://www.who.int/hiv/pub/drugresistance/hivdr-report-2019/en/.

Wickramathilaka, M. P. and Tao, B. Y. (2019) 'Characterization of covalent crosslinking strategies for synthesizing DNA-based bioconjugates', *Journal of Biological Engineering*. Journal of Biological Engineering, 13(1), pp. 8–17. doi: 10.1186/s13036-019-0191-2.

Woitiski, C. B. *et al.* (2011) 'Facilitated nanoscale delivery of insulin across intestinal membrane models', *International Journal of Pharmaceutics*. Elsevier B.V., 412(1–2), pp. 123–131. doi: 10.1016/j.ijpharm.2011.04.003.

Xiao, Z. *et al.* (2012) 'Engineering of targeted nanoparticles for cancer therapy using internalizing aptamers isolated by cell-uptake selection', *ACS Nano*, 6(1), pp. 696–704. doi: 10.1021/nn204165v.

Xie, X. *et al.* (2016) 'EpCAM aptamer-functionalized mesoporous silica nanoparticles for efficient colon cancer cell-targeted drug delivery', *European Journal of Pharmaceutical Sciences*. Elsevier B.V., 83, pp. 28–35. doi: 10.1016/j.ejps.2015.12.014.

Xing, J., Deng, L. and Dong, A. (2010) 'Chitosan/Alginate Nanoparticles Stabilized by Poloxamer for the Controlled Release of 5-Fluorouracil', *Journal of Applied Polymer Science*, 117(5), pp. 2354–2359. doi: 10.1002/app.

Yan, L., Rosen, N. and Arteaga, C. (2011) 'Targeted cancer therapies', *Chinese Journal of Cancer*, 30(1), pp. 1–4. doi: 10.5732/cjc.010.10553.

Yaqub, O. (2018) 'Variation in the dynamics and performance of industrial innovation: What can we learn from vaccines and HIV vaccines?', *Industrial and Corporate Change*, 27(1), pp. 173–187. doi: 10.1093/icc/dtx016.

Yin, L. (2013) 'Amphiphilic Polymers: Crystallization-assisted Self-assembly and Applications in Pharmaceutical Formulation'. Available at: http://hdl.handle.net/11299/163033.

Young, F. E. (1988) 'The role of the FDA in the effort against AIDS', *Public Health Reports*, 103(3), pp. 242–245.

Yu, C. *et al.* (2011) 'Novel aptamer-nanoparticle bioconjugates enhances delivery of anticancer drug to MUC1-positive cancer cells in vitro', *PLoS ONE*, 6(9), pp. 1–8. doi: 10.1371/journal.pone.0024077.

Yu, C. *et al.* (2012) 'We are IntechOpen , the world ' s leading publisher of Open Access books Built by scientists , for scientists TOP 1 %', in *Intech*, p. 13. doi: 10.1016/j.colsurfa.2011.12.014.

Yu, H., Nguyen, M. H. and Hadinoto, K. (2018) 'Effects of chitosan molecular weight on the physical and dissolution characteristics of amorphous curcumin–chitosan nanoparticle complex', *Drug Development and Industrial Pharmacy*. Informa Healthcare USA, Inc, 44(1), pp. 82–88. doi: 10.1080/03639045.2017.1373802.

Yu, K. *et al.* (2013) 'Copper ion adsorption by chitosan nanoparticles and alginate microparticles for water purification applications', *Colloids and Surfaces A: Physicochemical and Engineering Aspects*. Elsevier B.V., 425, pp. 31–41. doi: 10.1016/j.colsurfa.2012.12.043.

Zeng, M., Haase, A. T. and Schacker, T. W. (2012) 'Lymphoid tissue structure and HIV-1 infection: Life or death for T cells', *Trends in Immunology*. doi: 10.1016/j.it.2012.04.002.

Zhang, P. *et al.* (2019) 'Biocompatibility profile and in vitro cellular uptake of self-assembled alginate nanoparticles', *Molecules*, 24(3), pp. 1–12. doi: 10.3390/molecules24030555.

Zhang, S. *et al.* (2008) 'Polyethylenimine-coated albumin nanoparticles for BMP-2 delivery', *Biotechnology Progress*, 24(4), pp. 945–956. doi: 10.1002/btpr.12.

Zhang, X. and Zhang, P. (2017) 'Polymersomes in Nanomedicine - A Review', *Current Nanoscience*, 13(2), pp. 124–129. doi: 10.2174/1573413712666161018144519.

Zhou, J. and Rossi, J. (2017) 'Aptamers as targeted therapeutics: current potential and challenges have a patent pending on "Cell-specific internalizing RNA aptamers against human CCR5 and used therefore" [United States Patent HHS Public Access', *Nat Rev Drug Discov*, 16(3), pp. 181–202. doi: 10.1038/nrd.2016.199.

Zhou, J. and Rossi, J. J. (2014) 'Cell-type-specific, aptamer-functionalized agents for targeted disease therapy', *Molecular Therapy - Nucleic Acids*. doi: 10.1038/mtna.2014.21.

Zhu, M. *et al.* (2014) 'The effect of humic acid on the aggregation of titanium dioxide nanoparticles under different pH and ionic strengths', *Science of the Total Environment*. Elsevier B.V., 487(1), pp. 375–380. doi: 10.1016/j.scitotenv.2014.04.036.

Zhu, Q. *et al.* (2012) 'Inhibition of HIV-1 protease expression in T cells owing to DNA aptamer-mediated specific delivery of siRNA', *European Journal of Medicinal Chemistry*. Elsevier Masson SAS, 56, pp. 396–399. doi: 10.1016/j.ejmech.2012.07.045.

Zhu, Z. *et al.* (2019) 'Comparison of natural and synthetic surfactants at forming and stabilizing nanoemulsions: Tea saponin, Quillaja saponin, and Tween 80', *Journal of Colloid and Interface Science*, 536, pp. 80–87. doi: https://doi.org/10.1016/j.jcis.2018.10.024.

Zou, L. *et al.* (2016) 'Encapsulation of protein nanoparticles within alginate microparticles: Impact of pH and ionic strength on functional performance', *Journal of Food Engineering*. Elsevier Ltd, 178, pp. 81–89. doi: 10.1016/j.jfoodeng.2016.01.010.